UNIVERSITÀ
DEGLI STUDI DELLA
Tuscia

UNIVERSITÁ DEGLI STUDI DELLA TUSCIA

Dipartimento di Scienze Biologiche ed Ecologiche

Dottorato di ricerca in

Ecologia e gestione delle risorse biologiche

XXVI Ciclo

Spatial and temporal variability of dominant Phytoplankton Size Classes in the Mediterranean sea from Remote Sensing

Settore Scientifico Disciplinare – BIO/07

Tesi di dottorato di:

dott.ssa Annalisa Di Cicco

Coordinatore del corso

prof. Giuseppe Nascetti

Tutore

prof. Marco Marcelli

Co-tutore

dott. Salvatore Marullo

Index:

ABSTRACT

Thanks to the key rule that phytoplankton plays in the global Carbon cycle and in the regulation of the climate processes, information about the composition of its community structure is today one the most important scientific lines of research.

Recent trends in the comprehension of the community structure as well as the ecological state of the aquatic ecosystems are based on the identification of functional traits able to act as "non- taxonomic" descriptors. One of the most important descriptor for the phytoplankton community is considered the "cell size", thanks to the existent relationship between dimensions and pigmentary content, different taxa or stages of growth in the same taxon, photosynthetic efficiency and bio-optical phytoplankton properties. In some cases size is also able to supply information on the biogeochemical functions and roles of the community itself. In this context remote sensing technologies provide a great tool for a synoptic observation at spatial and temporal scale of the marine ecosystem.

In the recent years several physical, biological and ecological models have been proposed to estimate Phytoplankton Size Classes from remote sensing data.

The aim of this work is to investigate the spatial distribution and temporal variability of three dominant Phytoplankton Size Classes (PSCs) in the Mediterranean Sea during the SeaWiFS mission from 1998 to 2010.

This work is organized as follows. The first introductive chapter clarifies the base concepts of Size as community descriptor (section a), ecological rule of phytoplankton (section b), remote sensing technique in the Ocean Observation (section c) and characterizes the study area (section d). In the chapter 2, the *in-situ* (section a) and *remote* (section b) methods and data selected for this work with the algorithms investigated are represented. The third chapter shows the algorithm's validation and summarizes the results. Comments are exposed in the chapter 4. Conclusions and some directions of future work are indicated in the chapter 5.

1. INTRODUCTION

1.a The SIZE role in the comprehension of the community structure

Sallie Chisholm in her important treatise on the "Phytoplankton size" claims that ecologists divide in two great groups regarding the comprehension of the natural systems: one, that tries to explain nature by size, and the other that finds exceptions to the "established size-dependent rules" [Chisholm, 1992].

The principal goal of natural sciences has always been understanding the natural systems by a quantitative description that take into account of the energy flux and the interaction among powers, that results in different shapes and phenomena featuring biosphere at any scale level. "The system's dynamics are explained linking descriptors of state to descriptors of change" [Basset. et al., 2009].

Ecosystem is the reference natural system of the Ecology. The recent trends in the comprehension of the community structure and functioning, as well as to the ecological state of the aquatic ecosystems are also aimed to the research of functional traits able to act as "non- taxonomic" descriptors of community (Basset et al., 2009; Mouillot et al., 2006). "Size" is considered one of them. A great number of single organisms and community characteristics depend in a known manner on individual dimension. The "metabolic theory" of Brown et al. (2004), links closely the performance of "individuals" in terms of metabolism and energy transfer efficiency to the ecology of "population, community and ecosystems". There is a flow of energy and matter between the various ecological systems at different hierarchical scale dependent on environmental and individual characteristics that regulate the metabolism of the single organism and consequently, the features of each hierarchical level. According to this theory, body size is one of three key factors that affect individual metabolism and so community ecology, together with temperature and stoichiometry.

In this context, several studies based on this important "non-taxonomic" descriptor were conducted to perform the comprehension of different ecological and evolutionary processes as individual and population growth and biological cycle, populations interaction,

environmental forcing, species richness, ecological succession, bio-geographical distribution and system energy fluxes (Margalef, 1997; Vadrucci et al., 2007; Basset et al. 2009).

What is the advantage of the morphometric or "body size" descriptors?

Basset et al. (2009) provides different answers to this question in his new methodologies for the classification of the quality state of the aquatic ecosystems: cell size is easy to measure in quantitative, accurate and reproducible way, is easy to inter-calibrate, eliminates the problematic and the long times of taxonomic identification and "makes comparison between ecosystems easier, since it helps to resolve the difficulties resulting from the heterogeneity of taxonomic composition in different ecosystems" (Vadrucci et al., 2007).

On the basis of the different ecological hierarchical levels of investigation it is possible to identify several specific morphometric descriptors. For individual levels we can consider bio-volume, surface area or surface/volume ratio. Instead, for population and guild, there are body size-abundance distribution, body size-spectra or biomass size fractions of micro (>20 µm), nano (2-20 µm) and pico (<2 µm) phytoplankton (Sieburth, 1979).

In the present work we take into account biomass fractions, abundance distribution and bio-volume of the three Phytoplankton Size Classes (PSCs) related to Sieburth classification. I pay particular attention to bio-volume and biomass data, which are important in the determination of Carbon content and represent fundamental parameters in the studies on phytoplankton physiology and ecosystems energy flows (Vadrucci et al., 2007).

In the aquatic ecosystems the role of the individual dimension as phytoplankton community descriptor is based on the relationship between size and pigmentary content, different taxa or stages of growth in the same taxon, photosynthetic efficiency, bio-optical phytoplankton properties and water column dynamic (Chisholm, 1992; Organelli et al., 2007; Raven, 1998). J. A. Raven, in his important work "Small is beautiful" summarizes the influences of the phytoplankton cell size on its photosynthetic activity and its role in biogeochemical cycling, biodiversity and community (Raven, 1998). Size affects:

- maximum specific growth rate, i.e. in unicellular algae where smaller cells seems to have a larger fraction of biomass related to catalysis of growth and less to storage (Raven, 1998)
- photons acquisition, with a pigment "package effect", describing the Chlorophyll *a* efficiency in the light harvesting, smaller in the pico-phytoplankton component, implying

higher pigment-specific absorption coefficient for a given pigment content per unitary volume (Chisholm, 1992; Raven, 1998; Basset et al. 2009).

- nutrient solute and water fluxes across the plasmalemma, favoring the small sized cells in the oligotrophic water. This is due to the larger Surface/Volume ratio of small cell respect to the larger ones, that makes them efficient nutrient absorber in very low nutrient condition (Chisholm, 1992; Raven et al., 1998).
- loss of cells, because the probability of sinking out of the euphotic zone is greater in micro size cells than in smaller ones (Raven et al., 1998).

All this means that size affect the productivity of the phytoplankton cells.

1.b Phytoplankton and its ecology

1.b.1 Phytoplankton ecological role in the biogeochemical cycles

Phytoplankton (phyton = plant; planktos = wandering) consists in autotrophic free-floating microscopic algae that are mostly unicellular, although colonial or filamentous species also occur.

The great interest in the composition of the phytoplankton community is closely linked to the predominant position of this component in the climate regulation processes. With its activity of "biological pump", phytoplankton plays a very important role in the biogeochemical cycling of carbon, sequestrating atmospheric CO_2 from surface waters, which will be thus "stored" within the ocean.

The atmospheric CO_2 variation rate depends not only on human activity, that in the last 200 years have had a great weight, but also on biogeochemical and climatological processes and their interaction with the carbon cycle. There is a continuous and rapid exchange of CO_2 between the atmosphere and ocean. In this last one, the content of dissolved inorganic carbon (DIC) is 50 times higher than in the atmosphere. On a time scale of millennia the oceans determine the concentration of atmospheric CO_2 and not the opposite. The exchange is continuous at the surface level, at the air-water interface. The concentration of DIC in the ocean increases markedly below the first 300 m, where takes on values significantly greater than the value of balance between atmosphere and ocean surface. The

highest concentrations of DIC within the oceans are the result of two fundamental processes: the "solubility pump" (or physical pump) and the "biological pump" (Falkowski et al., 2000). The solubility pump is responsible for roughly 50% of the inorganic carbon gradient. The other 50% is a consequence of biological activity.

- The solubility pump efficiency depends on the thermohaline circulation and on latitudinal and seasonal changes in ocean ventilation. CO_2 is more soluble in cold and salty waters. Consequently, the oceans' ability to sequester atmospheric CO_2 is controlled by the formation of cold and dense water masses at high latitudes. These water masses are transported away and then fall, bringing into the ocean interior the CO_2, which is thus effectively removed from the atmosphere. Only when this deep water rises again to the surface (several hundred years later), the CO_2 will comes back in contact with the air. Human-induced warming and the possible consequent weakening of the thermohaline circulation could severely reduce the ability of the oceans to steal CO_2 to the atmosphere (Falkowski et al., 2000).

- The biological pump contributes to the absorption of CO_2 in the ocean interior through the photosynthetic activity of phytoplankton in the euphotic zone. This process reduces the partial pressure of CO_2 in the upper part of the ocean fixing the C inorganic into organic matter (OM), largely in the form of particulate material, and consequently promotes the absorption from the atmosphere. Thanks to the gravity force, about 25 % of this fixed carbon precipitates as persistent "rain" into the ocean, where it is then oxidized by respiration of heterotrophic bacteria and other organism (microbial loop), that convert it into inorganic nutrients, increasing so the DIC concentration (Falkowski et al., 2000). Much of this recycling takes place in the euphotic zone, where produced CO_2 can be turn again into OM by phytoplankton photosynthetic activity or exchanged with the atmosphere. The major influence on the climate there is when the OM reaches the bottom of the ocean before being decomposed and in geologic time becoming part of oil, gas hydrates and sedimentary rocks (Falkowski, 2002). The Carbon remaining in photosynthetic organism following their own respiratory costs is potentially available for consumption by other organisms. This Carbon, called Net Primary Production (NPP), provides the Energy requirements of all ecosystems. The contribution of the

phytoplankton to the NPP shows as the role of the Oceans in the Global Carbon Cycle is fundamental. Marine ecosystems, containing approximately 1% of the plant biomass, account for 45% of the productivity against the 55% contribute of the terrestrial ecosystem, that account approximately 99% of the plant biomass. The major efficiency per unit of biomass of the phytoplankton in the NPP is due to more rapid turnover of these marine primary producers with an average lifetime less than 1 week against the lifetime of terrestrial primary producers of a decade or more (Falkowski, 2001; Della Croce et al., 1997).

The principal factor in the maintenance of biological pump is the upward flux of inorganic nutrients from the ocean interior, especially fixed nitrogen and phosphate, essential for the photosynthetic activity of phytoplankton in the upper ocean (Falkowsky, 2001).

1.b.2 Biological and physical factor that control phytoplankton ecology

Distribution, abundance and production of phytoplantonic organisms are closely linked to the physico-chemical characteristics of the water column. Solar energy, through heat flux or momentum transfer by the wind, is the driving force for the whole ocean dynamics, affecting phytoplankton productivity at all spatio-temporal scales (Estrada et al., 1996), from ocean basin circulation, through localized areas of upwelling, down to small-scale turbulence that affects individual cells (Mann and Lazier, 2006). This mechanical energy caused by the Sun and called from Margalef “external energy” (Margalef et al., 1978) sustains the primary production, supporting the confluence of phytoplankton cells with light and nutrients, necessary factors for the photosynthetic activity. Light and nutrients have opposite gradient in the open ocean. External energy is so fundamental in the supplying of nutrients in the euphotic zone from the deep waters. Furthermore, at scale relative to the organism, turbulent water affects the exchange of metabolic molecules between the cell and the medium, with direct effect on the cellular growth and division. Size, shape, surface/volume ratio and motility appendage are different adaptations developed and used by different phytoplanktonic organism to prevent sinking and increase nutrient assimilation (Estrada et al., 1996). At the last, increase in turbulence may have affected the levels of light experienced by the cells (Mann and Lazier, 2006).

In this context the intensity of the turbulence in the column water is very important in the composition of the phytoplankton community.

Margalef (1978) suggested the close relationship existent between different combinations of nutrients concentration, turbulence intensity and distribution of phytoplankton assemblages. He showed the main phytoplankton life forms in an ecological space defined by these two environmental factors: the Margalef's "Mandala" (fig. 1.1).

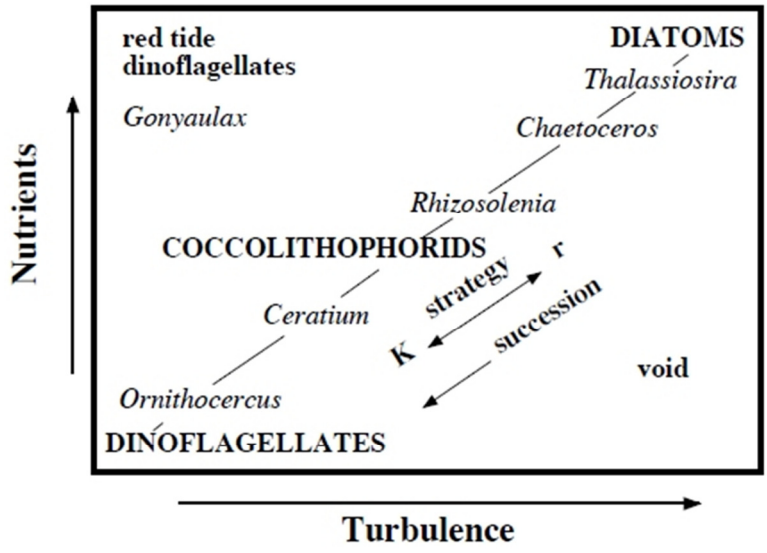

Figure 1.1 Margalef's Mandala (from the redrawing of Estrada et al. 1996 of Margalef et al., 1978)

On the Margalef view, a typical phytoplankton succession develops from high turbulence – high nutrient corner to the opposite low turbulence – low nutrient corner. The taxonomic classes are unlikely affected by different intensity of turbulence and concentration of nutrients. At high levels of both, the Diatoms, non-motile and characterized by fast potential growth rates, bloom. The high nutrients concentrations support their metabolism while the turbulence counteracts the lack of motility and the consequent greater tendency to the sinking. Coccolithophorids dominate the niche space featuring by intermediate environmental conditions. At the last, Dinoflagellates, that thanks to the presence of appendages can regulate their position in the column water and take advantage in the nutrients absorption, survive and predominate in stratified water (Margalef et al., 1978; Estrada et al., 1996).

Phytoplankton production depends strongly on turbulence. In a stratified water column the euphotic zone becomes over time depleted of nutrients as a result of uptake by the phytoplanktonic cells. In this finite layer there is enough light for photosynthesis and growth to take place. So the nutrient uptake becomes a limiting factor. In contrast, deeper water is nutrient-rich, due to the decomposition of organisms that sink and decay from the euphotic zone. In the absence of turbulence, the only mechanism for the transfer of nutrients from deep water to the euphotic layer is the molecular diffusion, an extremely slow process. In the real world, the ocean is filled with turbulent motion: the most common dynamical structures generated from wind stress at the surface, internal waves, changes in the bathymetry, divergences of surface currents, meandering and so (Mann and Lazier, 2006). The interaction between water masses with different features causes discontinuous areas of different physical, chemical and biological properties, each having different ecological implications. These areas are involved in the fertilization of the surface layers, in the production levels and are characterized by different organism distributions and community composition, following Margalef's principles. Typical of the Mediterranean Sea are cyclonic and anti-cyclonic mesoscale eddies (view section 1.d), where the deflection of the water movement due to the Coriolis force induces vertical water flux. In particular, cyclonic rotation in the northern hemisphere leads to spreading of water from the center, replaced so by the upwelling of cold, deep water, source of great concentration of nutrients (fig 1.2).

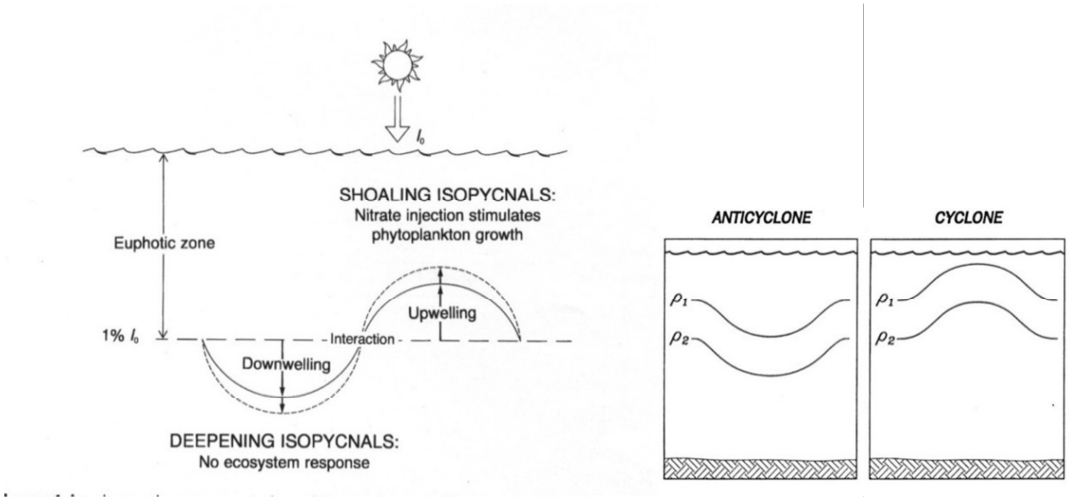

Figure 1.2 Schematic anticyclonic and cyclonic structures typical of the Mediterranean Sea (from McGillicuddy et al., 1998 & McGillicuddy et al., 1999).

The last important parameter to take in consideration in the influence of the phytoplankton productivity is the sea temperature. In particular the process of carbon

assimilation in the photosynthesis is enzymatically controlled and therefore temperature dependent (Falkowski and Raven, 2007). One of the main effects of the temperature is indirect (due to the Solar Energy) and is due to its influence on the stability of the water column. Temperature conditions the mixed layer depth, thus regulating the nutrients availability in lighted zone.

1.c Measuring the Size from space: satellite oceanography and Ocean Color

1.c.1 Passive remote sensing of Ocean Color

In the remote sensing of ocean color, a sensor mounted on a remote platform (i.e. satellite, aircraft, ship and so) recovers the radiometric flux reaching the sensor itself at several selected wavelengths in the visible and near-infrared domains of the electromagnetic spectrum. In a passive system of remote sensing, the primary source of the light is the sun, so the acquisition takes place only during the daylight hours. The sunlight, before reaching the sensor, can follow different pathways and so change in its properties due to the interaction of light with the atmosphere, the ocean and their components. The optical signal that reaches the detector is the result of photons that partly have been either (1) scattered by the atmosphere, (2) specular-reflected at the sea surface and (3) upwelled from the sea after have been back-scattered by the sea-water, undergone further absorption and scattered by the atmosphere on their way toward the sensor (IOCCG, 2000).

Water-leaving radiance is the only component of the total remotely-sensed radiance that is related to the water optical properties, and consequently to the composition of the investigated natural waters (fig.1.3). The remaining part of the detected signal constitutes noise. Only atmosphere-backscattered light represents more than 80% of the total radiance. This makes critically important in the remote sensing a good correction of the atmospheric and specular reflection contribute.

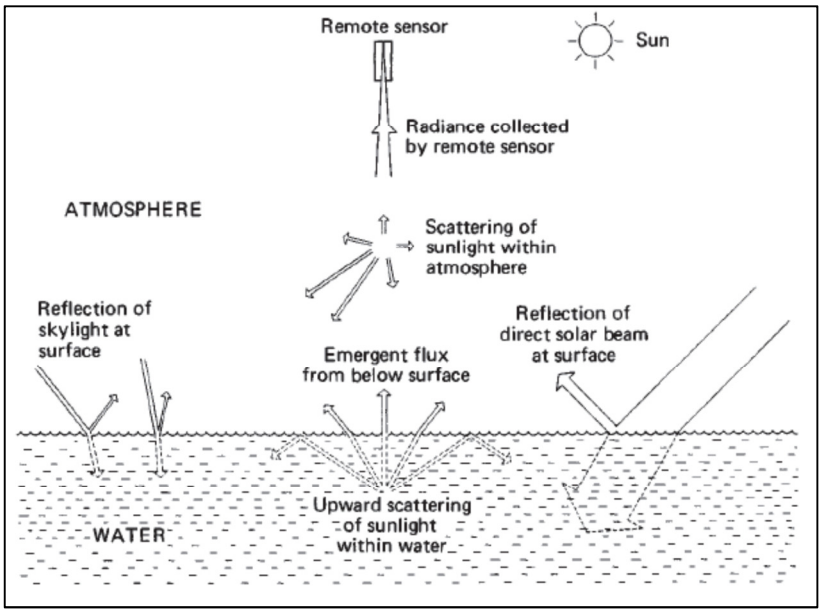

Figure 1.3 Sun light path and its interaction with the Atmosphere and the water medium before to be collect from the remote sensor (from kirk, 1983)

1.c.2 Light in the aquatic ecosystems: the physic behind the remote sensing

Light and its energy changes during its propagation through any medium are the basis of remote sensing optical methods of the earth investigation. Consequently, to understand the operation of the optical technologies and the meaning of the information which are able to provide, a quantitative study of the radiative transfer is necessary, and so the knowledge of the medium's optical properties. Natural waters, both fresh and saline, are optically very different from the pure water, that can be considered as a hypothetical medium devoid of substances other than water molecules themselves and inorganic salts dissolved in it (Mobley, 2004; IOCCG, 2000).

Natural waters are influenced by the presence of several inorganic and organic substances, suspended and dissolved. From an optical point of view, three are the main components characterizing their properties:

• Phytoplankton, and other microscopic organism that however have less influence on the optical properties

• Suspended inorganic material, consisting from river discharge or sediment re-suspension. It is relatively more important in coastal and inland waters than in the open ocean

• Yellow substances, called also "gelbstoff", "coloured-dissolved organic matter" (CDOM) or "gilvin". They consist of a group of organic, dissolved substances, represented by humic and fulvic acids and mainly arise from the phytoplankton cellular decay (IOCCG, 2000; Robinson, 2004).

The interaction between the water and these components characterizes the response of the water body to solar radiation (fig. 1.4).

When a photon gets into the water it can be either absorbed or scattered.

The absorption and scattering phenomena in the aqueous medium for light of a given wavelength are expressed in terms of the absorption ($a_{(\lambda)}$) and scattering ($b_{(\lambda)}$) coefficients, whose sum constitutes the attenuation coefficient ($c_{(\lambda)}$) [Kirk, 1983]. These are defined "Inherent Optical Properties (IOPs), properties that depend only by the medium and the substances it contains, and are unrelated to the geometrical structure of the electromagnetic field (Mobley, 2004). Taking into account the direction of the scattering in relation to the incident collimated light beam, the scattering coefficient is the sum of two components: forward scattering, b_f, and backscattering, b_b, coefficients, integrating over the "forward" and "backward" hemispheres respectively (Robinson, 2004).

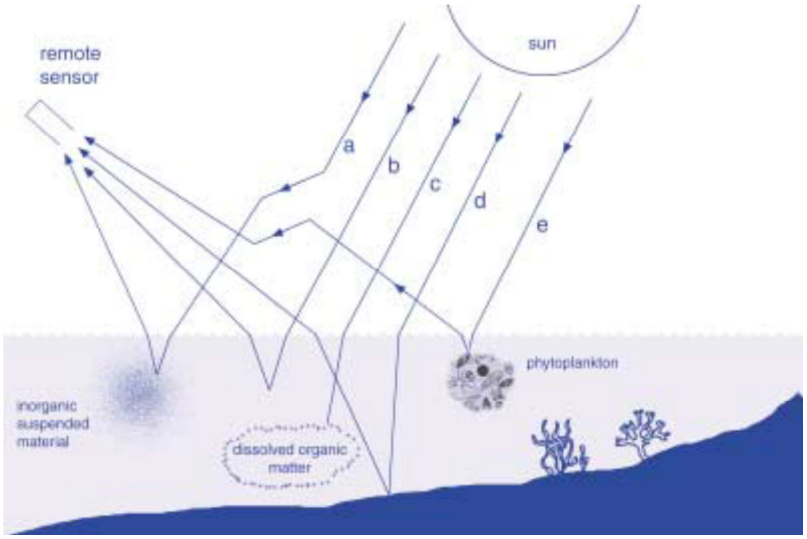

Figure 1.4 Principal water component characterizing the response of the water body to solar radiation from (IOCCG, 2000)

A photon can eventually be backscattered by a water constituent and reach the remote sensor. The direction of the scattering is affected by the size of the particles investigated.

Scattering can be elastic or inelastic. In the former, energy is conserved and the scattered photon has the same wavelength as the incident. In the aquatic environment the most important types of elastic scattering are those of Rayleigh (by water molecules) and Mie (by particulates and phytoplankton cells). On the contrary, inelastic scattering implies a loss of energy, and thus the scattered photon has a longer wavelength (spectral shift). Most common processes of inelastic scattering are Raman scattering caused by quantum effects between water molecules and fluorescence, typical of pigments (Robinson, 2004).

The presence and the different concentrations of the various constituents of natural waters, with their characteristic absorption and scattering (fig. 1.5), determine the optical properties of this medium, affecting brightness and color of the sea or other water bodies and creating the requirement for the operation of the remote sensing. In fact, for their definition, the total IOPs can be resolved in terms of their single component. The total absorption and scattering coefficients are the sum of the absorption and scattering of each constituent of the medium (Robinson, 2004).

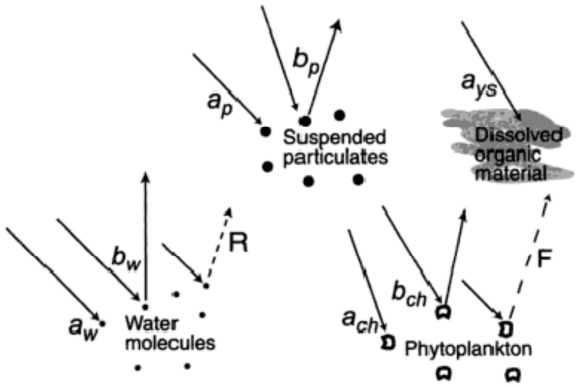

$$a = a_w + a_{Ch} + a_p + a_{ys}$$

$$b = b_w + b_{Ch} + b_p + b_{ys}$$

Figure 1.5 Total absorption and scattering of the water medium, equal to the sum of each component: water molecules (w), suspended particulates (p) and dissolved organic material (ys) (from Robinson, 2004)

The Lambert-beer law formulates the quantitative link between the IOPs and the concentration of each component of the medium, that is the base of the Ocean Color remote sensing:

$$a_n = C_n \, a_n^*$$

$$b_n = C_n \, b_n^*$$

where a and b are the absorption and scattering coefficients rispectively of the constituent n, C_n is its concentrations and a_n^* and b_n^* are the specific absorption and backscattering coefficients rispectively (Robinson, 2004). Unfortunately the satellite sensor are able to detect only the Apparent Optical Properties (AOPs). The AOPs are radiometric quantities, dependent both on the medium (i.e. on the IOP's) and on the directional distribution of the light field in the sea (Mobley, 2004). Since satellite sensors are unable to take over also the information relative to the angular distribution of the incident light, some assumptions about the geometry of the underwater light field are necessary to connect robustly the AOPs to the IOPs and than to estimate the concentration of the substancies present in the water. The experience shows that, in condition of open-sky, appropriate for ocean color remote sensing, some theoretical models based on simple relations between absorption and backscattering of the medium and its components and sub-surface water irradiance reflectance (the effectively apparent color of the sea; $R = \frac{E_u}{E_d}$, ratio of the upward to the downward irradiance) are good approximation for most marine situations. Among the most important models, it should be mentioned Morel and Prieur (1977)

$$\left(R = \frac{0.33 b_b}{a}\right)$$

when $\frac{b_b}{a}$ is less than 0.3, and Morel and Gentili (1993)

$$\left(R = f_1 \frac{b_b}{a}\right)$$

with f_1 that is function of sun angle, amount of sky light and chlorophyll concentration itself and can vary between 0.3 and 0.5 (Robinson, 2004).

Figure 1.6 shows the typical reflectance spectra for seawater dominated only by phytoplankton, yellow subtances and sediment respectively.

The spectral signature of pure seawater provides the baseline upon wich the spectral characteristics of other types of water are built by the addition of other scatterers and absorbers (fig. 1.7) – Robinson et al. (2004).

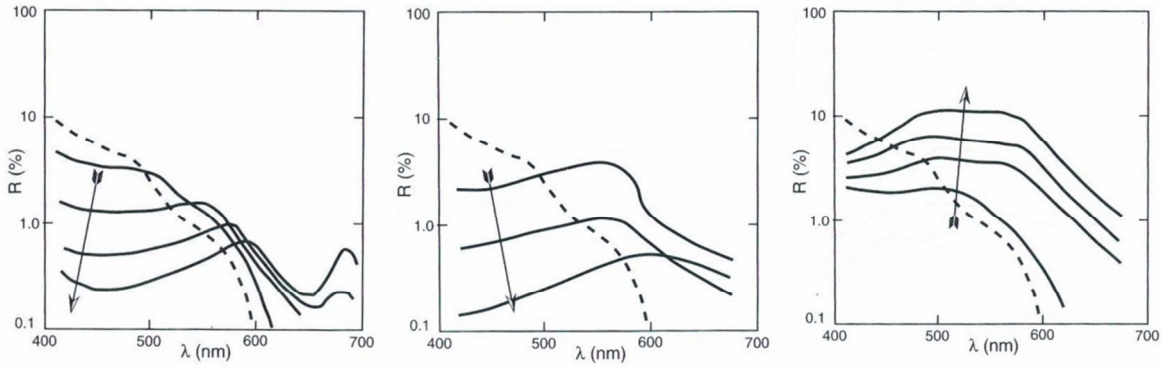

Figure 1.6 Reflectance spectra of seawater dominated only by phytoplankton (left), yellow substances (centre) and sediment (right) (from Robinson, 2004).

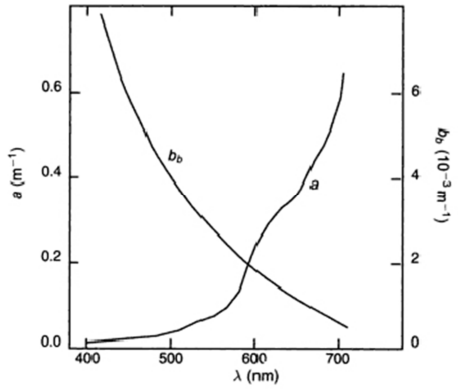

Figure 1.7 Spectral signature of pure sea water (Robinson, 2004)

In natural waters the reflectance spectra are generally more complex than those observed in figure 1.6. This is due to the influence of more than one constituent on the pure seawater at the same time. Because of this difficult interpretation of the spectra in quantitative terms of each costituent, Morel and Prieur in the 1977 divided all waters in two categories based on their optical properties (fig. 1.8):

• Case 1 waters: waters in which the Ocean Color of the sea is influenced by phytoplankton and its degradation products only. Typically these are open sea waters.

• Case 2 waters: waters whose optical properties are influenced not just by phytoplankton and related particles, but also by other substances, that vary independently of phytoplankton. These are more complex waters, generally related to coastal and inland waters (IOCCG, 2000) often influenced also by the bottom sea reflectance.

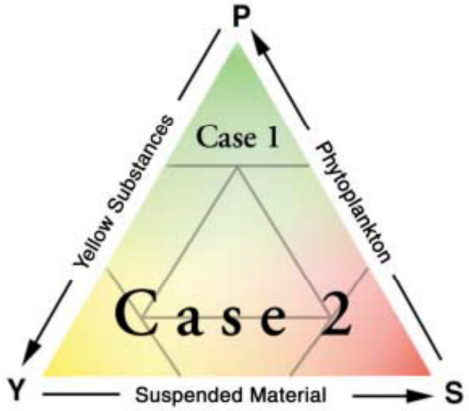

Figure 1.8 Diagrammatic representation of Case 1 and Case 2 waters (IOCCG, 2000)

Obviously, for their composition itself, the relation between AOPs and IOPs properties is more robust and easier in the case 1 than case 2 waters.

1.c.3 Satellite sensors for detecting Ocean Color: SeaWIFS era

The satellite remote sensing represents a very important resource in the Earth Observation and dynamic ecosystems understanding. This technique provides the great advantage of monitoring some biological and physical parameters at daily and global scale.

The first spectroradiometer fully dedicated to the Ocean color was the NASA's Coastal Zone Color Scanner (CZCS), an experimental sensor assembled on the Nimbus-7 satellite and operating from 1878 to 1986. The Coastal Zone was intended as a first test sensor. So the data were not systematically acquired and some different problems in the stability of an on-board calibration source for the radiometric correction and malfunctioning or sensor degradation occurred. Nevertheless, it proved the possibility to detect chlorophyll's information from satellite sensors and provided the first information on the spatial and temporal variability of the Ocean Primary production (Robinson, 2004).

The next sensor to be launched, on board of the SeaStar spacecraft on August 1997, was SeaWiFS (Sea viewing Wide Field of view-Sensor). This sensor was operating up to December 2010. It was a cooperative project between NASA and a private enterprise (Orbital Sciences Inc.). SeaWiFS sensor had six 20 nm spectral bands in the visible region, centered

on 412, 443, 490, 510, 555 and 670 nm, and two bands for atmospheric correction in the near infrared at 745-785 nm. The new sensor was designed on the basis of the CZCS experience. The new channels, in fact, provided better information that improved the precision of the chlorophyll and atmospheric correction algorithms (Robinson, 2004). Its sea level spatial resolution was 1.13 km (Kirk, 1983).

The purpose of the SeaWiFS project was to provide quantitative data on global ocean bio-optical properties to the Earth science community. The thirteen years of SeaWiFS data represent the first complete and accurate Ocean Color dataset. It was reprocessed several time to be definitively corrected from sensor drift and represent a very great resource of knowledge for the scientific community and was selected for this study.

The next spectroradiometers for the color of the sea were the two NASA's MODIS (Moderate Resolution Imaging Spectroradiometer) sensors, the first aboard of the TERRA (EOS AM) spacecraft, launched in the 2000, and the second on the AQUA (EOS PM) satellite, in orbit from the 2002. Aqua 's orbit around the Earth is sun-synchronous, near-polar, and circular. It passes from south to north over the equator in the afternoon (1.30 p.m.) and viewing the entire Earth's surface every 1 to 2 days. MODIS is acquiring, every day in every place, data in 36 spectral bands ranging in wavelength from 0.4 µm to 14.4 µm (Modis Technical Specifications [1]).

These different bands produce three different types of images with, respectively, 250 m, 500 m, and 1 km spatial resolution. The bands dedicated to the Ocean Color are six, as SeaWiFS, centered on 412, 443, 488, 531, 551 nm and have 1 km spatial resolution. The high resolution bands are important to improve the atmospheric correction and information for case 2 waters (i.e. Total Suspended Matter, TSM).

The first European Space Agency's Ocean Color sensor was the Medium Resolution Imaging Spectrometer (MERIS), launched in the 2001 and operated until April 2012. It covers most of the Earth surface in three days, providing information of Ocean Color with bands very similar to MODIS. MERIS had two important additional bands, one at 620 nm to improve the knowledge about case 2 waters and the other at 709 nm to clarify the background signal off the 681 nm fluorescence peak.

This European sensor was been very important for coastal and inland waters monitoring. In fact, although MERIS's spatial resolution in the normal mode monitoring was of 1.2 km, each band could have a maximum resolution of 300 meters (Robinson, 2004).

Today a number of other sensors operate in the visible wavebands, but with a less important scientific contribute for the Earth monitoring.

1.c.4 Current approach to detect size and taxonomy information from satellite technique

The approaches used to detect information on phytoplankton dimensions using remote sensing techniques are various and are based on different physical principles. Some of them give only size information; others are also able to estimate taxonomic classes on the bases of their specific optical properties, "directly" recovered by the sensors ("direct" methods). In the "indirect" methods the remote observation exploit the note relations existent between the Chlorophyll *a* and the different properties of specific phytoplankton groups.

The most important current approaches for detect dominant phytoplankton size classes designed for global application are based on:

1. Spectral response of optical properties
2. Phytoplankton abundance
3. Information in addition to ocean colour data
4. Satellite derived backscattering signal

1. Spectral-response algorithms utilize differences in the optical signatures of specific phytoplankton groups to distinguish among them:

   - **normalized water Leaving radiances (nwL)**:
     Alvain et al., (2005) and Alvain et al., (2008). This method, called PHYSAT, allows to identify nanoeucaryotes, Prochlorococcus, Synechococcus and diatoms in case 1 water. It is founded on an empirical correlation between AOPs properties (nLw) and a consistent global dataset of HPLC-based diagnostic pigments (data collected during nine cruises in the frameworkof the GeP&CO program). An implementation of Alvain et al., (2008) extends the detection to an additional group " phaeocystis-like". Coincident SeaWiFS nLw data between 412 and 555nm are extracted and normalized to remove the effect of the Chlorophyll *a*. These normalized spectra vary significantly

with in situ pigment composition, so the five groups can be distinguished (Alvain et al, 2005).

- **absorption (a):**

Ciotti et al., (2002) – They compared size-fractionated chlorophyll concentration and phytoplankton absorption spectra for a wide variety of natural communities of surface waters to estimate a "size" parameter from the phytoplankton absorption coefficient.

They found that more than 80% of the variability in the spectral shape of the phytoplankton absorption coefficient (from 400 to 700 nm) could be explained by the cell size of the dominant organism (considering 4 principal dimensional classes: pico-, ultra-, nano-, and micro-plankton), as a result of a strong covariation between dominant size and several factors controlling the spectral shape of the phytoplankton absorption coefficient, such as pigment packaging and concentration of accessory pigments.

From these results, they tried to reproduce the shapes of the phytoplankton absorption spectra using a spectral mixing model that took into account two spectra representative for smallest and largest cells and the complementary contribution of each of them.

- **reflectances (R)**:

Ciotti and Bricaud (2006) : the aim of this method was to retrieve information on cell size from ocean color measurements. The assumption is that change in phytoplankton cell size is the dominant factor that control the relationship between light absorption by phytoplankton and chlorophyll concentration (Ciotti et al., 2002; Bricaud et al. 2004). Under certain assumption it is possible derived the total absorption from reflectance. They selected the IOP model of Loisel and Stramski (2000) to retrieve the total absorption coefficients from reflectances at 5 SeaWiFS wavelengths (412, 443, 490, 510, 555 nm). In regions where phytoplankton absorption is significant and dominant this is a good method to retrieve changes in cell size from ocean color measurements.

2. Abundance based approaches: these approaches are based on the close link existent between the size of the phytoplanktonic cells and the trophic status of the environment (Margalef, 1967, 1978; Brewin, 2011). The trophic status can be expressed directly by

biogeochemical parameters such as Chlorophyll *a* or indirectly thorough variables such as the magnitude of a(λ) (Brewin et al., 2011).
Two of the three algorithms selected for this work are based on this approach:
Brewin et al. 2010/2011 and Hirata et al. 2011 (see section 2 for more details).

3. Ecological based approaches: ecological approaches use an integration of different type of data, ecological, geographical, temporal and physical data, in addition to ocean color, bio-optical characteristics, and remotely sensed physical parameters, to different phytoplankton groups. Among them, one of the most important is:
   Raitsos et al. (2008), in which the ensemble of these physical, ecological and bio-optical data, both *in-situ* that *remote*, was used as input to train an artificial neural networks. Their approach could discriminate four major phytoplankton functional types, diatoms, dinoflagellates, coccolithophores, and silicoflagellates, and showed an accuracy of more than 70% (Raitsos et. Al., 2008). Their results indicated that the two principal factors that contribute to the phytoplankton type identification are Sea Surface Temperature and spatio-temporal information.

4. Backscattering-based approaches: the sizes of the particles present in the medium are estimated by the particle size spectrum obtained from the satellite derived backscattering signal (see section 1.c.2). The third algorithm selected for this study, Kostadinov et al., 2009, is backscattering-based. For the description of this approach see the section 2.

1.d Study area and its characteristics: Mediterranean Sea

The investigation area is the whole Mediterranean Sea (fig. 1.9).

It is a mid-latitude and semi-enclosed sea with dimension, morphology, dynamics and external forcing that make it a "miniature model" for the comprehension of the global ocean complex processes, from the mesoscale to basin scale (Siokou-Frangou et al.,2010; Lacombe et al., 1981; Robinson and Golnaraghi, 1995). Respect to the other sea and oceans, the Mediterranean Sea has singular optical properties, with "oligotrophic waters less blue (30%) and greener (15%) than the global ocean", probably due to the lower value of Mediterranean

chlorophyll a (Volpe et al., 2007). This peculiarity makes necessary the development of regional bio-optical algorithms, more appropriate for the features of this sea.

The Mediterranean Sea is composed of two basins equal in size (fig. 1.9), one western and either eastern, connected by the Sicily Strait. The Adriatic Sea extends from the eastern basin northward between Italy and Balkans through the Strait of Otranto and the Aegean Sea between Greece and Turkey through several straits of the Grecian Island (Robinson et al., 2001).

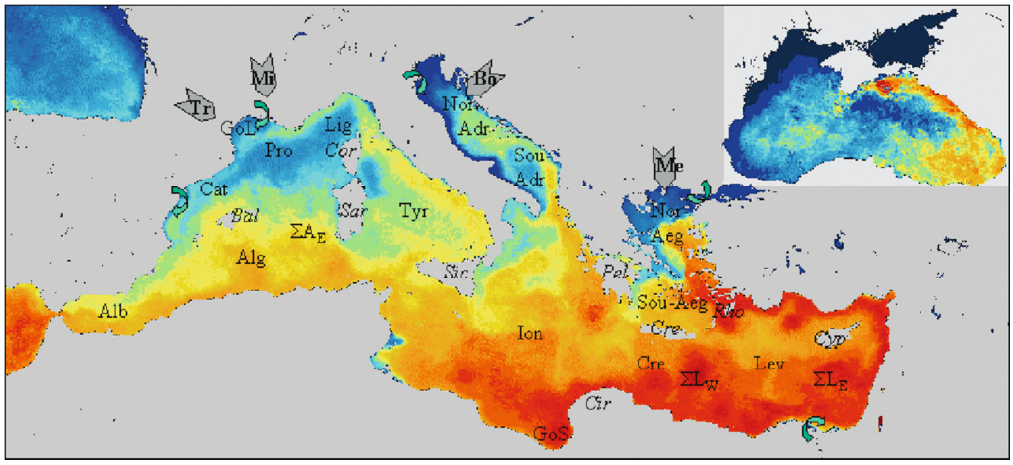

Figure 1.9 Basin and sub-basin of the Mediterranean Sea (SST maps from Millot et al., 2005)

The principal physical factors that move and regulate the Mediterranean circulation are water exchange through the various straits, wind stress and floating flux at the surface due to freshwater and heat fluxes (Robinson et al., 2001). The atmospheric processes that determine the general circulation of the basin are basic also in the production's seasonal cycles of pelagic systems, regulating indeed the fluxes of elements entering in the basin (Mann and Lazier, 2006, Siokou-Frangou et al., 2010).

The general circulation is complex because it is the result of the interaction of three predominant spatial scales: basin scale (with a thermohaline vertical circulation), sub-basin scale and mesoscale. These arise from different driving forces, from typical topographic and coastal influences and internal dynamical processes and generate free and boundary current (with relative jets, meanders and vortices), permanent or frequent cyclonic and anticyclonic gyres at sub-basin scale and smaller mesoscale eddies (Robinson et al., 2001).

The Mediterranean Sea is a concentration basin, with an anti-estuarine circulation characterized by freshwater input from the Atlantic through the Gibraltar Strait and an output flux of saltier and denser water (Millot et al., 2005; Robinson et al., 2001). The result is an open thermohaline cell that involved both western and eastern basin (through the Sicily channel) encompassing the upper layer of both basins. This cell is characterized by a dominant west-to-east surface transport and an east-to-west intermediate transport (Robinson et al., 2001; Siokou-Frangou et al., 2010).

Typical values for Atlantic Water (AW) incoming from Gibraltar are Temperature ~ 15–16 ◦C, Salinity ~ 36–37 ppt and densities of 1.026–1.027 Kg/m³ (Millot et al., 2005). Moving eastward, this water is continuously modified by the atmosphere, by the mixing with older AW surface or underneath waters. In its course the AW can be seasonally warmed or cooled, but overall, its salt content increases (up to 38–39 ppt) and it becomes denser (up to 1.028–1.029 Kg/m³). This water is markedly modified (referred as MAW, Modified Atlantic Water, to take into account its progressive change in T-S properties along its eastward flowing), but is not downwelled until the winter, when strong cold and dry northerly winds induce "marked evaporation (increase of salinity and loss of latent heat) and direct cooling (loss of sensible heat) of AW, resulting in a dramatic increase in its density (above 1.029 Kg/m³) which makes it sink", producing bottom, deep or intermediate waters (Millot, 2005).

Bottom water formation occurs in the Gulf of Lion at the western basin (WMDW, Western Mediterranean Deep Water) and in the southern Adriatic (EMDW, Eastern Mediterranean Deep Water) at the eastern basin. In the Gulf of Lion (NW MS), especially in winter, an important cyclonic circulation and the extreme atmospheric forcing produce intense convective events, which eventually reach the bottom (Sioukou Frangou at al., 2010). Deep mixing has been recently observed also in the north-eastern Levantine basin (LDW, Levantine Deep Water) during exceptionally cold winters (Robinson et al., 2001). Here, and generally over much of the Levantine basin, particularly in the north, intermediate water (LIW, Levantine Intermediate Water) is formed seasonally. The LIW is the warmest and saltiest intermediate water and the Mediterranean water mass produced with the largest volume. It is anywhere in the basin, just below the AW. The LIW, with the EMDW and WMDW, it is the water mass that prevalently contributes to the Mediterranean efflux toward the Atlantic Ocean. They continuously mix and, finally, outflow at 1000–1200m of depth thorough Gibraltar as a rather homogeneous water (Mediterranean Water, MW), which is colder (13.0–

13.5 ◦C), saltier (38.0–38.5 ppt) and denser (28.0–28.5 σ) than AW inflowing (Millot, 2005; Robinson et al., 2001).

Mediterranean surface circulation (100-200 m) (fig. 1.10) is characterized by along-slope counterclockwise gyres of AW and MAW at basin scale, that can bifurcate into vein or form branches. The southern Algerian and Libyo-Egyptian currents in the eastern ones, are markedly instable and generate mesoscale anticyclonic eddies (Millot, 2005).

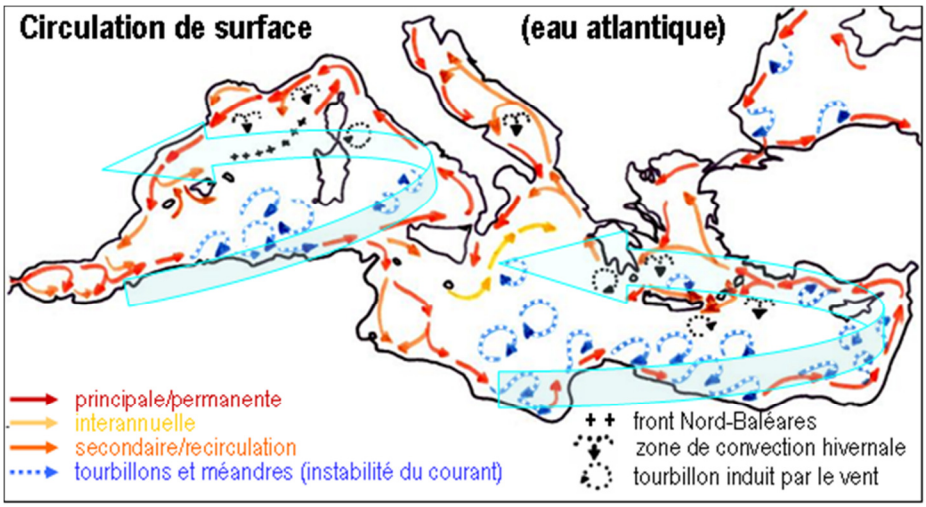

Figura 1.10 Mediterranean Surface Circulation [2]

The AW enters at Gibraltar. Water moves northeastward due to the orientation of the strait and at western of Alboran Sea describes two clockwise gyres, the first between Spain and Morocco and the second ones from Spain to Algeria. Out of Alboran, due to the Coriolis effect, the AW joins the Algerian Current, that moves along the Algerian slope. The Algerian current is often unstable and so generate mesoscale activity. Generally it produces small and short lived coastal eddies, but a few times per years the current produces a meander able to generate an anticyclonic eddy of 50-100 km in diameter in surface and induce a larger anticyclonic eddy in the deeper layer. These events, unable to pass the Sardinian Channel because too large and deeper, are guided by the topography towards the open sea. The instability of the Algerian current produce a very complex system of eddies Most of these "open sea eddies" have a life time up to 3 years (Millot, 2005).

This MAW, dispersed and amassed in the Algerian, tends to spread towards the Provencal and Catalan Basin, forming the North-Balearic front, which separates two drastically different sub-regions.

From the Algerian Current, MAW moves toward the Sicily channel. Part of this flux moves along Sicily and the Italian costs creating mesoscale activity that dominates the Tyrrhenian Sea with a quasi-permanent cyclonic gyre, which is mostly wind driven and displays strong seasonality (Robinson et al., 2001; Sioukou-Frangou et al., 2010). The Liguro-Provenço Catalan Current is created when this former flux meets the part of MAW from the west of the Corsica in the North West Mediterranean Sea. In this region, the mesoscale activity is more intense in winter, when this current becomes thicker and narrower. In the eastern basin, a jet of AW enters through the Straits of Sicily. In part meanders generating mesoscale eddies that tend to drift in the interior of the Ionia Sea, in part move southward in the regular flow of the South-Tunisian vein and afterwards Libyan vein along slope. The last one, moving eastward shows instability and produces mesoscale eddies, smaller and less well organized than the Algerian. The gyre goes on with the Libyo-Egyptian current. Millot and Taupier-Letage (2005) suggested that the instability of this current, as the southern Algerian current, develops important mesoscale activity with well-structured and energetic anticyclonic eddies. Leaded by the topography, these eddies can extended downward and moving toward the sea in western Levantine basin. Here they merge and interact with eddies of different origin from outside the zone as Mersa-Matruh (north of the Egyptian coast) or with Ierapetra, quasi permanent anticyclonic structures created every summer at southeast of Creta by the Meltem. When eddies decay, release AW that feeds the slope eastward current. The instability that generates eddies of various size is present in the whole southern part of the eastern basin gyre producing a Levantine system of anticyclonic eddies.

Other authors, based on large in situ data sets, support the idea of permanent, or recurrent, cyclonic and anticyclonic eddies and gyres interconnected by intense jets and meandering currents, as the Mid-Mediterranean Jet (See Rizzoli et al. 2014 for a comprehensive review).

When the current reaches the Rhodes Island, part of the flow moves northwestward into the Aegean Sea and bifurcates in two components, northern and southern respectively. The former, meeting the Black Sea outflow, is involved in the LIW formation. It is important to mention the cyclonic Rhodes Gyre in the North-West Levantine Sea, in which convective events during winter lead to the formation of intermediate water masses (Sioukou-Frangou 2010). The MAW, partly from Levantine basin and partly exiting from the Aegean sea, goes on in the eastern gyre toward the Ionian basin, where it bifurcates. The northern flux

penetrates in the Adriatic Sea. In the northern part of the basin, less dense water at the shelf is formed, due to the mixing with the Po runoff and to the Bora effect. In the south Adriatic, the convective winter events of the south Adriatic gyre leads to the formation of Adriatic Deep Water (Millot, 2005; Sioukou-Frangou et al., 2010). MAW that leaves the Adriatic Sea rejoins to the principal flux and proceeds in direction of Sicily, where it closes the eastern basin gyre.

2. MATERIALS AND METHODS

2.a Laboratory methods and field measurements

2.a.1. PSCs determination from "*in-situ*" data

Information about the composition of phytoplankton community structure can be obtained from the analysis of *in-situ* samples on the basis of different physical and biological properties. The method of cell counting and identification by the microscopic techniques has the greatest level of detail but is time demanding and needs of very great experience in the taxonomy knowledge.

In the last years, other important methods and techniques have reached maturity. The number and the dimensions of the fluorescent cells in a specific water sample volume can be identified directly by the flow-cytometer technique. Indirect information are also retrieved from the determination of light absorption spectra of pigments in the visible spectrum, commonly measured using the spectrophotometry techniques with the support of an auxiliary integrative sphere.

The morphometric descriptor used in this study is the biomass size fractions of micro- (>20 µm), nano- (2-20 µm) and pico- (<2 µm) phytoplankton, retrieved through the determination of the composition and concentration of the cell's pigmentary content by the High Pressure Liquid Chromatographic technique.

In order to fix the contribution of each Phytoplankton Size Classes to the Total Chlorophyll a (TChl a, which is the sum of Chlorophyll *a*, its allomers and epimers, Divinyl-chlorophyll *a* and Chlorophyllid *a*), the Vidussi et al. (2001) method has been selected for the definition of size's structure indices, based on the taxonomic meaning of several accessory pigments determined, together with TChl a, by HPLC technique. Vidussi and her collaborators identified from previous works (Gieskes et al., 1988; Goericke and Repeta, 1993; Claustre and Marty, 1995), seven principal Diagnostic Pigments ($\boldsymbol{DP}$, see table 2.1)

with taxonomic meaning, which are able to outline the size structure of the whole community. "$\sum \boldsymbol{DP}$" is the sum of all seven $\boldsymbol{DP}$ concentrations (mg m^{-3}):

$$\sum DP = [Zea] + [TChlb] + [Allo] + [19'\,Hex\text{-}fuco] + \\ + [19'\,But\text{-}fuco] + [Fuco] + [Peri] \quad (1)$$

Diagnostic Pigments	Abbreviations	Taxonomy	PSCs
Fucoxanthin	Fuco	Diatoms	Micro (> 20 µm)
Peridinin	Peri	Dinoflagellates	Micro (> 20 µm)
19'-hexanoyloxyfucoxanthin	19' Hex-fuco	Chromophytes and nanoflagellates	Nano (2-20 µm)
19'-butanoyloxyfucoxanthin	19' But-fuco	Chromophytes and nanoflagellates	Nano (2-20 µm)
Alloxanthin	Allo	Cryptophytes	Nano (2-20 µm)
Chlorophyll *b* + divinyl-chlorophyll *b*	TChl*b*	Green flagellates and prochlorophytes	Pico (<2 µm)
Zeaxanthin	Zea	Cyanobacteria and prochlorophytes	Pico (< 2 µm)

Table 2.1 Diagnostic Pigments used in this work and their reference taxonomic and size classes (Vidussi et al., 2001; Uitz et al., 2006).

The biomass fraction (f) associated with each size class is defined as:

$$\boldsymbol{f_{pico}} = ([Zea] + [TChlb])/\sum DP \quad (2)$$

$$\boldsymbol{f_{nano}} = ([Allo] + [19'\,Hex\text{-}fuco] + [19'\,But\text{-}fuco])/\sum DP \quad (3)$$

$$\boldsymbol{f_{micro}} = ([Fuco] + [Peri]/\sum DP \quad (4)$$

In Vidussi et al. (2001) $\sum DP$ is considered a valid estimator of TChl a, thanks to a significant linear dependence relationship founded between the two parameters. However they assumed an equal weight of each diagnostic pigment to TChl a, not taking into account the variation in the $\sum DP/TChla$ ratio due to different species and physiological states (Vidussi et al, 2001).

In order to obtain a more accurate quantification of each size class in terms of TChl a, Uitz et al. (2006), following the previous work of Gieskes et al. (1988), carried out a multiple

regression analysis between [TChl a] and the concentrations of the most important accessory pigments. They provided the best estimates of the seven "Total Chlorophyll a - diagnostic pigments" ratios ($TChla/DP$) for a global data set:

$$TChl = 0.86[Zea] + 1.01[TChlb] + 0.60[Allo] + 1.27[19'\,Hex\text{-}fuco] + \\ +0.35\left[19'\,But\text{-}Fuco\right] + 1.41[Fuco] + 1.41[Peri] \quad (5)$$

Therefore, according to Uitz et al. (2006), the fractions of the Total Chlorophyll a concentration associated with each of the three phytoplanktonic classes are:

$$\boldsymbol{f_{pico}} = (0.86[Zea] + 1.01[TChlb])/TChla \quad (6)$$

$$\boldsymbol{f_{nano}} = (0.60[Allo] + 1.27[19'\,Hex\text{-}fuco] + 0.35[19'\,But\text{-}fuco])/TChla \quad (7)$$

$$\boldsymbol{f_{micro}} = (1.41[Fuco] + 1.41[Peri]/TChla \quad (8)$$

In this study, these relationships have been applied to a Mediterranean subset of the SeaBASS HPLC pigment dataset (Werdell & Bailey, 2005) (fig. 2.1) to obtain *in-situ* concentrations of TChl a of each PSCs (biomass size fractions) for the validation and/or calibration of the algorithms selected, to identify the algorithm that better performs the optical and biological properties of the Mediterranean Sea. I take into account the whole complete *in-situ* data for the first 40 m of the water column. The statistical analysis for this work are performed by the IDL scientific programming language. The softwares used in support for graphic representation of the PSCs data are Origin, Past and Excel.

It should be noted, as reported previously by Vidussi et al. (2001), that the phytoplankton grouping based on the auxiliary pigments concentration does not strictly reflects the true phytoplankton size. This is because in the same taxonomic class there are species of different dimensions, that may be enclosed in more than one size classes. The same may occur in a single species at different stages of growth. Moreover, some taxonomic pigments may be present in small concentrations in other minor groups. Nevertheless, several investigations about the typical off shore composition of phytoplankton Mediterranean community have proven the validity of this approach (Siokou-Frangou et al., 2009; Vidussi et

al.,2001). In particular, using a method based on the diagnostic pigment's identification and quantification for the determination of the PSCs, it is important to consider that "micro" takes in Diatoms and Dinoflagellates in general, nano- includes all the Cryptophytes, nanoflagellates and Chromophytes and pico- phytoplankton is referred to Cyanobacteria, green tiny flagellates and Prochlorophytes (tab. 2.1).

2.a.2 SeaBASS Mediterranean *in-situ* data for the algorithms validation

The seven diagnostic pigments data used for the determination of the in-situ PSCs (fucoxanthin, peridininn, 19'-exanoyloxyfucoxanthin, 19'-butanoyloxyfucoxanthin, Alloxanthin, Total Chlorophyll *b* and Zeaxanthin), required for the algorithm validation, come from a Mediterranean subset of the SeaBASS HPLC pigments in-situ dataset (Werdell, & Bailey, 2005). This is a large HPLC pigment database. Data were collected in different cruises and in periodical activities of fixed mooring monitoring. In particular this subset consist of data from Propose cruise (1999, September - October), Boussole mooring (with sampling activities nearly every month from 2001 to 2006 and only in July for the 2008) and Boum cruise (2008, July). It includes stations sampled in case 1 waters in various trophic conditions. Figure 1 shows the location of the whole SeaBASS Mediterranean *in-situ* measurements.

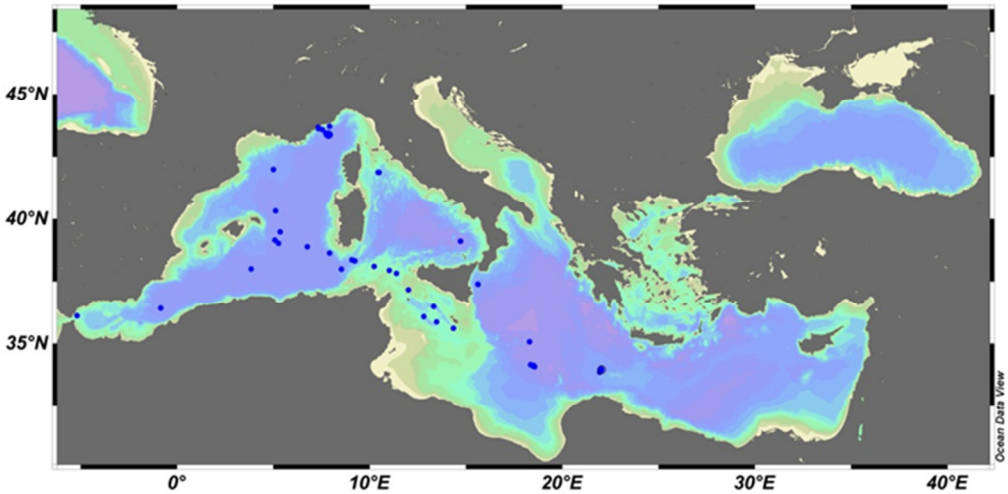

Figure 2.1 SeaBASS Mediterranean *in-situ* data used for the Algorithms validation

The field samples, collected by several teams, were analyzed in different laboratories using a variety of HPLC instruments and protocols, followed by a quality assurance process from SeaBASS. However, the different methodologies need to be taken into account for a coherent combination of the data sets.

The method of Vidussi et al. (2001), revisited by Uitz et al. (2006) has been applied on these pigments data for the determination of the phytoplanktonic biomass size fractions.

2.a.3 WMED-BIOOPT2012 Cruise: Sardinian Sea PSCs data

Particle size classes and taxonomy community composition were also investigated in the Sardinian Sea (fig. 2.2) during spring from *in-situ* collected data. WMED-BIOOPT2012 Cruise was conducted from 23/03/2012 to 09/04/2012.

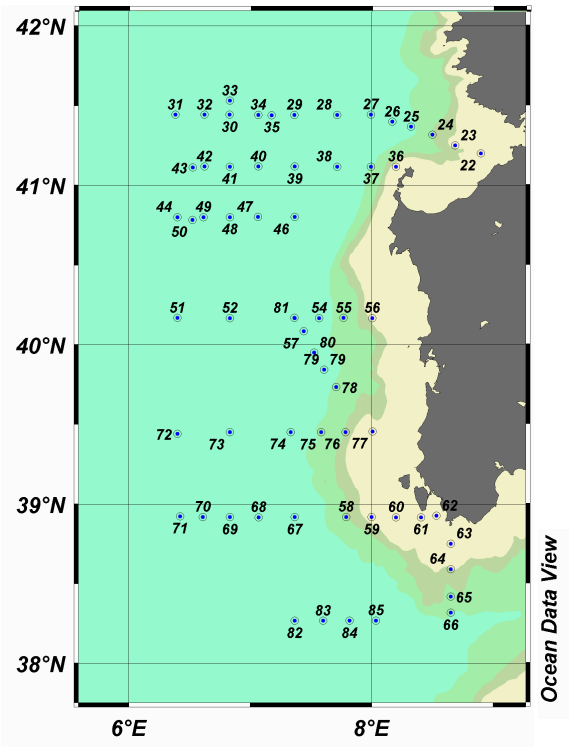

Figura 2.2 WMED-BIOOPT 2012 sampling map

Biological and physical ancillary parameters were collected in 100 stations using a SeaBird SBE911 plus Conductivity Temperature Depth (CTD) profiler equipped with a Sea Teach fluorometer. Maximum profiling depth reached 300 m.

Water samples for pigments determination were collected using a rosette Niskin bottle system at 65 stations, at three fixed depths of 2 m, 10 m and 25 m, taking into account the first optical depth at which the spectroradiometer satellite sensors can penetrate. Seawater from Niskin was pre-filtered by a planktonic net of 250 µm to remove zooplancton and macroalgae and stored in dark bottles. Known volumes of this water (from 1 to 4 L) were filtered using 25 mm GF/F Whatman glass fiber filters, with vacuum pressure lower than -25 KPa to preserve the integrity of the phytoplanktonic cells (Lazzara et al., 1990). The filters were collected in vials and stored in liquid nitrogen until the start of analysis, when they were frozen at -80°C. The pigments analysis (see table 2.2) were performed by High Pressure Liquid Chromatography (Varian system, with a C18 column). The method used in this work is a modified version (JFGOFS, 1994) of the UNESCO reference technique (Wright et al., 1991). The samples were extracted in 3 mL of methanol, sonicated for 20 minutes and conserved for 24h at 4°C. Pigments were detected from a detector UV-VIS 9050. The HPLC system was calibrated using pigments standard (DHI), as recommended by the Scientific Committee on Research, U. N. Educational, Scientific and Cultural Organization (UNESCO).

Pigments	Taxonomy	PSCs
Total Chlorophyll *a*	All	
Fucoxanthin	Diatoms	Micro (> 20 µm)
Peridinin	Dinoflagellates	Micro (> 20 µm)
19'-hexanoyloxyfucozanthin	Chromophytes and nanoflagellates	Nano (2-20 µm)
19'-butanoyloxyfucoxanthin	Chromophytes and nanoflagellates	Nano (2-20 µm)
Alloxanthin	Cryptophytes	Nano (2-20 µm)
Chlorophyll *b* + divinyl-chlorophyll *b*	Green flagellates and prochloro-phytes	Pico (<2 µm)
Zeaxanthin	Cyanobacteria and prochlorophytes	Pico (< 2 µm)

Table 2.2 Pigments detected with the HPLC from the WMED-BIOOPT2012 samples

These data were used to understand the phytoplankton community composition in the surface layer of the sea. To estimate the principal phytoplanktonic classes up to the Deep Chlorophyll Maximum (DCM) depth, the Hirata et al., (2009) algorithm was applied to the fluorescence profiles, calibrated to the Total Chlorophyll *a* in the all stations. This data were compared with Satellite phytoplankton size classes estimate, relative to the same period, to understand the effective potential and utility of the remote observation in the phytoplankton ecology.

The software used for the cruises data visualization is Ocean Data View 4. Data were interpolated by the Diva gridding.

2.b Optic methods and satellite measurements

2.b.1 Measuring the size from space: selected methods

• Brewin et al. (2010/2011) algorithm

The Brewin et al. (2010/2011) algorithm is a three component model of PSCs based on an empirical relationship observed between phytoplankton absorption at 443 nm and the Total Chlorophyll a. This algorithm is an extension of the Sathyendranath et al. (2001) and Devred et al. (2006) algorithms.

Understood the existence of a close relation between phytoplankton absorption and Total Chlorophyll a concentration, Sathyendranath and her collaborators tried to find the equation that better describes this relationship for parameterize the phytoplankton absorption (Sathyendranath et al., 2001) (fig. 2.3).

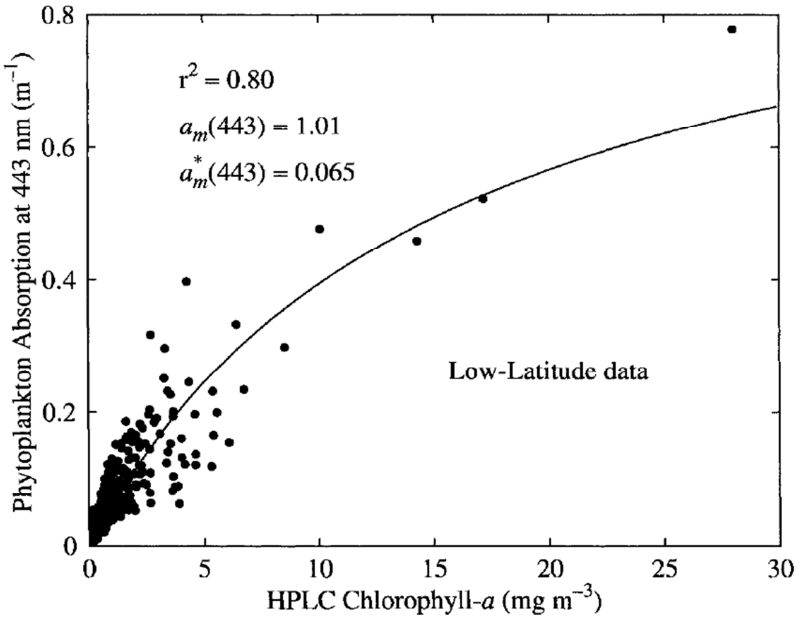

Figure 2.3 Absorption vs pigment data in a first test-fit of the Michaelis–Menten equation to the *in-situ* data (from Sathyendranath et al., 2001).

Thanks to the great differences in the optical properties and in the efficiency of harvesting light between the small and large phytoplankton cells (Chisholm, 1992; Raven, 1998; Basset et al., 2009), Sathyendranath and collaborators fitted Chlorophyll *a* concentrations versus phytoplankton absorption coefficients, derived from a dataset collected in various cruises developed both at high and low latitudes (e.i fig. 2.3) and obtained an exponential fit function. The underlying assumption is that TChl a concentration (C) is the sum of the concentrations of two distinct in size phytoplankton populations, one "small" (C_1), with an higher absorption coefficient and the other "large" (C_2), with a lower specific absorption coefficient. They parameterized the concentration of the first population (C_1), as a function of the total concentration (C),

$$C_1 = C_1^m[1 - exp(-S_1 C)] \tag{9}$$

C_1^m and S are the asymptotic maximum values and the initial slope respectively of the best fit equation.

The concentration of the second population is easily derived:

$$C_2 = C - C_1 \tag{10}$$

Brewin et al. (2010) extended this work to three size classes of phytoplankton populations. The TChl a concentration (C) is decomposed as the sum of pico- (C_1), nano- (C_2) and micro- phytoplankton (C_3) TChl a concentrations:

$$C = C_1 + C_2 + C_3 \tag{11}$$

Following Devred et al. (2006), Brewin et al. (2010) assumed that the large cells population is represented by micro-phytoplankton (C_3), and the small cells population $(C_{1,2})$ is the sum of the nano- and pico-phytoplankton. So the Sathyendranath et al. (2001) model becomes, for three components:

$$C_{1,2} = C_{1,2}^m\left[1 - exp\left(-S_{1,2}C\right)\right] \tag{12}$$

$$C_1 = C_1^m[1 - exp(-S_1 C)] \quad (13)$$

where $C_{1,2}^m$ and C_1^m, are the asymptotic maximum values for the dependent variables $C_{1,2}$, C_1, and $S_{1,2}$ and S_1 represent their initial slope respectively of the Sathyendranath et al. (2001) best fit equation.

So, it is simple to derive C_2 and C_3:

$$C_2 = C_{1,2} - C_1 \quad (14)$$

$$C_3 = C - C_{1,2} \quad (15)$$

These algorithms and their fixed parameters (Table 2.3) are derived from a global dataset of TChl a measures.

Using equations (13), (14) and (15), dividing for C, we obtain the fractions of each size classes (micro- nano- and pico- phytoplankton) expressed in terms of absolute values respect to the TChl a.

Population	Maximum C for given population	Initial slope
Nano- + Pico- phytoplankton	*0.775 mgm^{-3}* ($C_{1,2}^m$)	*1.152* ($S_{1,2}$)
Pico- phytoplankton	*0.146 mgm^{-3}* (C_1^m)	*5.118* (S_1)

Table 2.3 Parameters used in eq. (2) and (3) (from Brewin et al., 2011)

• Hirata et al. (2011) algorithm

Hirata et al. (2011) found a synoptic relationship between diagnostic pigments concentration representative of the PSCs and Total Chlorophyll a concentration (fig. 2.3).

They applied the Diagnostic Pigment Analysis (DPA), originally proposed by Vidussi et al. (2001) and modified by Uitz et al. (2006), to a global HPLC pigments dataset, to determine the relative abundance of each size classes respect to the satellite derived TChl a:

$$\boldsymbol{Micro} = [0.9117 + exp(-2.7330 * x + 0.4003)]^{-1} \quad (16)$$

$$\boldsymbol{Nano} = [1 - Micro - Pico] \quad (17)$$

$$\boldsymbol{Pico} = -[0.1529 + exp(1.0306 * x - 1.5576)]^{-1} - 1.8597 * x + 2.9954 \quad (18)$$

where x is the $log_{10}(Chl\ a)$.

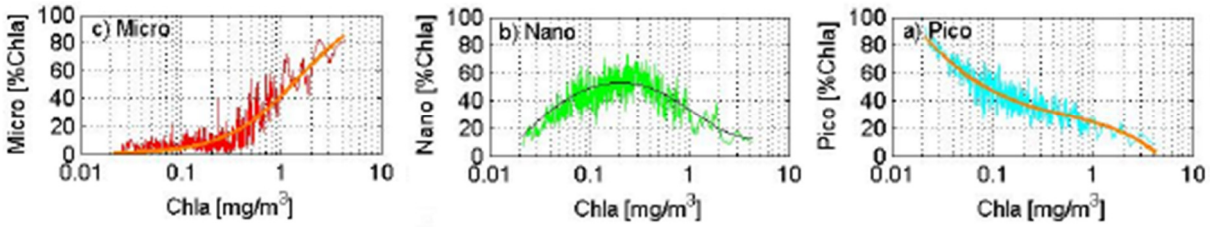

Figura 2.3 Hirata PSCs algorithms versus a global HPLC dataset (from Hirata et al., 2011)

Using the technique of DPA, Hirata and his collaborators derived also empirical algorithm for a several taxa associated to a specific Phytoplankton Functional Types (PFTs, see table 2.4).

PSCs/PFTs	Diagnostic Pigments	Estimation Formula
Microplankton (>20 µm)*[1]	Fucoxanthin **(Fuco)**, Peridinin **(Peri)**	1.41 (Fuco+Peri)/ TChl *a* *[2]
Diatoms	**Fuco**	1.41 Fuco/ TChl *a* *[2]
Dinoflagellates	**Peri**	1.41 Perid/ TChl *a* *[2]
Nanoplankton (2-20 µm)*[1]	19'Hexanoyloxy-fucoxanthin **(19'Hex)** Total Chlorophyll-*b* **(TChl-*b*)** 19'Butanoyloxy-fucoxanthin **(19'But)** Alloxanthin **(Allo)**	(X_n*1.27 19'Hex + 1.01 TChl *b* + 0.35 19'But + 0.60 Allo)/ TChl *a* *[3]
Green algae	**TChl *b***	1.01 TChl-*b*/ TChl *a* *[2]
Prymnesiophytes*[4] (Haptophytes)	**19'Hex, 19'But**	Nano – Green algae *[4]
Picoplankton (0.2-2 µm)*[1]	Zeaxanthin **(Zea)**, **19'Hex**, **TChl *b***	(0.86 Zea + Y_p 1.27 Hex)/ TChl *a* *[3]
Prokaryotes	**Zea**	0.86 Zea/ TChl *a* *[2]
Pico-eukaryotes	**19'Hex**, **TChl *b***	Pico – Prokaryotes
Prochlorococcus sp.	Divinyl Chlorophyll *a* **(DVChl *a*)**	0.74 DVChl- *a* /TChl *a*

*[1] Sieburth et al. (1978)
*[2] TChl *a* = 1.41 Fuco + 1.41 Perid + 1.27 Hex + 0.6 Allo + 0.35 But + 1.01 Chl-*b* + 0.86 Zea = Chl-*a* (Uitz et al., 2006)
*[3] X_n= proportion of nanoplankton contribution in 19'Hex; Y_p = proportion of picoplankton in 19'Hex, (Brewin et al., 2010).
*[4] The contributions of Allo to nanoplankton were only a few percent in Hirata et al. (2011) data set, so Haptophytes were approximated to Nano minus Green Algae.

Table 2.4. PSCs and PFTs represented by the combination of diagnostic pigments (from Hirata et al. 2011)

The work by Hirata and collaborators allows to understand the contribution of some of the main "taxonomic classes" of the phytoplankton to the Total Chlorophyll a. In particular,

they determine the singular contribution of Diatoms and Dinoflagellates to the Total micro-size biomass fraction. The empirical algorithms retrieved from their global dataset are:

$$\boldsymbol{Diatoms} = [1.3272 + exp(-3.9828 * x + 0.1953)]^{-1} \quad (19)$$

$$\boldsymbol{Dinoflagellates} = [Micro - Diatoms] \quad (20)$$

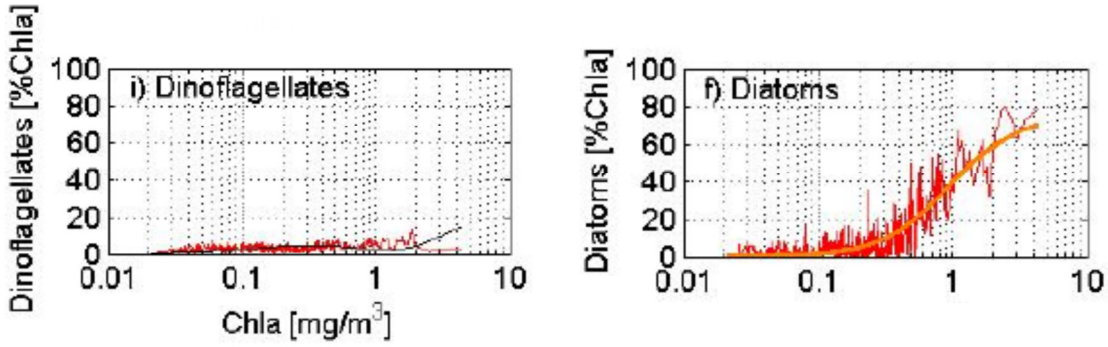

Figura 2.4 Hirata Diatoms and Dinoflagellates algorithms versus a global HPLC dataset (from Hirata et al., 2011)

• Kostadinov et al. (2009) algorithm

Kostadinov et al., (2009) developed a bio-optical algorithm based on the particle backscattering coefficient spectrum retrieved from ocean color observations, in particular from the normalized water-leaving radiances, following Loisel et al., (2006) model.

The particle size distribution (PSD) in the ocean surface has been found to follow the Junge-type power law size distribution (Junge, 1963; Kostadinov et al., 2009):

$$\boldsymbol{N(D)} = N_0 \left(\frac{D}{D_0}\right)^{-\xi} \quad (21)$$

where *N(D)* is the number of particles per volume of seawater normalized by the size bin width, *D* is the particle diameter, D_0 is a reference diameter (2 µm), N_0 is the particle differential number concentration at D_0 , and ξ is the Junge slope of the PSD. The Junge slope, ξ, and the reference abundance, N_0, are the two unknown parameters of the Junge-type size distribution. Kostadinov and collaborators estimated the parameters of the power law PSD (ξ and N_0) as a function of the particulate backscattering spectrum from Mie theory,

deriving the backscattering coefficient from the spectrum of satellite-observed normalized water-leaving radiance, analytically and empirically related (Gordon et al., 1988; Reynolds et al., 2001; Kostadinov et al., 2007).

Applying Mie theory, the backscattering efficiency of an individual particle (Q_{bb}) is a function of light wavelength in vacuum (λ), the diameter of the particle itself (D) and the particle's "complex index of refraction" relative to the medium (m). The backscattering properties of the total assemblage (b_{bp}) will be the sum of all particles' efficiencies multiplied by the respective cross-sectional area of all particles of a given size:

$$b_{bp}(\lambda) = \int_{D_{min}}^{D_{max}} \frac{\pi}{4} D^2 Q_{bb}(D, \lambda, m) N_0 \left(\frac{D}{D_0}\right)^{-\xi} dD \qquad (22)$$

The equation (22) provides the link between satellite measurable optical properties, namely, the spectral particle backscattering coefficient, and the parameters of the assumed underlying power law PSD (ξ and N_0). Kostadinov et al., (2009) performed Monte Carlo simulation to establish an operational relationship between $b_{bp}(\lambda)$ and the PSD parameters.

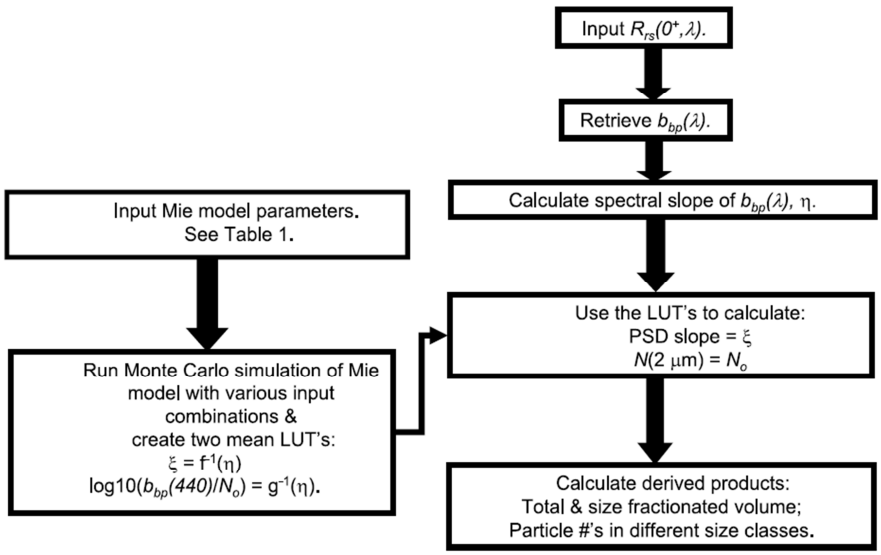

Figure 2.5 Flow diagram of the operational steps of this backscattering based method (from Kostadinov et al., 2009)

The total number of particles per unit volume of seawater in a given size range can be found by integrating equation (1) from a minimum size, D_{min}, to a maximum size, D_{max},

partioning the PSD into distinct classes. In this work has been used the Sieburth et al., (1978) classification of phytoplankton in pico-, nano- and pico-size particles.

2.b.2 Satellite "input" data for the three algorithms

All the satellite data used in this study as input for the three algorithms were obtained in scientific format (HDF and/or NetCDF) and was processed with original programs written in IDL language. Mediterranean climatological maps based on the SeaWIFS era period (1998-2010) were produced for the all parameters investigated for this study.

• Brewin et al. (2010/2011) and Hirata et al. (2011): case 1 – case 2 merged Chl a

Ten years (from 2 January1998 to 10 December 2010) of daily SeaWiFS Chlorophyll a estimates were used as input for Brewin et al. (2010/2011) and Hirata et al. (2011) algorithms. These data were downloaded from the MyOcean Ocean Colour Thematic Assembling Centre (MyOcean OC TAC). The specific product used, case 1 - case 2 merged Chlorophyll (Chl1,2), takes into account the different optical properties of the offshore and inshore waters. So two different algorithms were applied on the reflectance: the MedOC4 algorithm (Volpe et al., 2007) for the case 1 waters and the Ad4 (Berthon and Zibordi, 2004) for the case 2.

The exact identification of the two water types is performed by taking into account the whole light spectrum from blue to NIR bands for both two water types from in situ data (D'Alimonte et al., 2003). For the waters with intermediate features, a weighted average of the two former algorithms were applied, based on the distance between the actual reflectance spectrum and the two reference reflectance spectra for the case 1 and 2 waters respectively [3].

According to Morel and Berthon (1989), satellite Ocean Color products are representative of the "surface" layer, defined as having a thickness corresponding to one attenuation length with respect to PAR. This surface layer corresponds to 1/5 of the euphotic depth (Ze), understood, in its operative definition, as the depth where the downwelling PAR irradiance is reduced to 1% of its value at the surface. Taking into account the role of the

entire euphotic zone in the phytoplankton ecology, in this study the bio-optical model of Morel and Berthon (1989) has been applied to estimate the concentration of the Chlorophyll *a* over the Ze. This model categorized the profiles into seven trophic situations and computed a mean vertical profile for each, according to surface Chlorophyll *a*. The basis of this approach are the highly significant relationships between the pigment content of the euphotic layer and the relative Chlorophyll *a* concentration within the first penetration depth (founded by the analysis of 4000 Chlorophyll *a* vertical profile).

Following this model, estimates of TChl *a* data have been produced and used as input for the Brewin model. So, together with micro- nano- and pico- fraction of "surface" TChl *a*, with the Brewin algorithms has been estimated the same type of data also over Ze.

• Kostadinov et al. 2009: remote sensing reflectance (Rrs)

The input data used for the Kostadinov et al.(2009) algorithm are daily SeaWiFS remote sensing reflectances at 412, 443,490, 510 and 555 nm, operationally produced by the Group for Satellite Oceanography (GOS-ISAC) of the Italian National Research Council, in Rome, for the entire SeaWIFS era. These products are derived from standard processing. The Rrs is the ratio of upwelling radiance to down-welling irradiance at each wavebands considered. It can also be expressed as the ratio of normalized water leaving Radiance (nLw) and the extra-terrestrial solar irradiance (F0). Raw data are routinely processed up to Level-3 with the SeaWiFS Data Analysis System (SeaDAS) software package available from NASA website [4] (Volpe et al., 2012).

The Group for Satellite Oceanography (GOS) collects raw data Near Real Time and when the ancillary data are available perform the processing of the Delayed Time product, in which standard masking criteria for detecting clouds or other contamination factors are routinely applied, as for land, cloud, sun glint, atmospheric correction, high total radiance, large solar zenith angle (70 deg), large spacecraft zenith angle (56deg), coccolithophorids, negative water leaving radiance, and normalized water leaving radiance at 555 nm 0.15 Wm^{-2} sr^{-1} (McClain et al., 1995). These products are remapped at 1 km spatial resolution using cylindrical equi-rectangular projection [5].

2.b.3 Sea Surface Temperature (SST) data

For the sea surface temperature (SST) study, the AVHRR (Advanced Very High Resolution Radiometer) Pathfinder Version 5.2 (PV5.2) data were used, obtained from the US National Oceanographic Data Center (NODC) and the Group for High Resolution Sea Surface Temperature (GHRSST). The data has been provided at level 3 with a spatial resolution of 4 Km.

The PV5.2 project is the latest reanalysis of the AVHRR data, developed by the University of Miami's Rosenstiel School of Marine and Atmospheric Science (RSMAS) and the NOAA (National Oceanographic Data Center) NODC. This project was supported in part by a grant from the NOAA Climate Data Record (CDR) Program for satellites [6]. The PFV5.2 data are an updated version of the Pathfinder Version 5.0 and 5.1 collection described in Casey et al. (2010). Multichannel sea surface temperature (SST) products have been constructed operationally from the five and six channel of the (AVHRR) by NOAA's National Environmental Satellite. Pathfinder data comes from different NOAA satellites, NOAA-14 (1/22/95 – 10/11/2000), NOAA-16 (10/12/00 -12/31/02), NOAA-17 (01/01/03 – 06/04/05), and NOAA-18 (06/05/05 – 12/31/09) satellites.

2.b.4 MODIS data for the WMED-BIOOPT 2012

Contemporary with the *in-situ* sampling of the WMED-BIOOPT 2012 cruise satellite images of TChl *a* have been processed. Ocean Color MODIS data for this work were downloaded directly by the NASA website [7] at level L1A (Level L1A data products in MODIS contain the raw radiance counts, spacecraft and instrument telemetry and calibration data). Data processing was carried out by the SeaDAS utility, an image analysis package for the processing, display, analysis, and quality control of ocean color data, supplied by the same NASA [4]. The processing consists of 4 steps:

- step 1: generation of a separated Geo-file that contains the navigation data for the geolocation;
- step 2: L1B data are generated. These files contain the calibrated at-aperture (top-of-atmosphere) radiances and are used to produce L1A products;

- step 3: generation of the L2 TChl *a* product applying MedOC3 algorithm (Santoleri et al., 2008), that contains geophysical values data for each pixel, derived from the L1B radiances by applying atmospheric corrections, and bio-optical algorithms. L2 product data are geolocated data;
- step 4: geophysical parameters contained in the L2 product were remapped onto a cylindrical projection. For each of them were created a data file and a thematic map to display the data.

Hirata et al., 2009 algorithm has been applied to these TChl *a* data to obtain information on the phytoplankton PSCs and on the Dinoflagellates and Diatoms component. Results are compared with the in-situ measurements.

3. RESULTS

3.a Validation of the PSCs algorithms

3.a.1 Models versus *in situ* data

For the validation and/or calibration of the two abundance based algorithms (Hirata et al., 2011 and Brewin et al., 2010/2011), I have used TChl *a* data obtained from *in situ* data only, rather than directly validate satellite estimate. This procedure is usually applied for algorithms validation, in order to separate error components due to the models itself from other sources of error due to atmospheric correction or satellite chlorophyll algorithms.

Fig. 3.1 and 3.2 describe the matching between the size-specific fraction of Total Chlorophyll *a* concentration derived from in-situ diagnostic pigments versus the PSCs obtained by the Brewin and Hirata models respectively. Both algorithms show a general better qualitative performance when applied to the Mediterranean SeaBASS subset (fig. 3.1 and 3.2 on the right, respectively) respect to the original global case study (fig. 3.1 and 3.2 on the left, respectively).

In particular, for the Mediterranean dataset, the plots indicate that Hirata et al. (2011) underestimate the micro-phytoplankton (Figure 3.2, a) and slightly overestimate the pico-phytoplankton (Figure 3.2, c). Instead, a good agreement is pointed out between the Hirata model and the nano size class (Figure 3.2, b). Brewin et al. (2010/2011), on the other hand, performs better the micro-component (Figure 3.1, a) but underestimates slightly the pico-phytoplankton at low TChl *a* value (Figure 3.1, d) and strongly the whole nano component (Figure 3.1, c), compared with the Hirata algorithm. So, both abundance models show either strengths or weaknesses for the Mediterranean Sea.

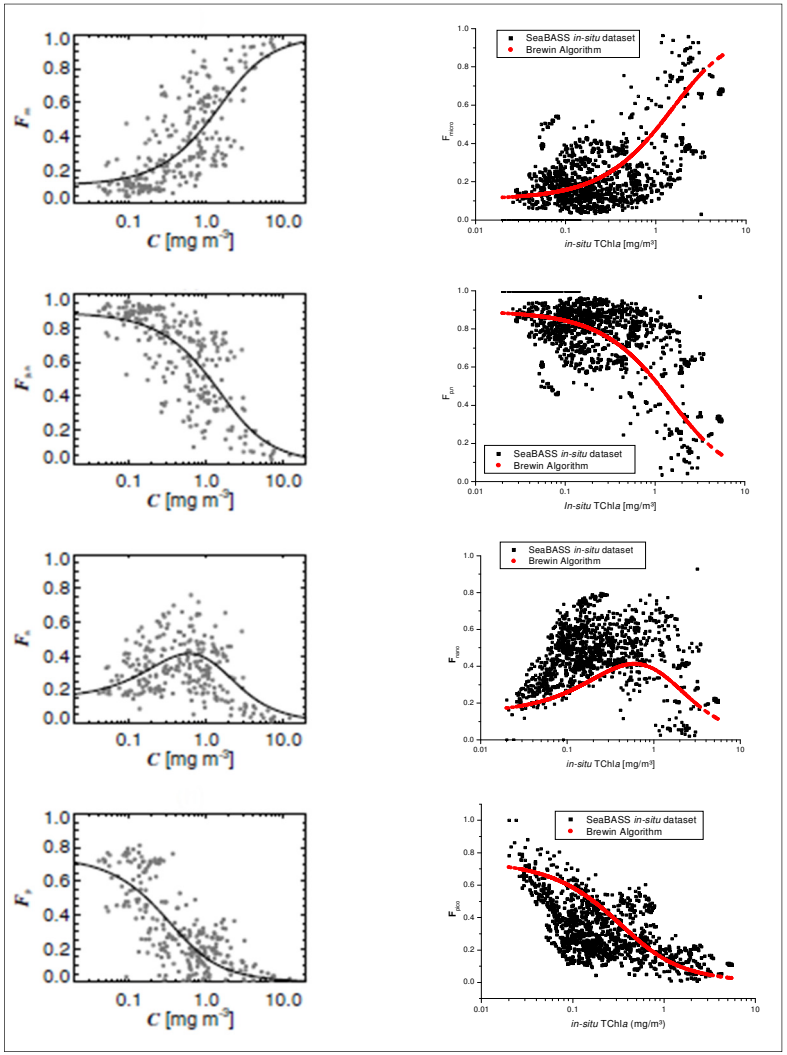

Figure 3.1 Brewin model versus PSCs from in-situ measures (global dataset on the left, from Brewin et al, 2011, Mediterranean SeaBASS dataset on the right) for micro (a), nano&pico (b), nano (c) and pico (d) phytoplankton.

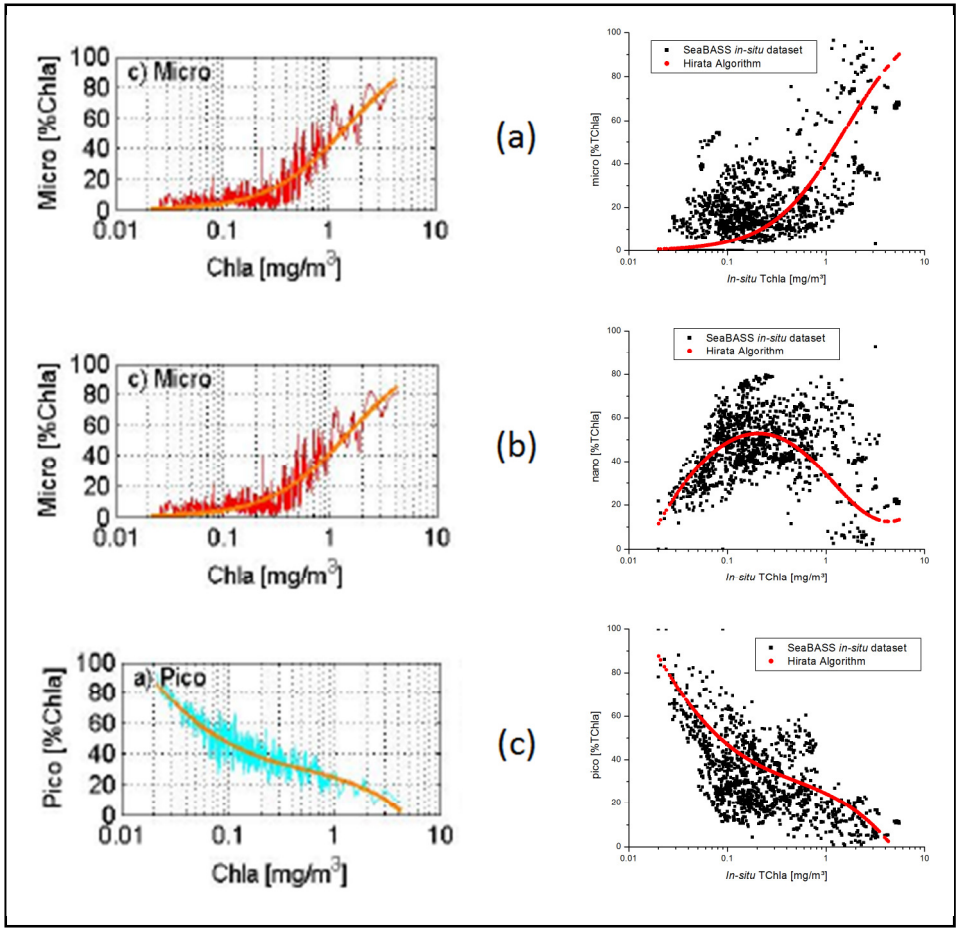

Figure 3.2 Hirata model versus PSCs from in-situ measures (global dataset on the left, from Hirata et al, 2011, Mediterranean SeaBASS dataset on the right) for micro (a), nano (b) and pico (c) phytoplankton.

3.a.2. Mediterranean determination of pigment coefficients

The Uitz et al. (2006) equations, used in this first step to determine the TChl a fraction of each PSCs from *in-situ* data pigments, are based on a multiple regression analysis applied on a global dataset.

Gieskes and his collaborator in the 1988 carried out a multiple regression analysis of the concentrations of Chlorophyll *a* and the principal accessory pigments that they founded in their samples. The partial slopes of such regressions provided the best estimates of the Chlorophyll *a* to these diagnostic pigments ratios (for the data set considered). Uitz et al., (2006) applied this approach to the three specific size-groupings proposed by Vidussi et al. (2001) on a Global pigments database. To better test the performances of the Brewin and Hirata models, following Uitz et al., (2006) I applied the Geskies approach to the SeaBASS Mediterranean Pigments sub-set, performing a new multiple regression analysis to evaluate whether different pigmentary composition of the Mediterranean phytoplankton community can occur (fig 3.3). The analysis were carried out on 1017 individual samples, where Total Chlorophyll *a* and all the seven selected biomarker pigments were available at the same time. The new coefficients (Wp) are given in Table 3.1, with their standard deviation.

Pigments Biomarker	Uitz coefficients	New coefficients (Wp)	Wp Standard deviation
Fuco	1.41	1.740	0.015
Peri	1.41	1.172	0.119
19' Hex-fuco	1.27	0.861	0.021
19' But-fuco	0.35	0.405	0.138
Allo	0.60	2.088	0.085
TChl *b* *	1.01	1.624	0.076
Zea	0.86	1.999	0.089

Table 3.1 - Comparison between Uitz et al. 2006 global coefficients and new Mediterranean coefficients with their standard deviation for the in-situ determination of PSCs.

On the basis of this analysis, the best estimates of the seven "Total Chlorophyll a - diagnostic pigments" ratios ($TChla/DP$) for a Mediterranean data set is:

$$TChla = 1.999[Zea] + 1.624[TChlb] + 2.088[Allo] + 0.861[19'\ Hex\text{-}fuco] + 0.405[19'\ But\text{-}Fuco] + 1.74[Fuco] + 1.172[Peri] \quad (1)$$

and the new algorithms for the determination of the contribution of each PSCs to the TChl *a* are:

$$\boldsymbol{f_{pico}} = (1.999[Zea] + 1.624[TChlb])/TChla \quad (2)$$

$$\boldsymbol{f_{nano}} = (2.088[Allo] + 0.861[19'\ Hex\text{-}fuco] + 0.405[19'\ But\text{-}fuco])/TChla \quad (3)$$

$$\boldsymbol{f_{micro}} = (1.74[Fuco] + 1.172[Peri]/TChla \quad (4)$$

The coefficient of determination (r^2) between the SeaBASS *in-situ* Total Chlorophyll *a* and that estimated with the new coefficients (Cw) is 0.99, with a p-value < 0.001.

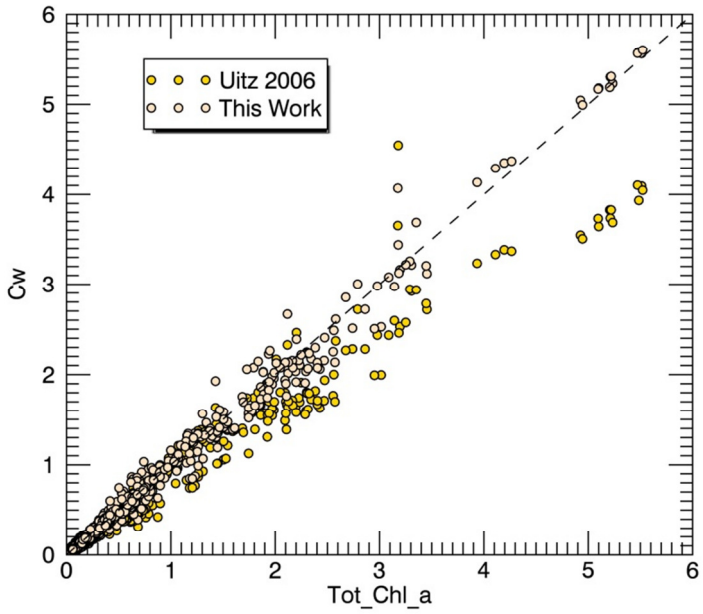

Figure 3.3 Comparison between Total Chl *a* calculated from Uitz coeffcients and from new ones versus SeaBASS in situ Total Chl *a*

The match between the two models considered and the in-situ PSCs improves when these new algorithms are applied to the Mediterranean SeaBASS *in-situ*. This points out a better performance of Brewin algorithm than Hirata for all Phytoplankton dimensional classes (Figure 3.3).

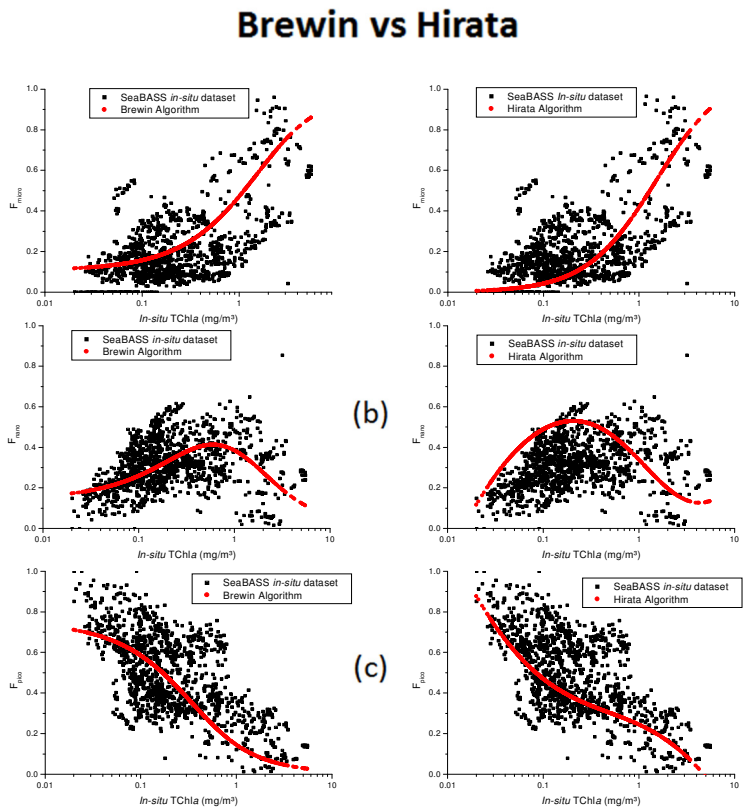

Figure 3.4 Brewin (on the left) and Hirata (on the right) models versus PSCs obtained applying recalculated coefficients on the Mediterranean SeaBASS in-situ measures for micro (a), nano (b) and pico (c) phytoplankton.

These considerations are supported by basic statistical analysis parameters: Mean Bias Error (MBE), Root Mean Square Error (RMSE) and Pearson correlation coefficient (R),

$$MBE = \frac{\sum_{i=1}^{N}(x_i - y_i)}{N}$$

€

$$RMSE = \sqrt{\frac{\sum_{i=1}^{N}(x_i - y_i)^2}{N}}$$

$$R = \frac{\sum_{i=1}^{N}(x_i - \bar{x})(y_i - \bar{y})}{\sqrt{\sum_{i=1}^{N}(x_i - \bar{x})^2}\sqrt{\sum_{i=1}^{N}(y_i - \bar{y})^2}}$$

€

where x_i represents the PSCs estimated by the model, y_i the PSCs estimated by Diagnostic Pigments, N is the total number of the matchup data and the bar indicates the arithmetic average (R is dimensionless, MBE and RMSE have the same dimension of x and y). These parameters were calculated for Brewin and Hirata models both with old (Uitz et al., 2006) that new coefficients (Table 3.2 and 3.3).

	Mean Bias Error				Root Mean Square Error			
	Brewin (Uitz)	Brewin (new)	Hirata (Uitz)	Hirata (new)	Brewin (Uitz)	Brewin (new)	Hirata (Uitz)	Hirata (new)
F_{micro}	0.0411	**0.0525**	-0.0549	-0.0435	0.1517	**0.1523**	0.1697	0.1634
F_{nano}	-0.1602	**-0.0088**	-0.0221	0.1293	0.2118	**0.1128**	0.1384	0.1902
F_{pico}	0.1191	**-0.0437**	0.0770	-0.0858	0.2065	**0.1727**	0.1526	0.1728

Table 3.2 – Mean bias Error and Root Mean Square Error between PSCs obtained by the models and PSCs from Diagnostic Pigments calculated for Brewin and Hirata models with old (Uitz et al., 2006) and new coefficients ("+" represents overestimation, "-" underestimation).

MBE and RMSE show that the in situ PSCs obtained with the new coefficients performs better with the Brewin model than with Hirata. Furthermore, the error for the Brewin model versus the PSCs with new coefficients is more uniform and reasonable for the whole dimensional classes than the error obtained from Brewin and Hirata models with the old coefficients (Table 3.2).

Pearson Correlation Coefficient (R)		
	Brewin (Uitz)	Brewin (Us)
F_{micro}	0.6185	**0.6329**
F_{nano}	0.3722	**0.3912**
F_{pico}	0.5469	**0.6195**

Table 3.3 – Pearson Correlation Coefficient between PSCs obtained by the Brewin et al. (2010/2011) model and PSCs from Diagnostic Pigments calculated with old (Uitz et al., 2006) and new coefficients.

On the basis of the statistical results described above, the Brewin algorithm has been selected for the detailed study, at basin and sub-basin scale, of the biomass associated with each Phytoplanktonic Size Class for the whole SeaWIFS era (1998-2010). Model input are the case 1-case2 merged Chlorophyll maps produced by CNR in the MyOcean OC TAC.

On the other hand, the Hirata approach gives the opportunity to estimate the abundance of some taxonomic classes that represent specific functional groups. Therefore, this algorithm has also been considered as a tool to investigate the structure of the phytoplankton population in terms of taxonomic classes in some specific area characterized by intense mesoscale activity.

3.b Seasonal variability of Phytoplankton Size Classes at Basin Scale

In figures 3.5 to 3.16 SeaWIFS ten years climatology, from 1998 to 2010, are showed for Total Chlorophyll *a* (surface and over Ze applying the Morel model), micro-, nano- and pico-size particles density from the Kostadinov et al. (2009) algorithm, and biomass fraction of micro-, nano- and pico-phytoplankton (surface and over Ze) from the Brewin et al., (2010/2011) model. For the same period, the SST climatological maps have also been presented.

• Surface Total Chlorophyll *a* (mg m^{-3})

The climatological maps of Surface TChl a for the Mediterranean Sea show the typical cycle of temperate areas, with higher values in late winter/early spring and lower values in the maximum stratification summer period. In agreement with the dynamical characteristic of the Mediterranean sea, the general trend shows lower value of TChl a (< 0.2 mg m^{-3}) in the eastern basin than in the western one for the whole year. Only some coastal areas of the eastern basin, dominated by important river runoff, present always high TChl a concentrations (> 1.2 mg m^{-3}). These areas are the North Adriatic Sea, the Gulf of Gabès and the south-eastern area of the Levantine basin that is influenced by the outflow of the Nile river. High TChl a values are also present in the North Aegean Sea. A very small increase in the biomass values can be observed in the cyclonic Rhodes Gyre in March (more evident in the Total Chlorophyll *a* over Ze).

In the western basin, greater variability is revealed, that underlines the seasonality of the phytoplankton blooms, except in the summer months when very low concentrations of TChl a (similar to the eastern one) predominate. The more productive zones seem to be the

Alboran Sea, the Gulf of Lion, the Liguro-Provençal and part of the Catalan Basins, the cyclonic area in the North Tyrrhenian Sea, and to a minor extent, the Southern Algerian basin (in particular along the Algerian current). High TChl *a* values are also evident along the whole Italian peninsula. Relatively high values of TChl *a* (from 0.2 to 1.2 mg m^{-3}) are also observed in the Alboran Sea, entrained by two anticyclonic gyres, in particular by the western Alboran gyre well visible almost throughout the year.

The TChl *a* concentration in the whole open waters of the Mediterranean Sea ranges from 0.02 to 0.2 mg m^{-3} in summer and begins to increase from November/December at first along the Algerian current (0.4-0.8 mg m^{-3}) and later in the whole western basin (0.2-0.7 mg m^{-3}). In the Tyrrhenian Sea, in particular in the South, the TChl *a* values remain lower, except in the North Tyrrhenian Cyclone. As expectable, the surface Total Chlorophyll *a* reaches the up level (1.3-1.4 mg m^{-3}) at March and April in the North-western basin (Gulf of Lion and Liguro-Provençal and Catalan Basin).

• Over Ze Total Chlorophyll *a* (mg m^{-3})

The general trend of the TChl *a* estimated over the entire euphotic zone is very similar to the surface one, with values equal or greater than in the surface layer. This is more evident in the whole western basin, in the Adriatic sea, along the coastal shelves and in particular areas of the eastern basin as the Rhodes gyre, that in March shows values of ~ 0.5 mg m^{-3}. From November to March, the surface TChl *a* concentration increases initially in the Alboran basin (where the presence of the western and eastern Alboran gyres is evident), then along the southern and northern coasts and so towards the entire basin in December/January. In February, almost the whole western basin shows TChl *a* values greater than 0.5 mg/m³, with a minimum value lower than 0.25 mg/m³ exactly in the center of the Lion's Gulf. In March, the important bloom in the North-western basin becomes well evident. In April, TChl *a* reaches the higher value for Mediterranean open sea waters, with a concentration of ~ 1.5 mg/m³. In the eastern basin, the greater concentration in the TChl *a* value can be observed in areas with particular dynamical condition as the Sicily channel, the North Adriatic sea and along the Italian coasts , the North Aegean Sea, the Rodhis Gyre, in the Gulf of Gabès and in the south-eastern area of the Levantine basin interested by the outflow of the Nile river. In the remaining part of the basin the TChl *a* concentrations never exceeds 0.2-0.25 mg m^{-3} (except

for the coastal areas), with maxima values in the winter/spring months and minima in summer.

• Kostadinov 2009: micro, nano and pico-size particles density (log10 (n° particles m^{-3}))

The analysis of the number of particles in the unitary volume of water shows, without any exception, that the pico-size component dominates, everywhere and every time, followed by the nano-particles and the micro-particles at last. All three size components present higher values always in the western basin than in the eastern one. Seasonal effects, typical of the temperate areas, are evident in the whole basin.

In the western basin:

- the micro-size component shows values from ~ 10^3 to 10^8 (n° particles m^{-3}).

The open sea areas where the n° of particles are generally higher are the Alboran sea, Gulf of Lion, Liguro-Provençal and part of Catalan Basins, cyclonic area in the north Tyrrhenian Sea and only in winter/spring months the Southern Algerian basin. However, these areas present great variability in the absolute values. In summer, they show a density of ~ 10^6 particles m^{-3}, against ~ 10^3 to 10^4 in the remain part of the sub-basin. The minimum values are in July and August. From September-October, in the whole western basin, the values starts to increase. In December in the Alboran Sea, along the Algerian/Tunisian current, in the Gulf of Lion and Provençal basin values up to 10^8 n° particles m^{-3}, ~ 10^5 in the whole sub-basin and lower values always in the southern Tyrrhenian Sea can be observed. In February, we can see higher values (~ 10^7 – 10^8) in the whole sub-basin, with an evident minimum, in the southern-Tyrrhenian and in the center of the Lion's Gulf (~10^6 particles m^{-3}). The highest micro-size particles density is reached in March-April, in the Alboran Sea, Gulf of Lion and Liguro-Provençal basin, with values of ~ 10^8 (particles m^{-3}).

- the nano-size component shows values from ~ 10^8 to 10^{11} (n° particles m^{-3}). From the climatological maps, it can be seen that the distribution of the nano particles is similar to the micro ones. The areas with greater densities are the same for both sizes of particles, but the values of the number of particles per unit of volume's water are higher in the nano-component than in the micro, with ~ 10^{11} (n° particles m^{-3}) in March and April against the ~ 10^8 (particles m^{-3}) for the micro. A minimum of particles in the center of the Lion's Gulf is evident in February. The remaining part of the sub-basin shows values that varies from ~ 10^9 to 10^{10}

(n° particles m^{-3}) in March, to ~ 10^8 - 10^9 (n° particles m^{-3}) in late spring/summer. The minimum value is found in August in the southern Tyrrhenian Sea (<10^8 particles m^{-3}).

- the pico-size component shows values from ~ 10^{10} to 10^{13} (n° particles m^{-3}) and is always the most abundant one. Also for the pico-size component the typical richest areas are the same, the Alboran sea, Gulf of Lion, Liguro-Provençal and part of Catalan Basins, cyclonic area in the central Tyrrhenian Sea, only in winter/spring months the Southern Algerian basin and various coastal zones. Typical values in March in these areas are of ~ 10^{12} (n° particles m^{-3}), up to 10^{12} - 10^{13} along the coast Italy and the Lion's Gulf coast. Minima values (between 10^{10} - 10^{11} n° particles m^{-3}), found in August everywhere in the less productive zone.

<u>In the eastern basin:</u>

- the micro-size component shows values from ~ 10^2 to 10^7 (n° particles m^{-3}) in the whole eastern basin, except in the North-Adriatic Sea and along the entire Italian peninsula, in the North-Aegean Sea, in the Sicily channel, in the Gulf of Gabès and in the south-eastern area of the Levantine basin influenced by the outflow of the Nile river, where values of ~ 10^{10} (n° particles m^{-3}) are also reached. In particular, the North-Adriatic Sea and the area in front of the Nile delta, are characterized by maxima density of micro-particles during the whole year. The lowest values are found in the southern Ionian and Levantine basins, decreasing from March to late summer.

In the Rhodes gyre, the maps show a maximum density of micro-particles of ~ 10^6 (n° particles m^{-3}) in March. From January to March the higher concentrations are reached in the Adriatic Sea, Northern Ionian Sea, Sicily channel and Aegean Sea. From April to August the density of the particles decrease above overall the basin, showing minima in the Southern area with ~ 10^2 number of particles per m^{-3} of water against ~ 10^4 in the northern basin, ~ 10^6 in the North Aegean sea and always higher values in North-Adriatic Sea, in the Gulf of Gabès and in the south-eastern area of the Levantine basin influenced by the outflow of the Nile river. From October/November the densities start up to increase again in the whole basin, in the North-western part more than in the South-Eastern one.

- the nano-size component shows values from ~ 10^7 to 10^{10} (n° particles m^{-3}) in the whole sub-basin, except in the productive areas previously mentioned, in which values higher than 10^{11} are also reached. The seasonal maps of nano-component show the same trend observed for the micro-component but with higher densities compared with it.

The lowest values are reached in summer in the southern Ionian and Levantine basins (in particular in the South-eastern Levantine) where valued of to ~ 10^7 (n° particles m^{-3}) are observed. The highest density is always in the North Adriatic Sea for the whole year (> 10^{11} n° particles m^{-3}).

- the pico-size component in the eastern sub-basin shows values from ~ 10^{10} to 10^{12} (n° particles m^{-3}), except in its typical productive areas in which values of ~ 10^{13} are also reached. In the highly productive areas, the trend is similar to the one observed for micro- and nano- ones for the typical areas of higher values. In particular in the North Adriatic Sea the density of the particles reache ~ 10^{13} (n° particles m^{-3}). Such high values are also observed along the Italian coast (mainly in winter and spring months) in the Gulf of Gabès and the south-eastern area of the Levantine basin influenced by the outflow of the Nile river. In the Levantine and Ionian basins the difference between North and South is not so evident as for the other size components. Values are more homogeneous also in summer, with density of ~ 10^{11} (n° particles m^{-3}) and minima in the South-eastern part of the sub-basin and along the Tunisian-Libyan coasts with values of ~ 10^{10} (n° particles m^{-3}).

• TChl *a* fractions (surface & over Ze) of micro, nano and pico-phytoplankton (mg m^{-3})

These maps show the fractions of the Total Chlorophyll *a* for each phytoplanktonic size-component. The maps are expressed in % of TChl *a* and thus are compensative. In general all maps show a typical trend: at lower concentrations of Total Chlorophyll a the pico-size component represents the major part of the biomass, both in the surface layer that in the estimate over the euphotic layer (although in this last case the contribution of the other classes to the TChl *a* is greater). On the contrary, when the TChl *a* reaches higher values, the contribution of the micro-component becomes more evident (even more considering the whole euphotic layer). The nano component always shows intermediate values (both in surface that in euphotic zone), generally from 20 to 40% of the TChl *a*, up to 50% in the more productive areas and times. Typical coastal areas with the highest TChl *a* concentration of the Mediterranean Sea are: the North Adriatic Sea, the Gulf of Gabès, the south-eastern area of the Levantine basin influenced by the outflow of the Nile river, the Northern Aegean Sea, the Northern coast of the Gulf of Lion and of the North-western Alboran Sea. In such areas the micro contribution to the TChl *a* is predominant, with values higher than 50-60% for the all

months, up to 80-90% of the TChl *a* in some cases (i.e. North Adriatic Sea). Obviously, in the same areas, the contribution of the nano- and pico-size classes is minimum, with the pico component shows the lowest values, close to 0-10% of TChl *a*. This is observable in both surface and entire euphotic layers.

In the eastern basin:

In the eastern Mediterranean basin, the principal contribution to the TChl *a* is due to the pico-phytoplankton. It constitutes ~ the 60% of the TChl *a* from December to March. In spring, summer and first part of Autumn, its contribution increases up to 70-80%. From November, it starts to decrease and in December reaches again the ~ 60% of total TChl *a*. When the whole euphotic layer is considered, the values are a bit lower, with ~ 40-50% in winter up to ~ 50-60% in the other months. Contemporary, the nano component represents the ~ 20-30% (30-40% over Ze) in the winter months and decrease up to ~ 15-20% (20-30% on Ze) from late spring to autumn. The remaining TChl *a* is supplied by the micro component, that in winter – early spring represents ~ the 10-15% (~ the 15-20% taking in consideration the euphotic layer). From April to the early autumn, it decreases to ~ 5-10% (10-15% over Ze) of TChl *a*, with minima values in summer, and it increases again from November-December. In specific areas with higher content of Total Chlorophyll as the Rhodes gyre, the cyclonic area in the Northern Ionian Sea and part of the Adriatic Sea, the ratio between pico, nano and micro is different, with a greater proportion of the micro- and nano-size classes against to the pico in the more productive periods of the year (typically in March).

In the western basin:

The western basin shows a more pronounced seasonality. TChl *a* concentration presents a greater spatial and temporal variability and, consequently, the relative contribution of the three size classes to the TChl *a* shows also variability.

It can been observed in typical bloom areas such as the Liguro-Provençal basin, the Gulf of Lion, the Alboran Sea and the North Tyrrhenian cyclonic gyre. Here, from February to May TChl *a* concentration increase from ~ 0.2-0.4 mg m-³ to 1.2-1.3 (in April in the Liguro-Provençal basin). This is linked to a rapid increase of the micro component on the Total Chlorophyll *a*, that reaches values as high as the 50-60%, against the 35-40% of nano and the 10-15% of the pico (similar values are observed over Ze). For the remaining part of the year, these ratios change in favor of the pico component, but in the Liguro-Provençal basin and in

the Alboran sea the value of micro and nano remain always a few greater than in the other areas.

In the remaining part of the western basin, in summer the situation is similar to that of the eastern basin: pico contributes to the TChl *a* of ~ 60-70% (50-60% over Ze), nano ~ 15-25% (25-35% over Ze) and micro-phytoplankton ~ 5-15% (15-25 over Ze).

Starting from October, the TChl *a* concentration slowly increases, first in the Alboran Sea and along the Algerian and Spain coasts and then (December-January) in the whole open western Mediterranean Sea with values of 0.5-0.7 mg m^{-3}. At the same time, a weak increase in the micro and nano and decrease in the pico contributions is observed. In spring, values of ~ 15-25% of micro, ~ 25-35% of nano and 5.0-60% of pico-TChl a can to be observed in the surface layers of the Algerian Basin and the South-eastern Tyrrhenian Sea.

• Sea Surface Temperature

The spatial distribution of the SST shows gradients from West to East and from North to South. The eastern basin is warmer than the western one, and in general, the southern Mediterranean Sea is warmer than the North. The colder areas are the North Adriatic Sea (with a SST of ~ 7°C in January-February, that increase in Spring and reaches ~ 25/26°C in August), the Gulf of Lion (with minimum values of ~ 10-12°C in March-April and maximum values ~ 20-22°C in July-August), the Liguro-Provençal basin (that in November reaches the 15°C) and the Alboran Sea, particularly from late spring to late autumn.

The warmest area is the eastern part of the eastern Mediterranean basin, where values as high as ~ 30°C are reached in August.

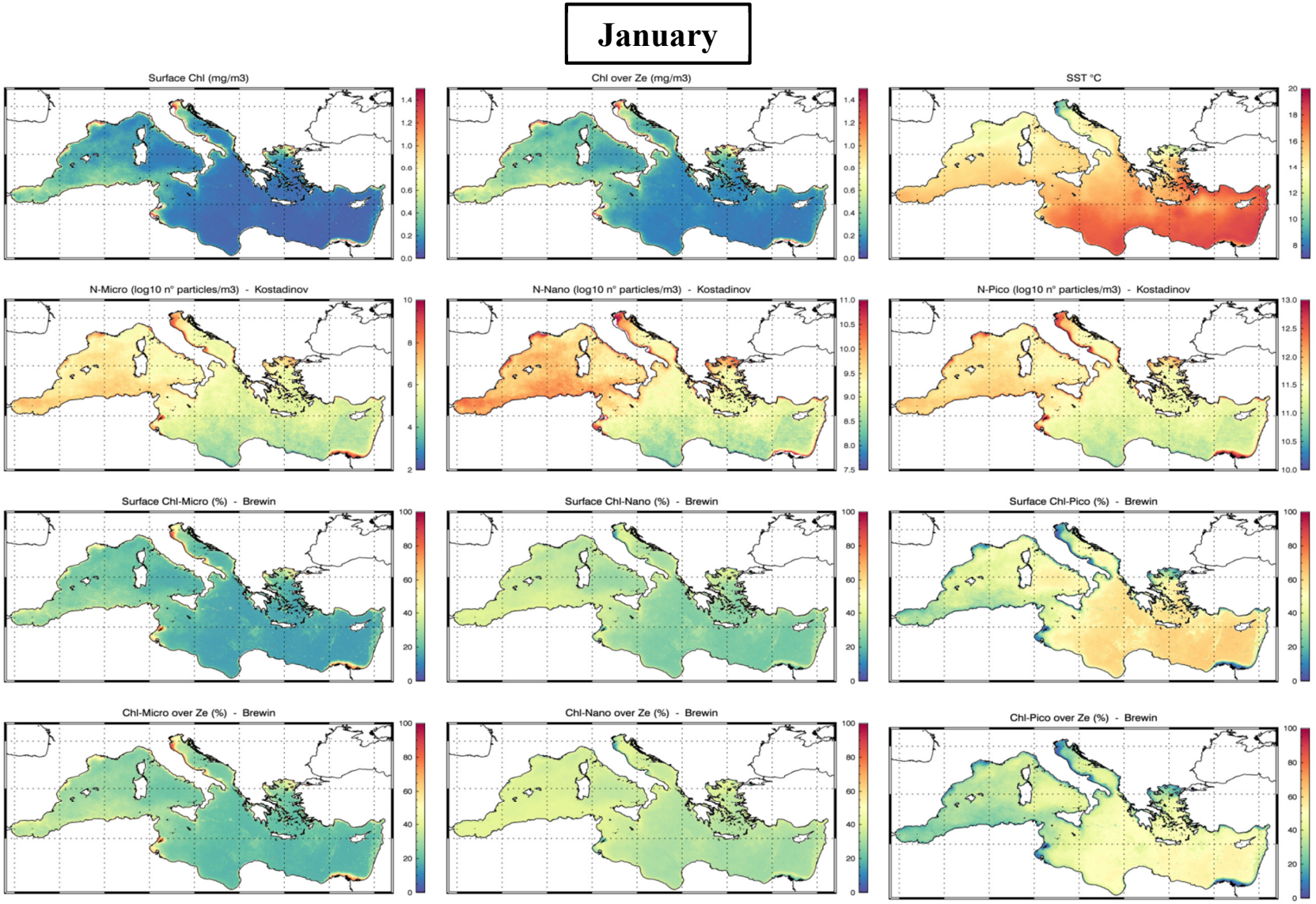

Figure 3.5 Climatological maps: January

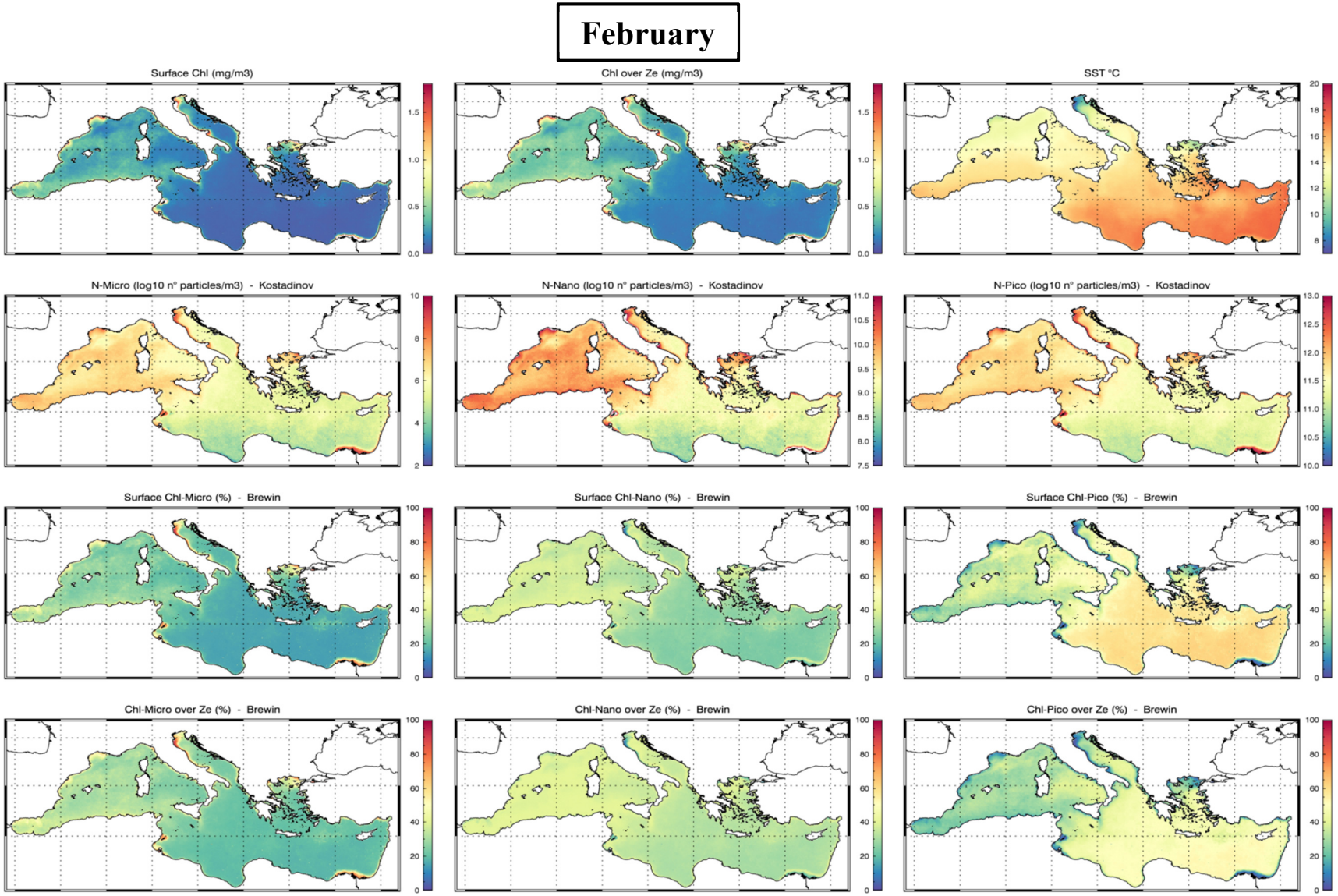

Figure 3.6 Climatological maps: February

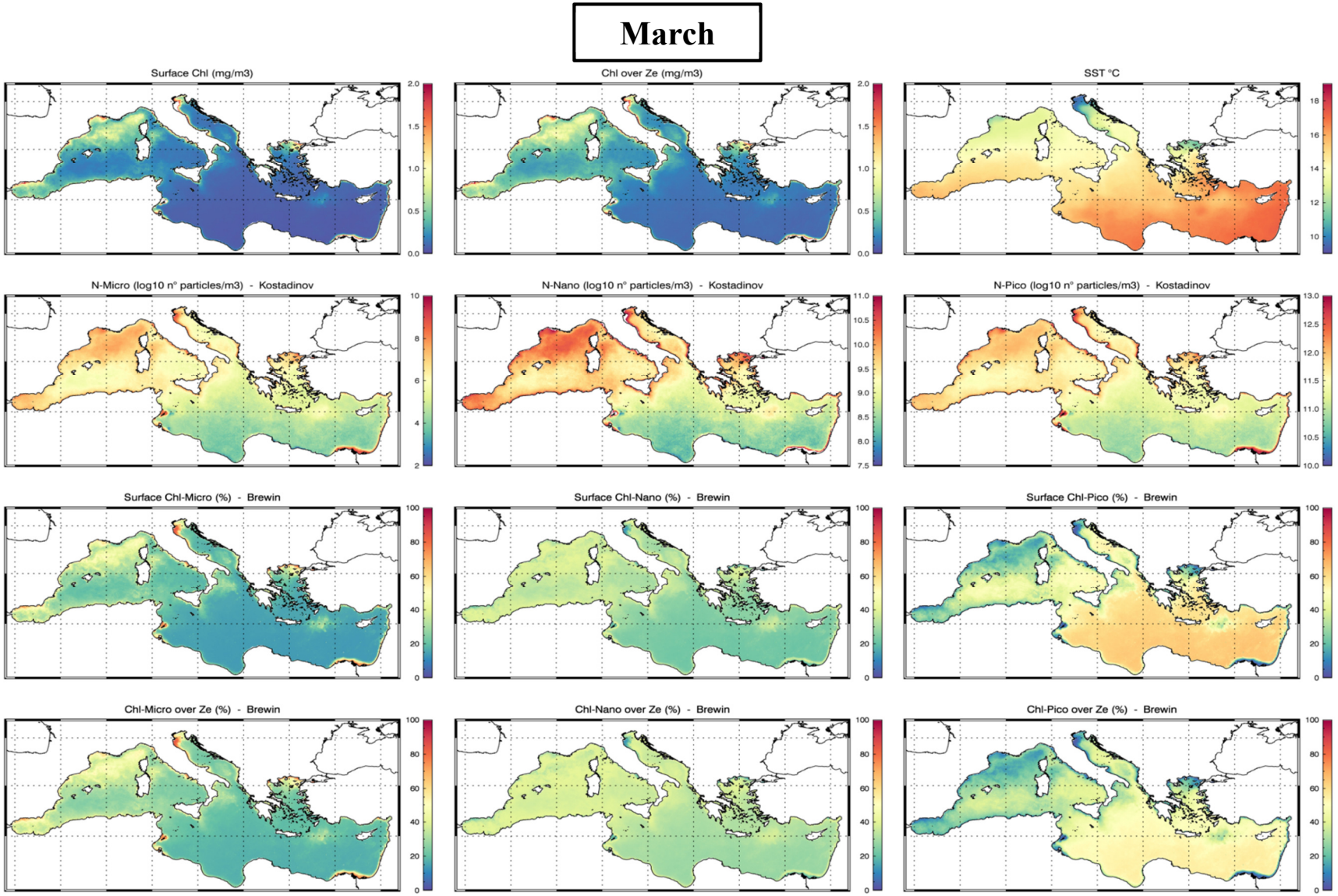

Figure 3.7 Climatological maps: March

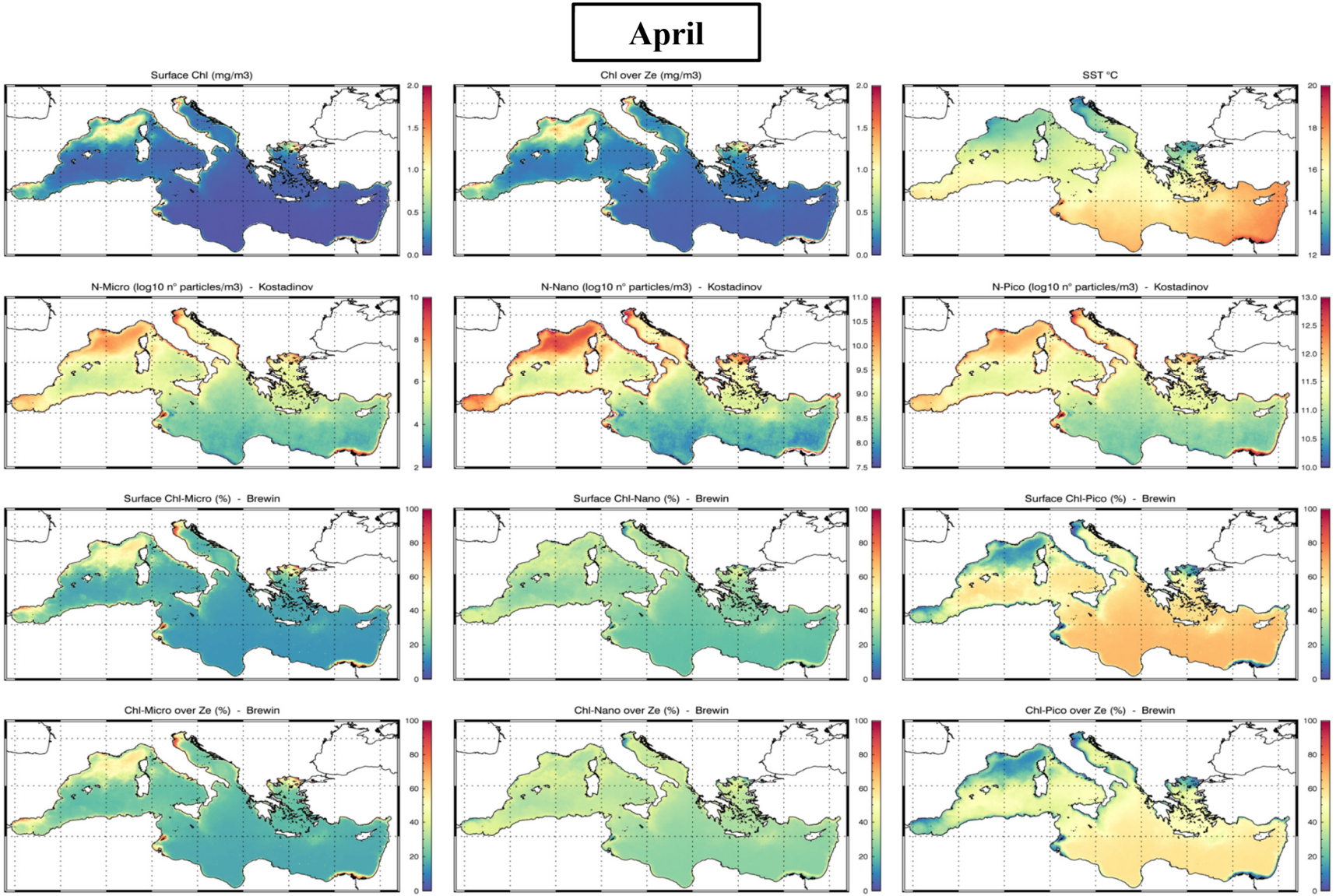

Figure 3.8 Climatological maps: April

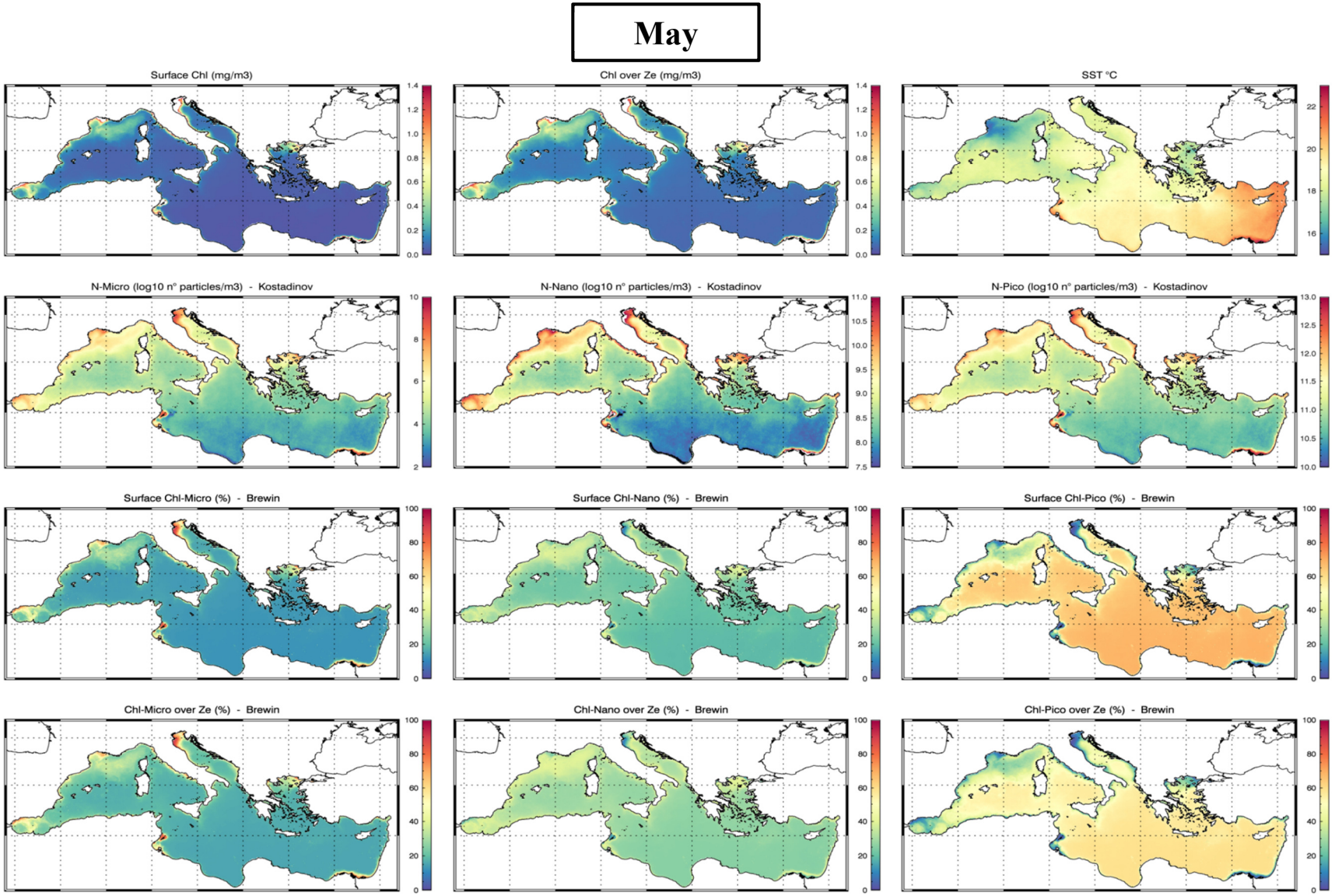

Figure 3.9 Climatological maps: May

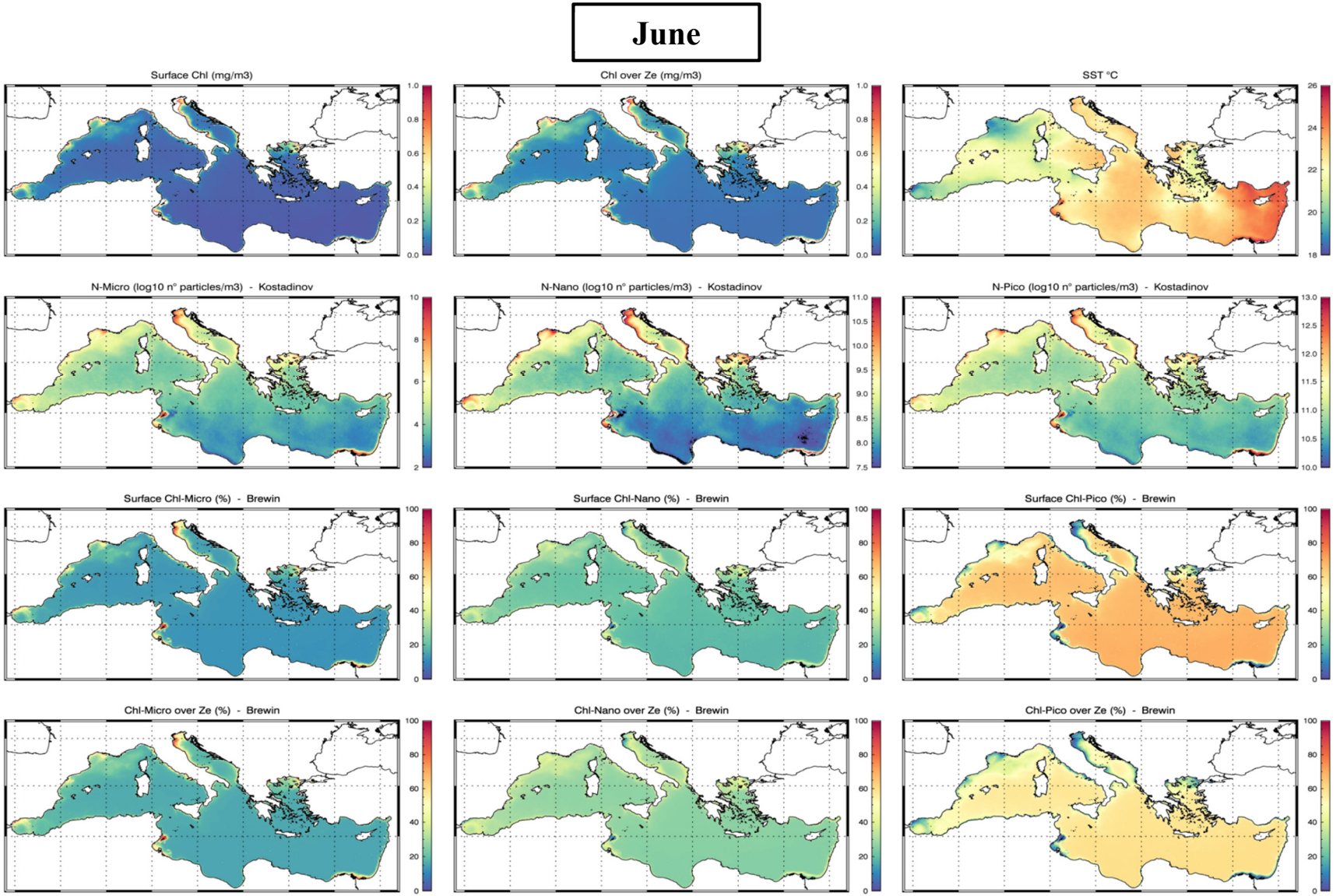

Figure 3.10 Climatological maps: June

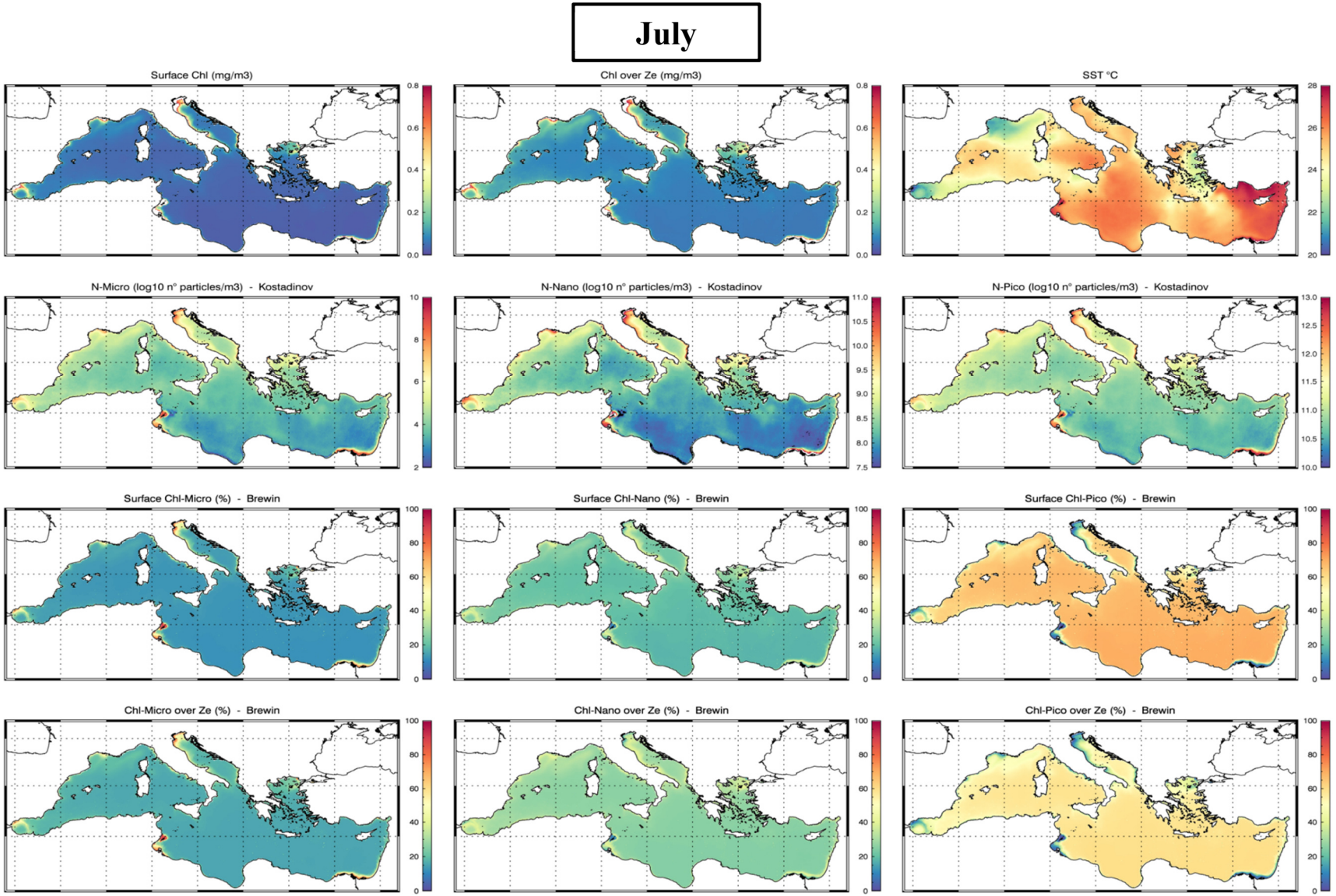

Figure 3.11 Climatological maps: july

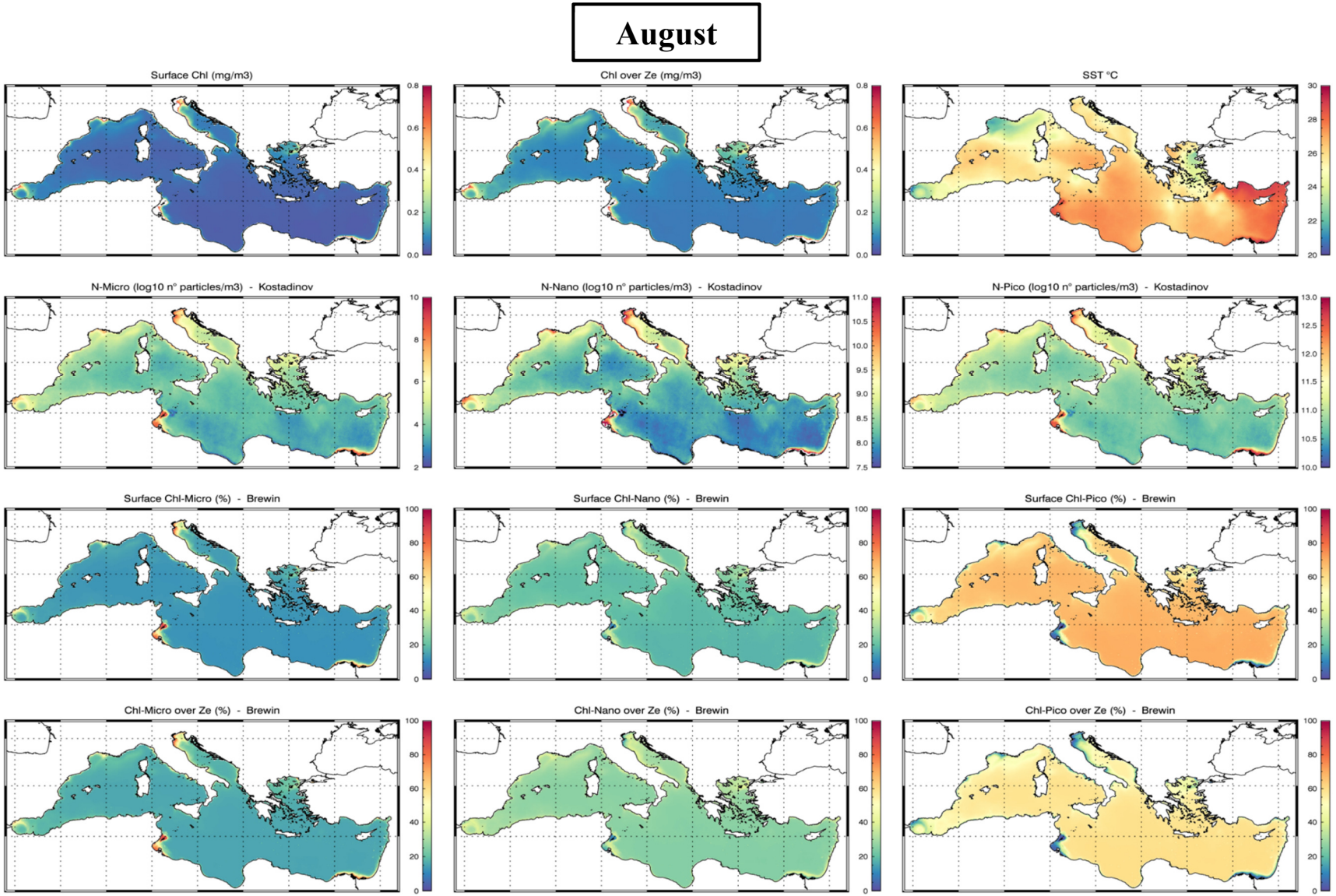

Figure 3.12 Climatological maps: August

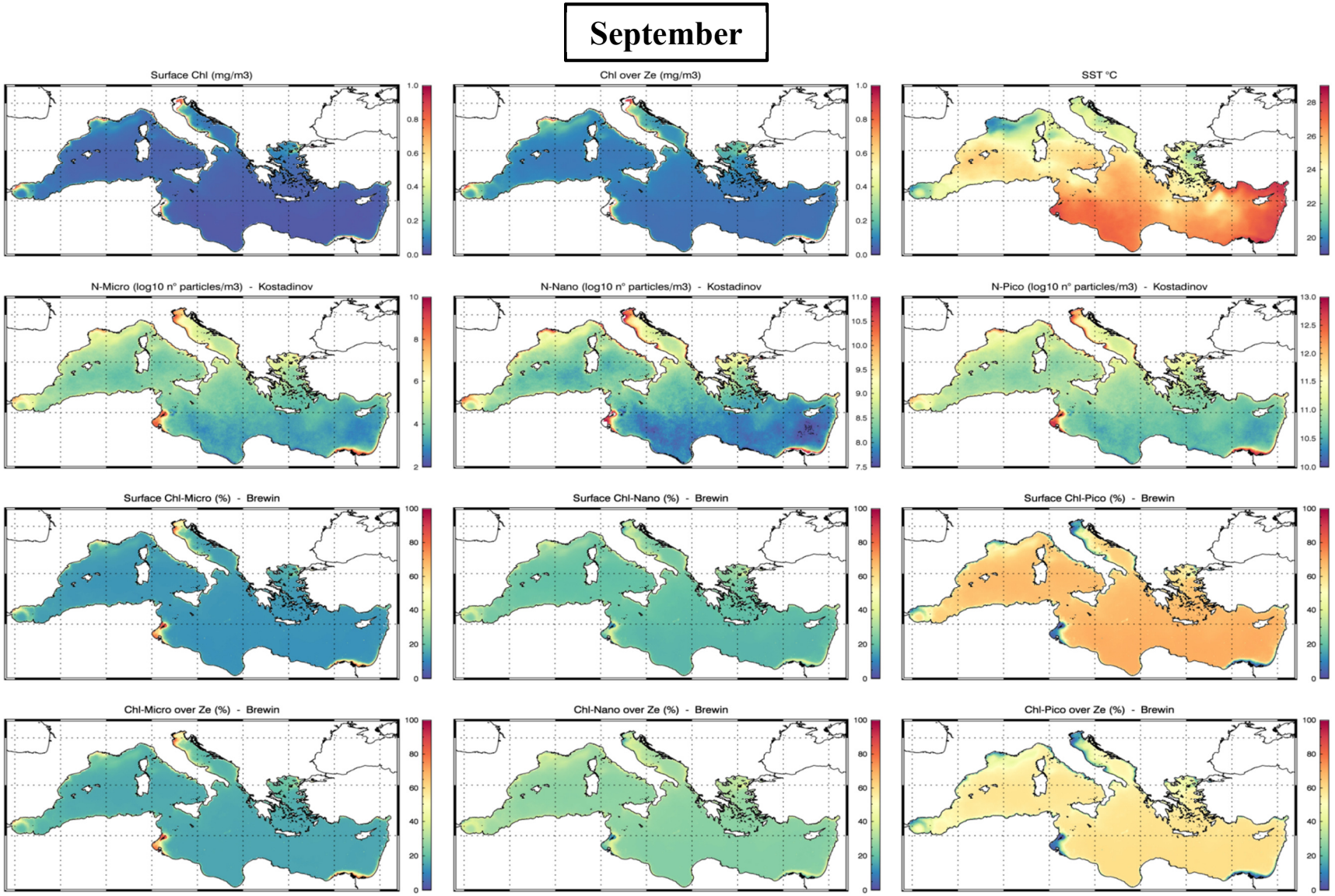

Figure 3.13 Climatological maps: September

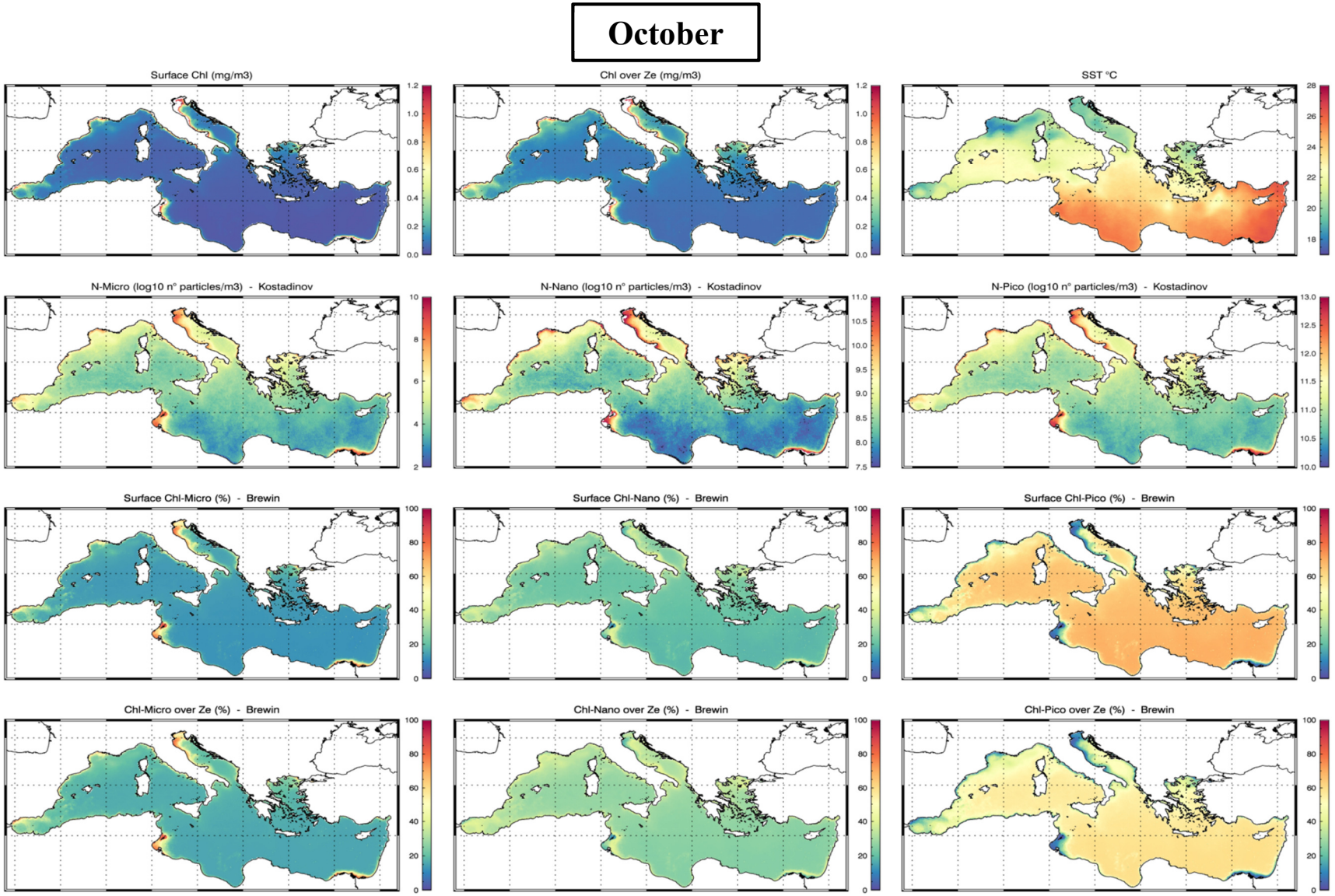

Figure 3.14 Climatological maps: October

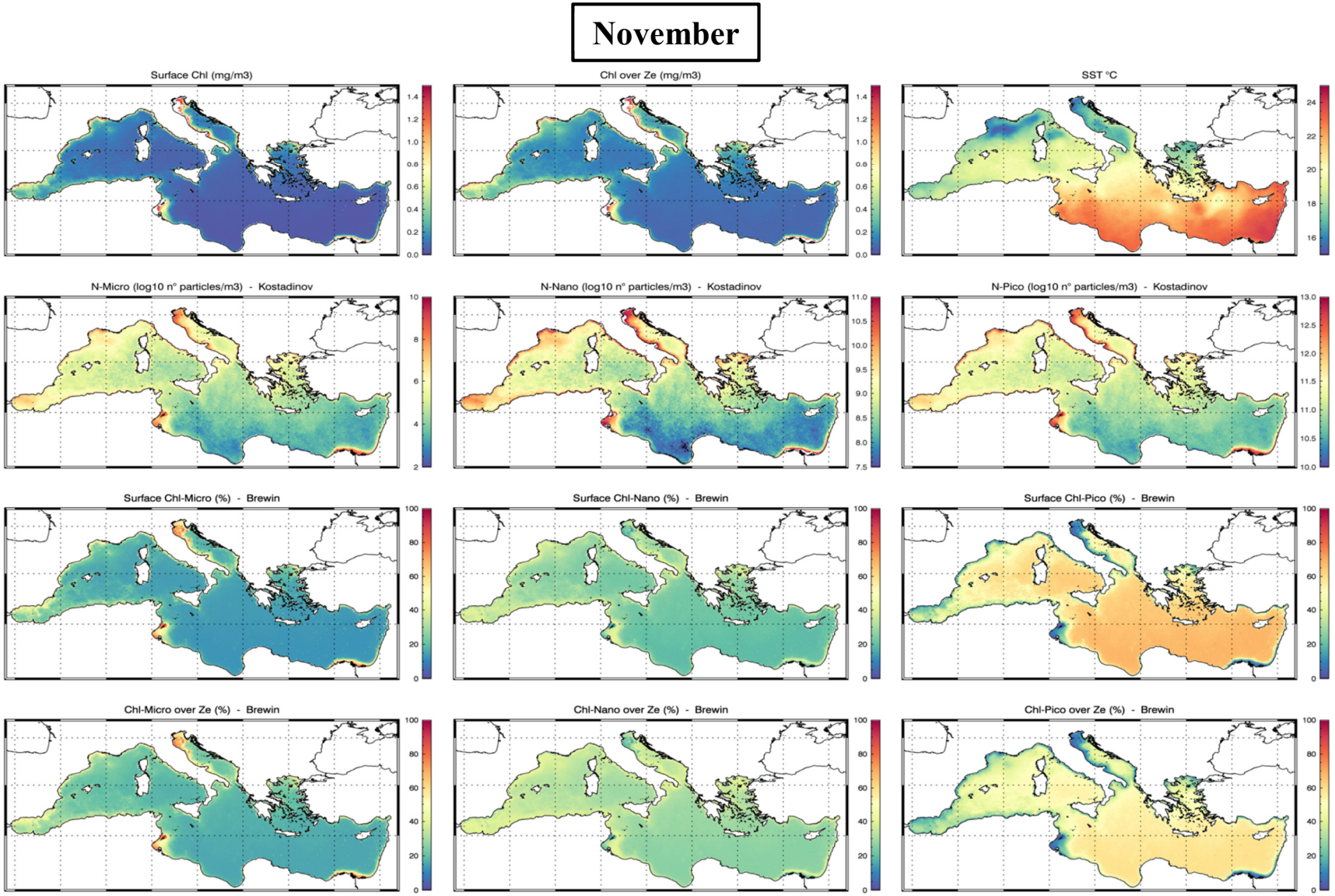

Figure 3.15 Climatological maps: November

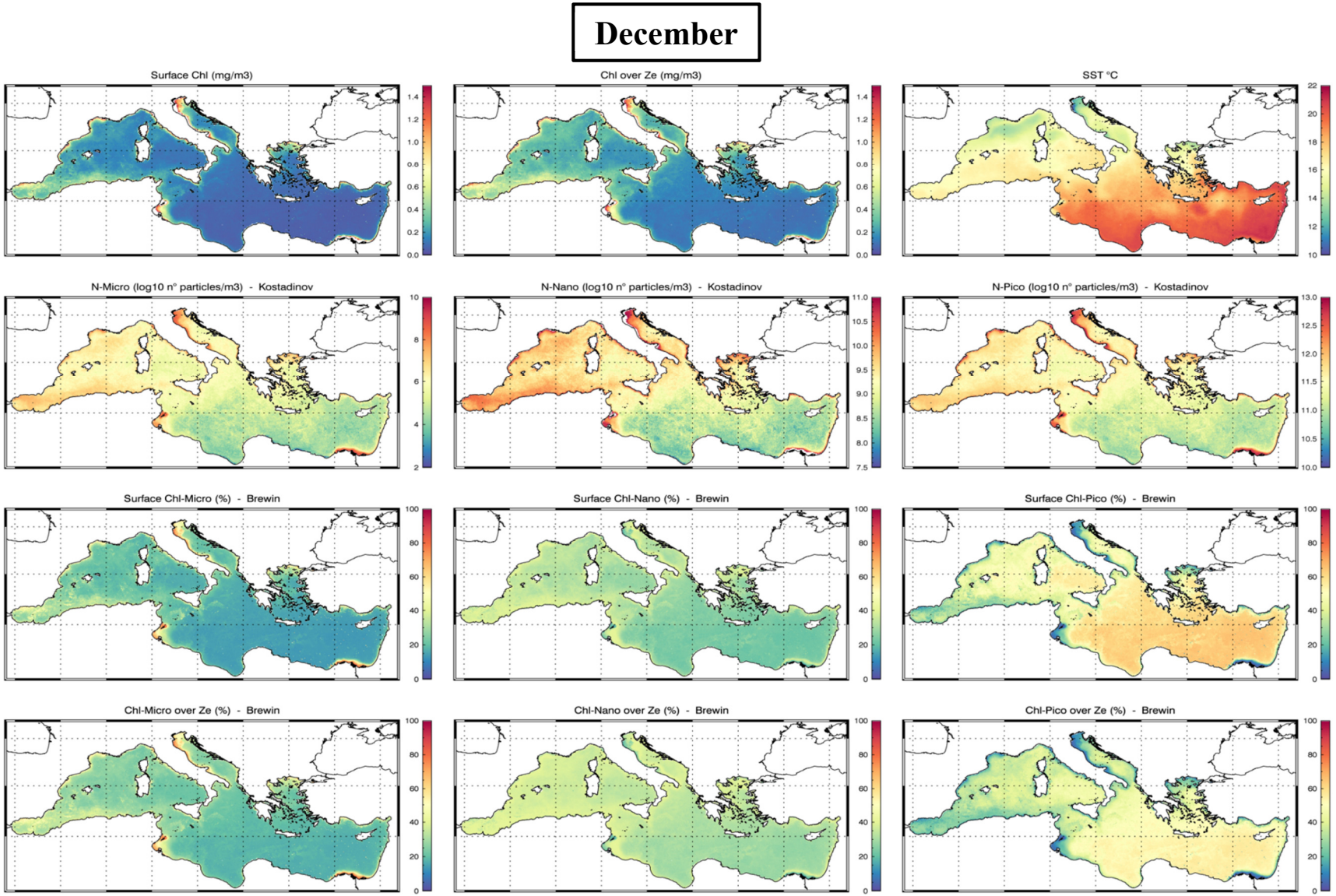

Figure 3.16 Climatological maps: December

3.c Variability of Phytoplankton size classes at Regional Scale

3.c.1 D'Ortenzio clusters regions

To better understand and appreciable the variability in the spatial and seasonal distribution of the phytoplantonic size classes, trends based on the regionalization proposed by D'Ortenzio and Ribera (2009) are shown. They identified seven "clusters" for the TChl *a* spatial distribution, on the basis of ten years of the SeaWiFS satellite surface Total Chlorophyll *a* concentration observations: three areas are considered of "no bloom", one presents "intermittently" blooms, the fifth is a typical "bloom" area and the sixth and seventh are two "coastal" regions. In figure 3.17 the geographical spatial distribution of this cluster is reported.

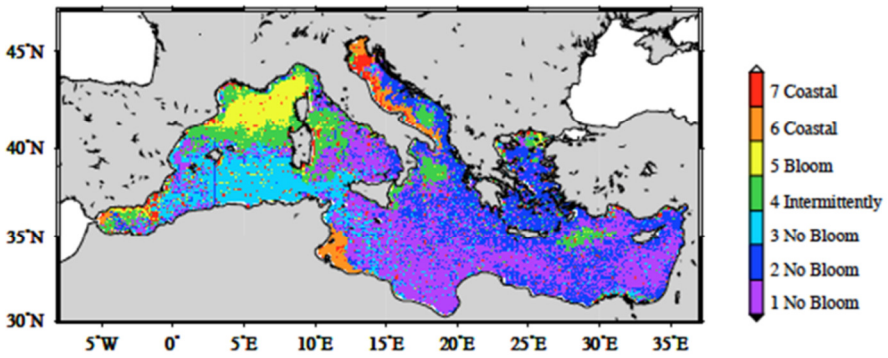

Figure 3.17 D'Ortenzio clusters regions: spatial distribution (from D'Ortenzio and Ribera, 2009)

• Seasonal variability

Seasonal trends of Total Chlorophyll *a* (surface and over Ze), Sea Surface Temperature, particle densities and volume for the three size classes (from Kostadinov et al., 2009), TChl *a* concentration (surface and over Ze) represented by each size class (from Brewin et al., 2010/2011) have been investigated for the cluster regions (figures 3.18-3.24):

Cluster 1 – No bloom area (fig. 3.18)

This cluster, as evidenced by the figure 3.17, includes principally the southern and eastern part of the eastern Mediterranean sub-basin (partly of the Ionian and partly of the

Levantine) and the highly oligotrophic waters of the southeastern Tyrrhenian Sea. Some scattered "no bloom" pixels are also observed in the Algerian and Catalan basin.

- Surface and Over Ze Total Chlorophyll *a* present an identical trend, with different concentration values. Surface TChl *a* increases from ~ 0.04 mg m^{-3} in August to ~ 0.15 mg m^{-3} in February. In the same periods TChl *a* over Ze increases from ~ 0.08 to ~ 0.23 mg m^{-3}. The trend show a slow increase from the Autumn, reaching the maxima value in February-March and starting to decrease up to the summer minima values.

- SST shows a minimum (~ 15.5°C) in February-March, reaching ~ 16.5°C in April. Then, from April to July, increase of ~ 3°C per months and reaches the maximum value of ~ 27°C in August.

- Particles densities show, all around the year, the predominance of the pico component with values varying from ~ $5.5x10^{10}$ (n° particles m^{-3}) in June-August to ~ $2.5x10^{11}$ (n° particles m^{-3}) in February. In the same months the minimum for nano is ~ $1.1x10^{8}$ (n° particles m^{-3}) and for micro is ~ $3.7x10^{3}$ (n° particles m^{-3}), the maximum for nano is ~ $1.5x10^{9}$ (n° particles m^{-3}) and for micro is ~ $2.8x10^{5}$ (n° particles m^{-3}). The three size classes follows the seasonal trend of the Total Chlorophyll *a*.

- Particles volumes in the cluster 1 follow a similar trend as the densities. For the pico-size particles, we can observe values ranging from ~ $9.6x10^{-9}$ (m^3 particles m^{-3}) in summer (June-August) to ~ $5.5x10^{-8}$ (m^3 particles m^{-3}) in February. In the same months the minimum for nano is ~ $1.4x10^{-9}$ (m^3 particles m^{-3}) and for micro is ~ $3.6x10^{-11}$ (m^3 particles m^{-3}). The maximum for nano is ~ $2.7x10^{-8}$ (n° particles m^{-3}) and for micro is ~ 3.0x10-^{9} (m^3 particles m^{-3}).

- Also in the TChl *a* content (surface and over Ze) for pico, nano and micro component the trend is similar. Pico strats from maximum concentration between ~ 0.065-0.07 (mg m^{-3}) in February and minimum of ~ 0.025 (mg m^{-3}) in summer. Nano ranges from ~ 0.045 to ~ 0.01 (mg m^{-3}) and micro from ~ 0.035 to ~ 0.075 (mg m^{-3}) in the same months.

	Chl (surf)	**Chl (Ze)**	**Pico-density**	**Nano-density**	**Micro-density**	**Pico-Volume**	**Nano-Volume**	**Micro-Volume**	**Pico-Chl(surf)**	**Nano-Chl(surf)**	**Micro-Chl(surf)**	**Pico-Chl(Ze)**	**Nano-Chl(Ze)**	**Micro-Chl(Ze)**
Max	0.15 Feb	0.23 Feb	$2.5x10^{11}$ Feb	$1.5x10^{9}$ Feb	$2.8x10^{5}$ Feb	$5.5x10^{-8}$ Feb	$2.7x10^{-8}$ Feb	$3.0x10^{-9}$ Feb	0.07 Feb	0.05 Feb	0.03 Feb	0.09 Feb	0.08 Feb	0.06 Feb
Min	0.04 Aug	0.08 Aug	$5.5x10^{10}$ Jul	$1.1x10^{8}$ Jul	$3.7x10^{3}$ Jul	$9.6x10^{-9}$ Jul	$1.4x10^{-9}$ Jul	$3.6x10^{-11}$ Jul	0.03 Aug	0.01 Aug	0.01 Aug	0.04 Aug	0.02 Aug	0.01 Aug

Table 3.4 Cluster 1 maxima and minima parameters values

Cluster 2 – No bloom area (fig. 3.19)

This cluster includes principally the northern part of the eastern basin (in the Ionian sub-basin, except a districted area related to the fourth cluster) and part of the Levantine non involved in the first cluster, Aegean Sea (except the North), the no bloom waters of the Adriatic Sea and a small part of the South-eastern Tyrrhenian Sea. Few isolated pixels can be found in the western Alboran gyre.

In this cluster the trends are very similar to the those observed in the previous one, and presents the same seasonality. TChl *a* shows a maximum in February and a minimum in August with values of ~ 0.14 and ~ 0.05 mg m^{-3} respectively. Concentrations of Total Chlorophyll *a* over the euphotic zone are slightly higher than for the surface, with extreme values ranging from ~ 0.22 to 0.1 mg m^{-3} in the same months. The minimum for the SST is reached in March (~ 15.52 °C), while the maximum of temperature is observed in August (~ 26.32 °C). The density of particles, obtained applying the Kostadinov model, exhibits higher values in February with ~ $2.6x10^{11}$ (n° particles m^{-3}) for pico, ~ $1.5x10^{9}$ for nano and ~ $2.6x10^{5}$ for micro, and lower values on July for all of the three size classes of particles. The volume behaves similarly, with higher values in February with ~ $5.6x10^{-8}$ (m^3 particles m^{-3}) for pico, ~ $2.6x10^{-8}$ for nano and ~ $2.8x10^{-9}$ for micro, and lower values on July with ~ $1.2x10^{-8}$ (m^3 particles m^{-3}) for pico, ~ $2.1x10^{-9}$ for nano and ~ $6.6x10^{-11}$ for micro are observed. The biomass fractions show lower values in August for all the three components, with ~ 0.03 (mg m^{-3} of TChl *a* – surface) for pico, ~ 0.013 for nano and ~ 0.11 for micro, corresponding to 0.05, 0.03 and 0.02 mg m^{-3} of TChl *a* – over Ze. The maximum values for pico (0.06 and 0.08 mg m^{-3} of surface and over Ze TChl *a* respectively), nano (~ 0.04 and 0.074 mg m^{-3}) and micro (0.056 mg m^{-3} TChl *a* over Ze) occur in February. However, the maximum concentration of micro surface Total Chlorophyll *a* occurs in March (~ 0.03 mg m^{-3}).

	Chl (surf)	**Chl (Ze)**	**Pico-density**	**Nano-density**	**Micro-density**	**Pico-Volume**	**Nano-Volume**	**Micro-Volume**	**Pico-Chl(surf)**	**Nano-Chl(surf)**	**Micro-Chl(surf)**	**Pico-Chl(Ze)**	**Nano-Chl(Ze)**	**Micro-Chl(Ze)**
Max	0.14 Feb	0.22 Feb	$2.6x10^{11}$ Feb	$1.5x10^{9}$ Feb	$2.6x10^{5}$ Feb	$5.6x10^{-8}$ Feb	$2.6x10^{-8}$ Feb	$2.8x10^{-9}$ Feb	0.06 Feb	0.04 Feb	0.03 Mar	0.09 Feb	0.07 Feb	0.06 Feb
Min	0.054 Aug	0.097 Aug	$6.9x10^{10}$ Jul	$1.6x10^{8}$ Jul	$6.8x10^{3}$ Jul	$1.2x10^{-8}$ Jul	$2.1x10^{-9}$ Jul	$6.6x10^{-11}$ Jul	0.03 Aug	0.01 Aug	0.01 Aug	0.05 Aug	0.03 Aug	0.02 Aug

Table 3.5 Cluster 2, maxima and minima parameters values

Cluster 3 – No bloom area (fig. 3.20)

The third cluster is located in the western Mediterranean Sea, mainly the Algerian basin, with some extension eastward toward Sicily, and westward toward the Alboran Sea.

These areas show a seasonal trend of the Total Chlorophyll *a* similar to that of the cluster 2 (no bloom), but with values twice then those recorded there (maxima in February, ~ 0.3 mg m^{-3} in surface layer and ~ 0.41 over Ze and minima in August, ~ 0.059 in surface layer and ~ 0.1 mg m^{-3} over Ze). This is highlighted especially in the volume of particles and in the fractions of TChl *a*. In the winter months, from December to February, the volume of the nano particles reaches that of the pico particles, with value higher than in cluster 1 and 2 (table 3.6 for the maxima values in February). Also the micro volumes increase and, all around the year, a smaller distance between micro, nano and pico component is observed. The volume and the density of the particles increase from October to February. Regarding the biomass fractions, the nano concentration for surface TChl a exceeds the pico and micro ones from December to late March (and from November to April considering the whole Ze). The micro-fraction values increase and, in the estimate of the TChl a over Ze, surpass the pico concentrations from late November to March. In general, the distances between the three classes are smaller than for the previous clusters. The seasonality of the SST is similar to that of the other cluster, with oscillations between ~ 26.13 °C in August and ~ 14.74 °C in February.

	Chl (surf)	**Chl (Ze)**	**Pico-density**	**Nano-density**	**Micro-density**	**Pico-Volume**	**Nano-Volume**	**Micro-Volume**	**Pico-Chl(surf)**	**Nano-Chl(surf)**	**Micro-Chl(surf)**	**Pico-Chl(Ze)**	**Nano-Chl(Ze)**	**Micro-Chl(Ze)**
Max	0.31 Feb	0.41 Feb	$5.0x10^{11}$ Feb	$5.0x10^{9}$ Feb	$2.5x10^{6}$ Feb	$1.3x10^{-7}$ Feb	$1.3x10^{-7}$ Feb	$3.2x10^{-8}$ Feb	0.1 Feb	0.11 Feb	0.096 Feb	0.12 Feb	0.16 Feb	0.14 Feb
Min	0.06 Aug	0.10 Aug	$7.1x10^{10}$ Aug	$1.7x10^{8}$ Aug	$7.6x10^{3}$ Aug	$1.3x10^{-8}$ Aug	$2.2x10^{-9}$ Aug	$7.4x10^{-11}$ Aug	0.031 Aug	0.014 Aug	0.013 Jul	0.05 Aug	0.03 Aug	0.023 Aug

Table 3.6 Cluster 3 maxima and minima parameters values

Cluster 4 – Intermittently area (fig. 3.21)

This cluster includes part of the Northern Aegean Sea, the Rodhes gyre, the South Adriatic Sea, the North Tyrrhenian cyclonic gyre, the boundaries of the North-Western Mediterranean Sea cyclonic area, part of the Alboran sea and some regions of the northern Ionian basin.

Contrary to the previous clusters, the maximum of the TChl a (both at the surface and over Ze) is observed in March rather than in February. In these regions, concentrations are higher than in the previous ones and the excursion from spring to summer is more pronounced (see table 3.7 for minimum and maximum values). The trends of the densities and volumes of the size-particles are very similar to that of the third cluster, except for the maxima values that in the intermittently areas are shifted to March. The major differences are noticeable in the TChl a concentration of each size class. Nano-TChl *a* concentration is higher than the pico from January to late April in the surface layer and from November to May in the euphotic layer. The micro-component shows surface concentrations greater than for nano during the whole year, except from January to February when they are nearly the same. The situation is different when the full euphotic layer is considered. In this case micro dominates over nano only from February to June. In summer, nano has concentration slightly higher than micro while in Autumn they are nearly equal. Surface concentrations of micro overpass those of the pico-component from January to late May. In the following months, the pico component is the dominant one up to December at the surface, and from June to November in the whole euphotic depth.

The SST are slightly lower than the other cluster, with a minimum of ~ 13.9°C in February and maximum of ~ 25.5°C in August.

	Chl (surf)	**Chl (Ze)**	**Pico-density**	**Nano-density**	**Micro-density**	**Pico-Volume**	**Nano-Volume**	**Micro-Volume**	**Pico-Chl(surf)**	**Nano-Chl(surf)**	**Micro-Chl(surf)**	**Pico-Chl(Ze)**	**Nano-Chl(Ze)**	**Micro-Chl(Ze)**
Max	0.38 Mar	0.49 Mar	$5.8\text{x}10^{11}$ Mar	$6.0\text{x}10^{9}$ Mar	$3.2\text{x}10^{6}$ Mar	$1.5\text{x}10^{-7}$ Mar	$1.5\text{x}10^{-7}$ Mar	$3.4\text{x}10^{-8}$ Mar	0.1 Mar	0.13 Mar	0.15 Mar	0.12 Mar	0.18 Mar	0.19 Mar
Min	0.09 Aug	0.14 Aug	$9.5\text{x}10^{10}$ Aug	$2.8\text{x}10^{8}$ Aug	$1.7\text{x}10^{4}$ Aug	$1.8\text{x}10^{-8}$ Aug	$4.0\text{x}10^{-9}$ Aug	$1.6\text{x}10^{-10}$ Aug	0.04 Aug	0.02 Aug	0.025 Aug	0.06 Aug	0.04 Aug	0.037 Aug

Table 3.7 Cluster 4 maxima and minima parameters values

Cluster 5 – Bloom area (fig. 3.22)

This cluster is centered in the Northwestern basin and includes the Liguro-Provençal basin and the Gulf of Lion.

In this area, the TChl a concentrations reaches in April the highest values for the open sea waters of the Mediterranean Sea, with maxima of ~ 0.8 mg m^{-3} at the surface and ~ 0.9 mg m^{-3} in the euphotic layer. Note that these concentrations refer to an average of all the pixels in the cluster over a month, resulting in values definitely lower than the maximum of TChl a

concentrations observed in the more active area of the bloom. The particles density shows always the predominance of pico, followed by nano and micro. Comparing their trends between this cluster and the former, a greater increase in the all three components becomes evident, especially from February to April. The maximua of the pico density and volume occur in March (table 3.8). Regarding to the volume particles, nano component predominates from December to May, and pico for the remaining part of the year. The micro component, differently by the other cluster, increases more quickly from January to March while, from March to April, the micro volume is equal to pico.

The trend of the Total Chlorophyll *a* is evident in the biomass fraction. In this cluster the values of surface TChl *a* relative to the three size classes are very similar from June to December. From January to May, nano and micro component increase more rapidly than pico. In particular from February to May the contribution of the micro component to the TChl *a* is predominant. Similar trends are observed in the euphotic zone, but with a greater relative contribution of the micro-phytoplankton on the TChl *a* concentrations (see the table for the maximum and minimum values).

The Sea Surface Temperature shows the same trend as other clusters but with lower value (maximum in August of ~ 24.2°C and minimum in February of ~ 11°C)

	Chl (surf)	Chl (Ze)	Pico-density	Nano-density	Micro-density	Pico-Volume	Nano-Volume	Micro-Volume	Pico-Chl(surf)	Nano-Chl(surf)	Micro-Chl(surf)	Pico-Chl(Ze)	Nano-Chl(Ze)	Micro-Chl(Ze)
Max	0.81 Apr	0.91 Apr	$9.3x10^{11}$ Mar	$1.8x10^{10}$ Mar	$2.2x10^{7}$ Mar	$2.8x10^{-7}$ Mar	$5.9x10^{-7}$ Mar	$2.8x10^{-7}$ Mar	0.128 Mar	0.262 Apr	0.42 Apr	0.135 Mar	0.30 Apr	0.48 Apr
Min	0.12 Aug	0.17 Aug	$1.3x10^{11}$ Aug	$5.0x10^{8}$ Aug	$4.5x10^{4}$ Aug	$2.7x10^{-8}$ Aug	$7.6x10^{-9}$ Aug	$4.7x10^{-10}$ Aug	0.047 Aug	0.031 Aug	0.037 Aug	0.068 Aug	0.053 Aug	0.052 Aug

Table 3.8 Cluster 5 maxima and minima parameters values

Cluster 6 – Coastal area (fig. 3.23)

Cluster 6 includes the north Adriatic Sea and its western coast, the Gulf of Gabès and a small part of the Alboran Sea, in proximity of the Gibraltar strait.

As expected, TChl *a* trends in coastal area are very different to other regions of the Mediterranean Sea. In this case, TChl *a* shows two maxima, both at the surface and over Ze. The higher maximum is observed in November (~ 0.67 mg m^{-3}). The concentration decreases up to March, when one of the two annual minima is detected (the other one is in June). The second maximum, smaller than that in November, occurs in May (~ 0.67 mg m^{-3}). The

densities of the particles always show the dominance of the pico-size component respect to nano and micro. The values show a regular trend for the whole year with minima in June for all three components. Volume trends show a similar behaviour, but the differences between minima and maxima values are more pronounced (table 3.9). The Brewin model results for this cluster show that TChl a trend is better represented by the micro component since it is the dominant component of the TChl a concentration. For this component, two maxima are observed in May and November.

The SST has the same trend of the other cluster with a minimum in February of ~ 13.4°C and a maximum in August of 26.3°C.

	Chl (surf)	Chl (Ze)	Pico-density	Nano-density	Micro-density	Pico-Volume	Nano-Volume	Micro-Volume	Pico-Chl(surf)	Nano-Chl(surf)	Micro-Chl(surf)	Pico-Chl(Ze)	Nano-Chl(Ze)	Micro-Chl(Ze)
Max	0.77 Nov	0.86 Nov	$7.9x10^{11}$ Dec	$7.6x10^{9}$ Dec	$3.2x10^{6}$ Dec	$1.9x10^{-7}$ Dec	$1.7x10^{-7}$ Dec	$3.6x10^{-8}$ Dec	0.12 Dec	0.22 Nov	0.43 Nov	0.13 Dec	0.26 Dec	0.47 Nov
Min	0.53 Mar & Jun	0.60 Jun	$2.3x10^{11}$ Jul	$1.2x10^{9}$ Jul	$1.9x10^{5}$ Jul	$5.0x10^{-8}$ Jul	$2.2x10^{-8}$ Jul	$2.0x10^{-9}$ Jul	0.07 Jul	0.12 Jul	0.28 Mar	0.09 Jul	0.15 Jul	0.032 Mar

Table 3.9 Cluster 6 maxima and minima parameters values

Cluster 7 – Coastal area (fig. 3.24)

The last cluster is coastal and is located in the North Adriatic Sea. The Total Chlorophyll *a* starts from a minimum in July of ~ 0.22 mg m^{-3} to reach its maximum in February (0.53 mg m^{-3}). In terms of particles densities the pico component is always the dominant one. For the other two components a predominance of the nano sized particles density respect to micro one is observed. Similar ratios occur when volumes are considered, except from December to March when the nano component of the total volume is equal to that of pico. The micro component shows a greater variability, both in terms of number than of volume of particles. The same behaviour is observed in all clusters. The contribution of the micro component to the TChl *a* is the dominant one. This component has two maxima, the first one in November and the second one between February and March with similar intensities of about 0.25 mg m^{-3}. The minima are observed in July, when the nano concentration, generally predominant over the pico class, becomes closer to that one of the pico biomass. The same trends are evident in the euphotic layer, but with greater values (see table 3.10).

SST trends are similar to those of the other clusters, with a maximum in August (25.8 °C) and a minimum in February (13.5 °C).

Table 3.10 Cluster 7 maxima and minima parameters values

	Chl (surf)	Chl (Ze)	Pico-density	Nano-density	Micro-density	Pico-Volume	Nano-Volume	Micro-Volume	Pico-Chl(surf)	Nano-Chl(surf)	Micro-Chl(surf)	Pico-Chl(Ze)	Nano-Chl(Ze)	Micro-Chl(Ze)
Max	0.53 Feb	0.63 Feb	$6.8x10^{11}$ Feb	$3.7x10^{9}$ Feb	$3.2x10^{6}$ Feb	$1.7x10^{-7}$ Feb	$1.8x10^{-7}$ Feb	$4.5x10^{-8}$ Feb	0.11 Feb	0.16 Feb	0.27 Mar	0.12 Feb	0.2 Feb	0.31 Mar
Min	0.22 Jul	0.28 Jul	$1.4x10^{11}$ Aug	$5.5x10^{8}$ Aug	$5.0x10^{4}$ Aug	$3x10^{-8}$ Aug	$8.5x10^{-9}$ Aug	$5.0x10^{-10}$ Aug	0.05 Aug	0.06 Aug	0.1 Jul	0.07 Aug	0.08 Aug	0.12 Jul

Figure 3.18 – Cluster 1: ***no blooming areas***

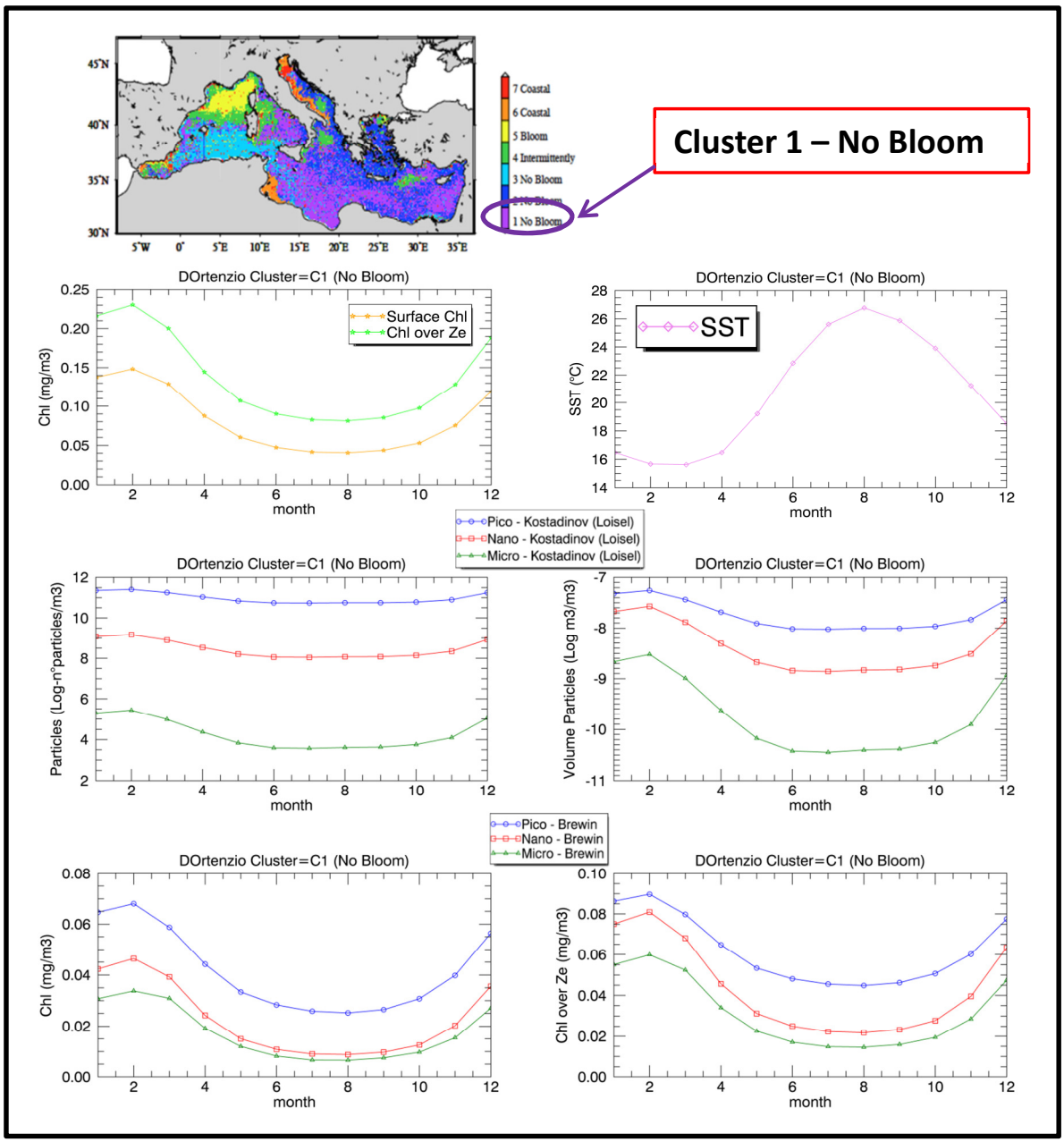

Figure 3.19 – Cluster 2: ***no blooming areas***

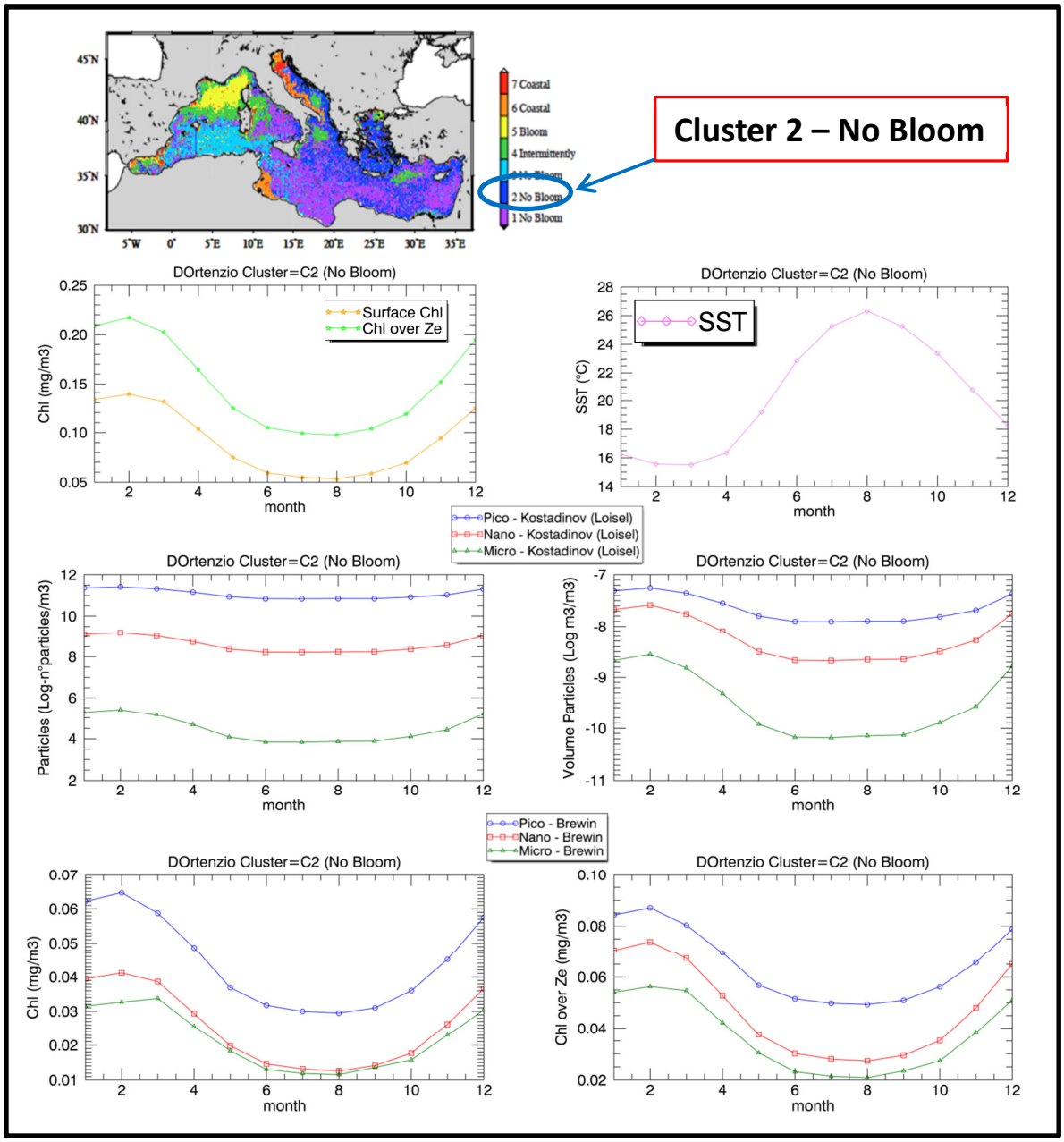

Figure 3.20 – Cluster 3: ***no blooming areas***

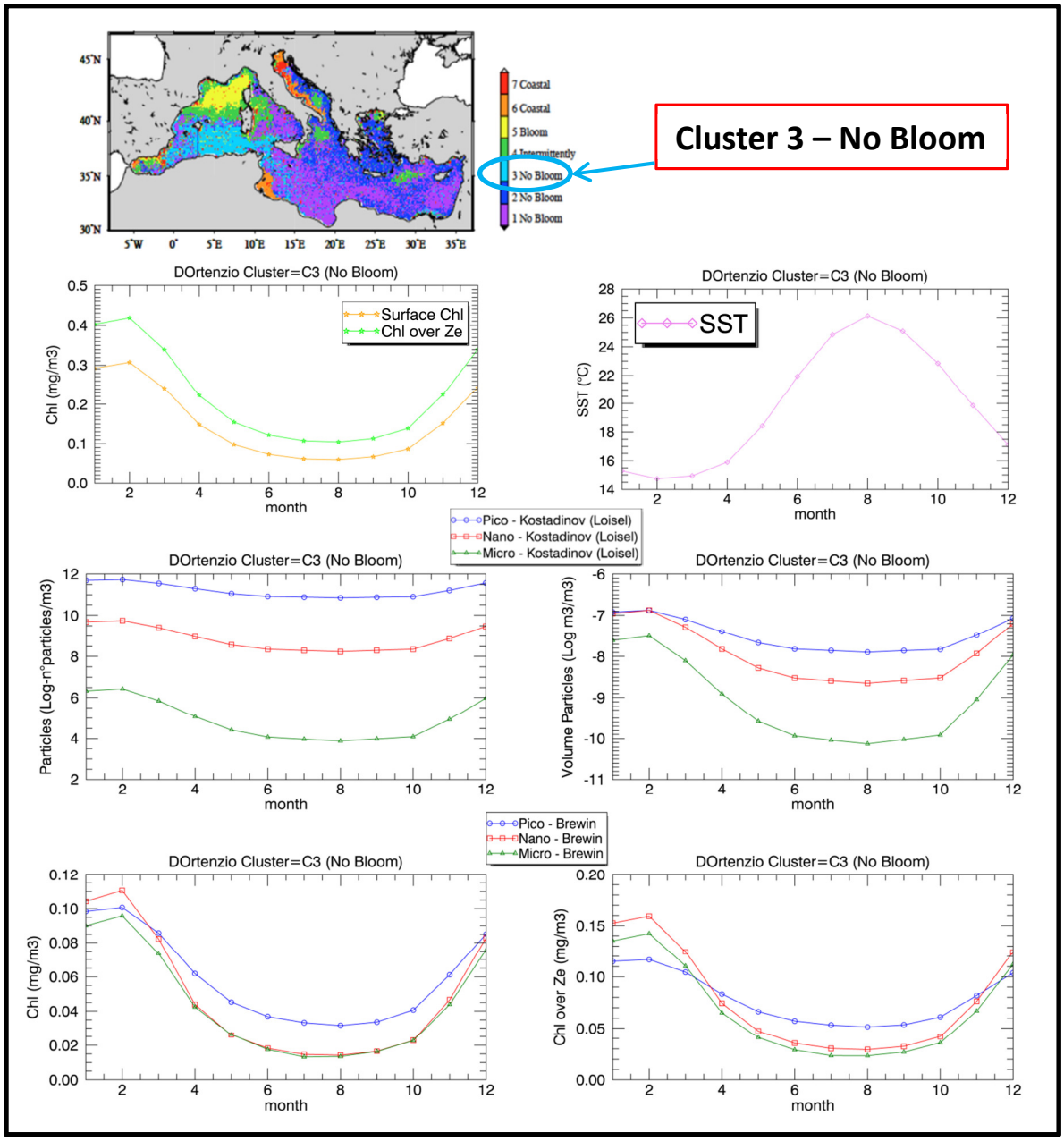

Figure 3.21 – Cluster 4: ***intermittently blooming areas***

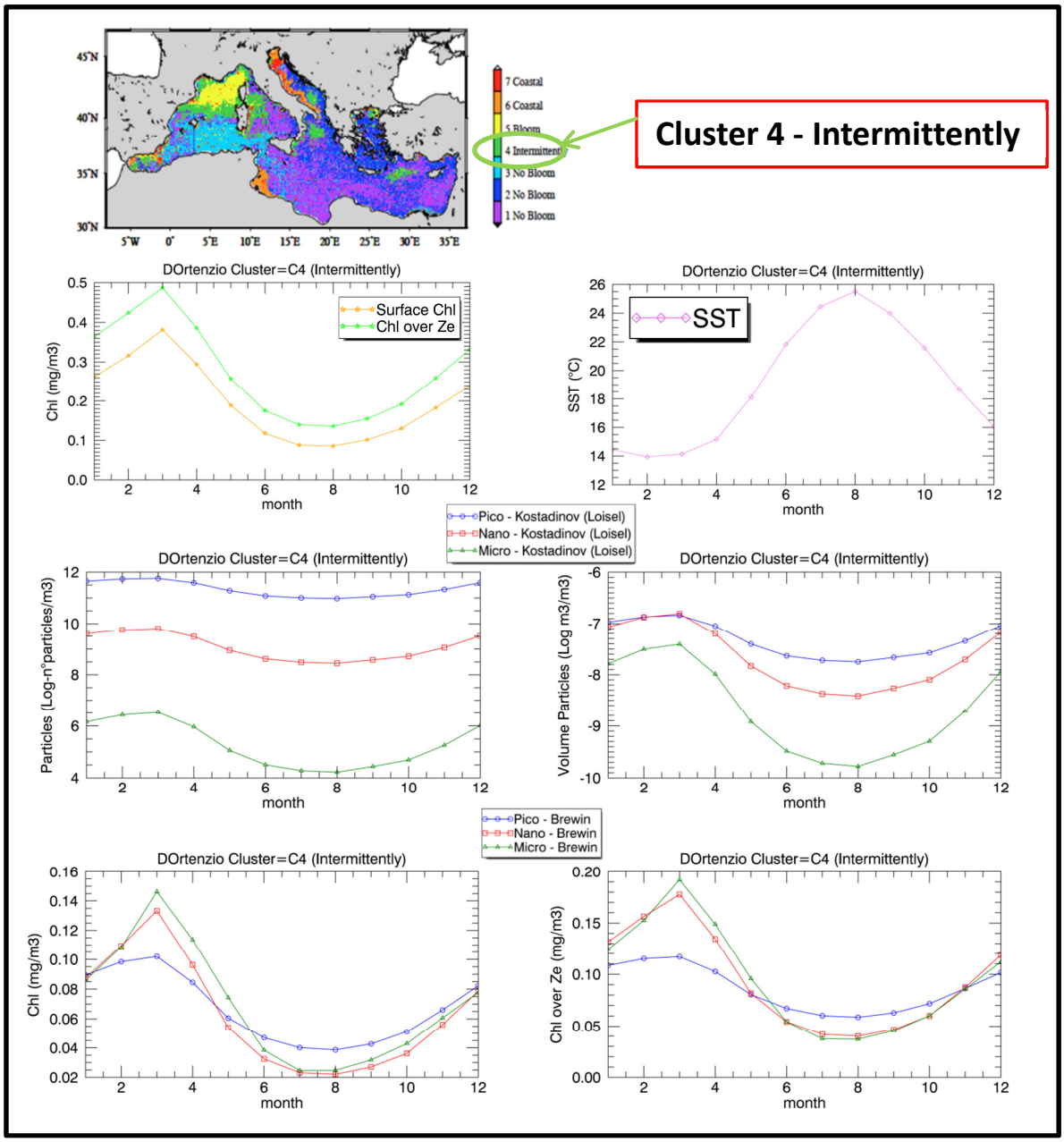

Figure 3.22 – Cluster 5: ***blooming areas***

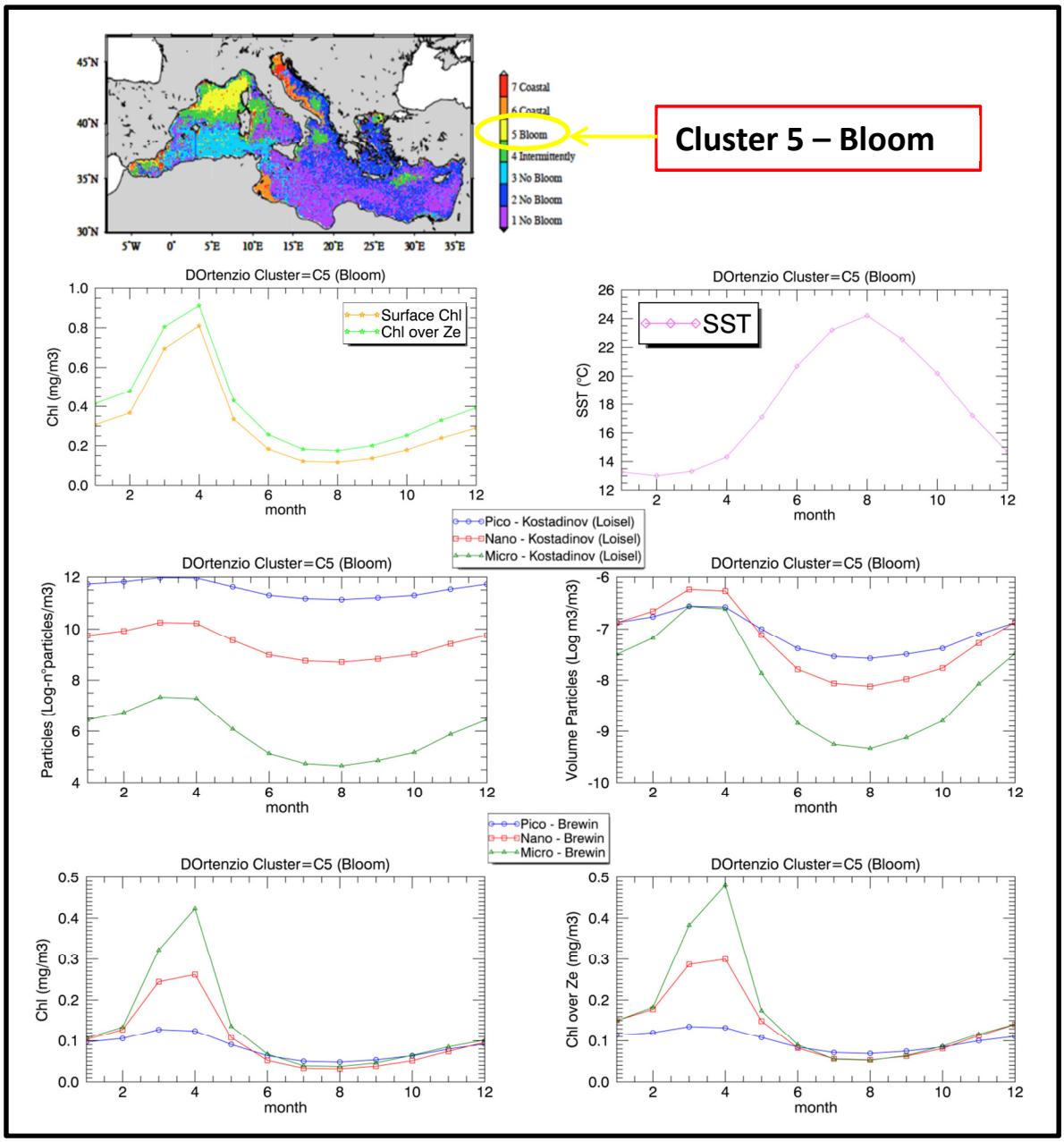

Figure 3.23 – Cluster 6: ***coastal areas***

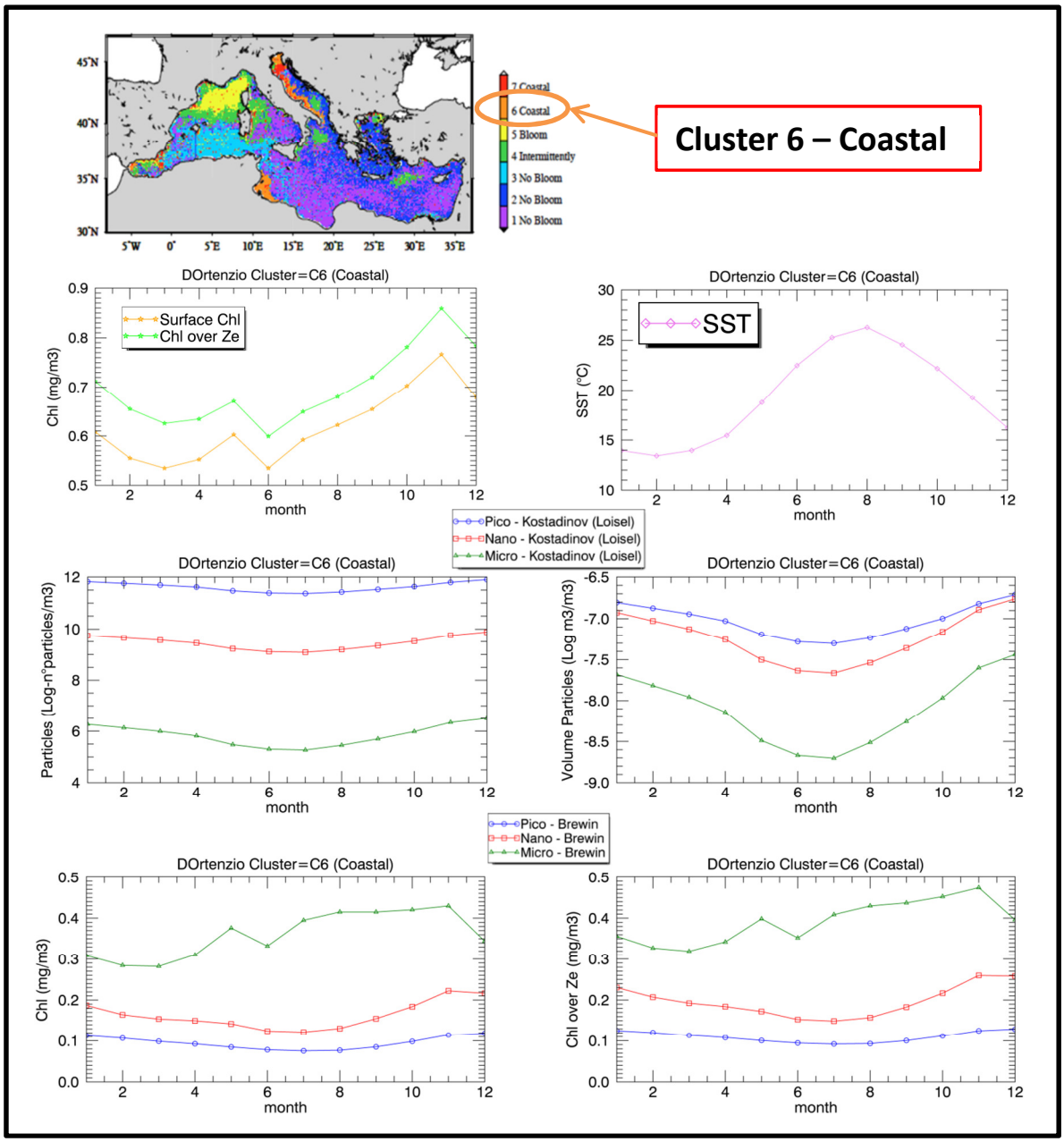

Figure 3.24 – Cluster 7: ***coastal areas***

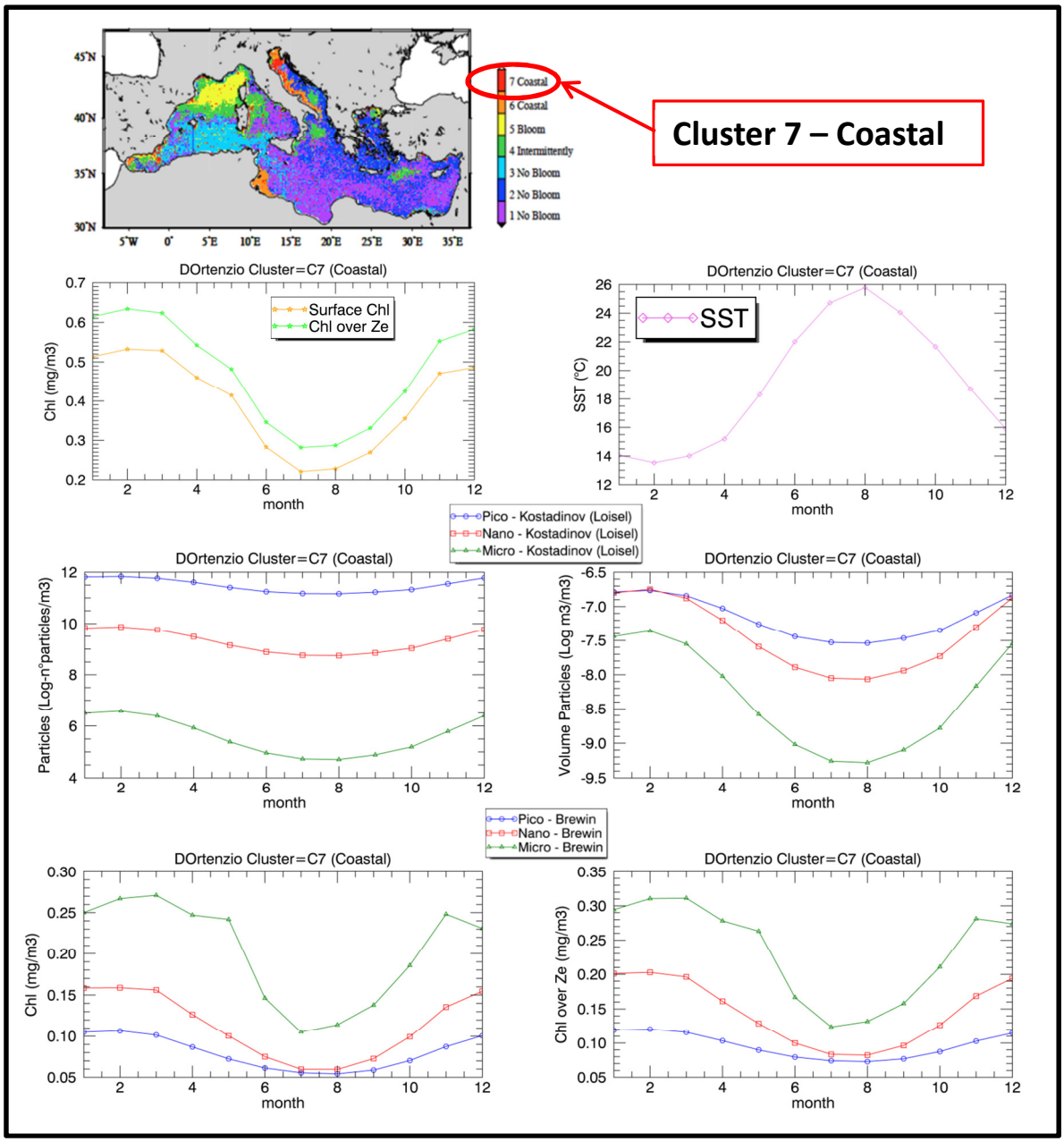

• Interannual variability

The interannual variability of micro-, nano- and pico-size classes in terms of surface Total Chlorophyll *a* concentration (Brewin et al., 2010/2011) and density of particles for the three size classes (Kostadinov et al., 2009) is shown in figures 3.25 and 3.26 for each cluster.

The plots underline the typical seasonality with maxima value in winter/spring and minima in summer. A secondary local maximum is often observed in autumn for all the three particle size components. In the case of TChl *a* fracions this secondary maximum is present only at cluster 5.

For the Brewin algorithm (fig. 3.25) pico-TChl *a* concentrations dominates always in the oligotrophic clusters 1 and 2, followed by nano and micro. In cluster 1 higher maxima value are observable in the 1999, from 2004 to 2006 and in 2009, in the cluster 2 in 1999, 2006 and 2009. In cluster 3, nano and micro contributions become increasingly important. In this regard, pico-TChl *a* concentration prevails only in summer. At higher TChl a concentrations nano dominates, followed by micro. The highest value of TChl *a* in these areas are evident in the 2003. High values are also observed in 2006 and 2009. A similar situation can be observed in cluster 4 (intermittently blooming area), but nano and micro contributes are nearly equivalent. Higher TChl a concentrations are observed in the 2005, 2006, 2009 and 2010. In the blooming (cluster 5) and coastal (clusters 6 and 7) areas the micro component of the TChl a clearly dominates, followed by the nano and pico contributions. Maxima detectable for cluster 5 are present in 2005 and 2009 and in clusters 6 and 7 in 2001. In the blooming area, the contribution of nano is also significant, although in the late winter/spring the micro is dominant. In coastal areas the micro fraction is strongly dominant on the other two size components.

The Kostadinov model shows the dominance of the pico-size particles density for all clusters, followed by nano and then by micro. The seasonality typical of the temperate areas is always evident but clearer in the more eutrophic clusters. In these clusters, the differences between minima and maxima are more pronounced, in particular for cluster 5.

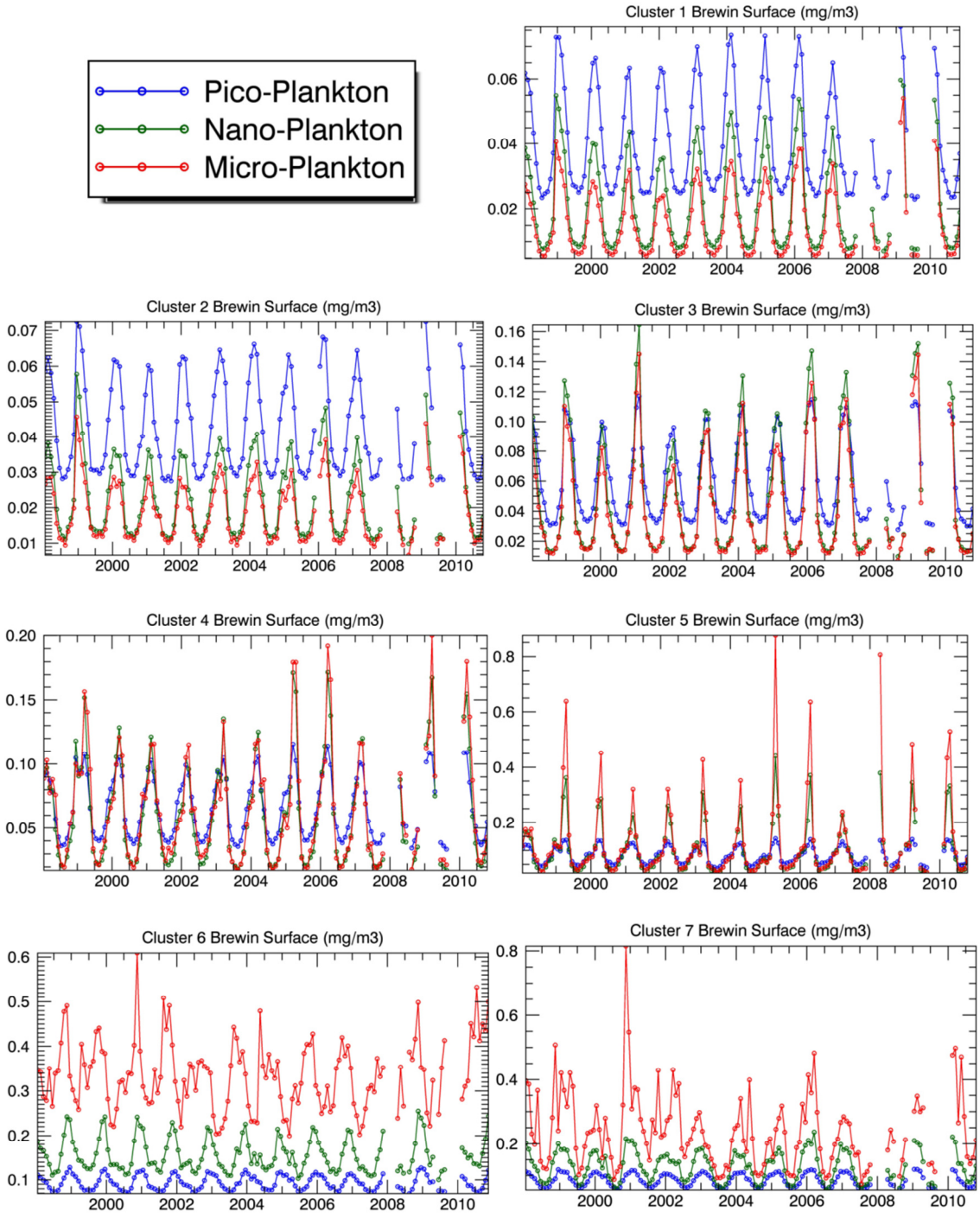

Figura 3.25 Interannual variability of micro-, nano- and pico-size classes in terms of surface Total Chlorophyll a concentration , obtained from Brewin et al., 2010/2011)

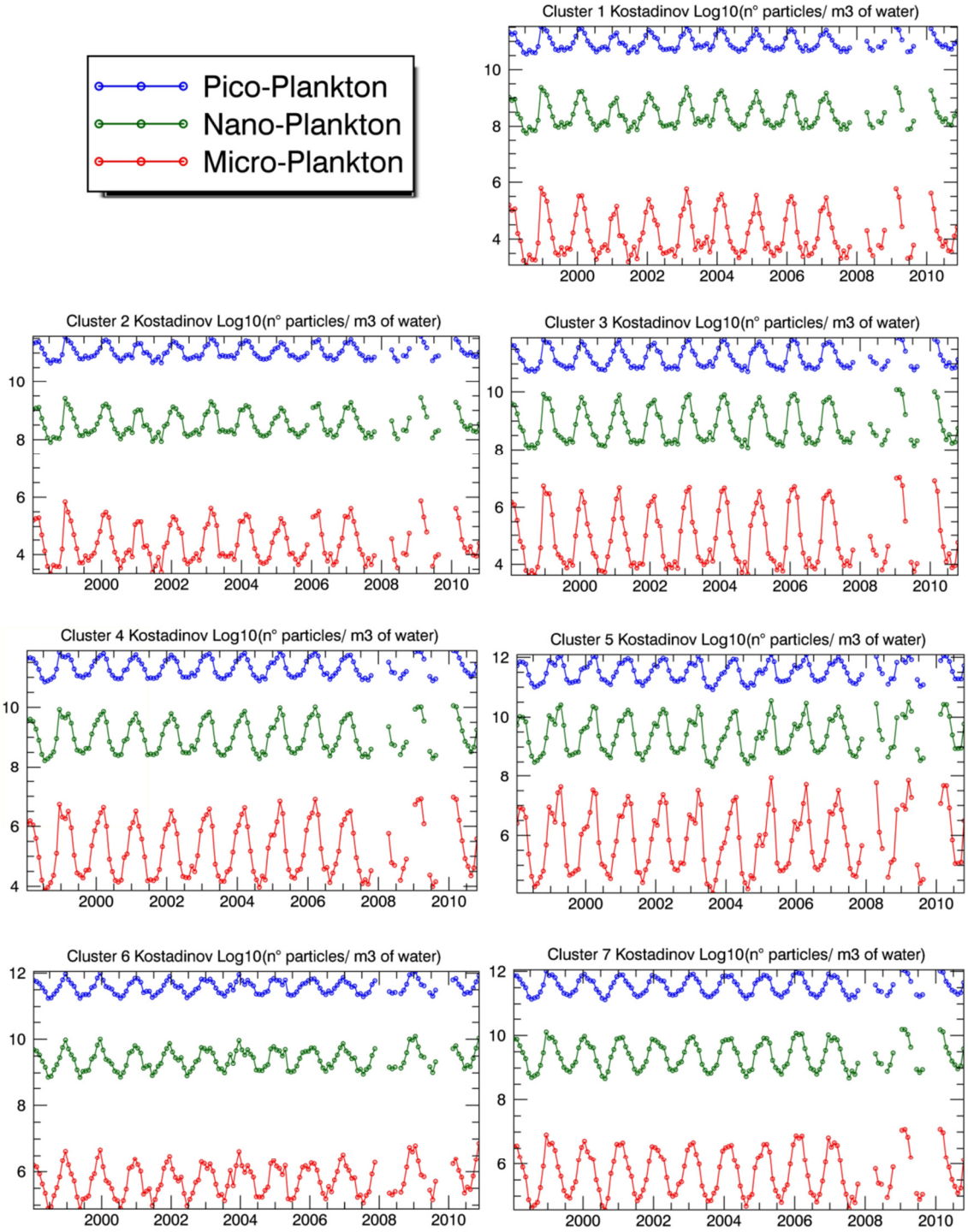

Figura 3.26 Interannual variability of the density of particles for the three size classes obtained from Kostadinov et al., 2009 algorithm

3.d A case study at Mesoscale: Sardinian sea

3.d.1 *In-situ* data

The regression analysis of the pigmentary content related to the phytoplanktonic samples collected during the WMED-BIOOPT2012 in the first 25 m of the water column shows an high linear correlation between the Total Chlorophyll *a* versus all the three size components (fig 3.27). In particular, pico-size is represented by Total Chlorophyll *b* and Zeaxanthin, nano-size by 19'-hexanoyloxyfucoxanthin, 19'-butanoyloxyfucoxanthin and Alloxanthin and micro-size by Fucoxanthin and Peridinin.

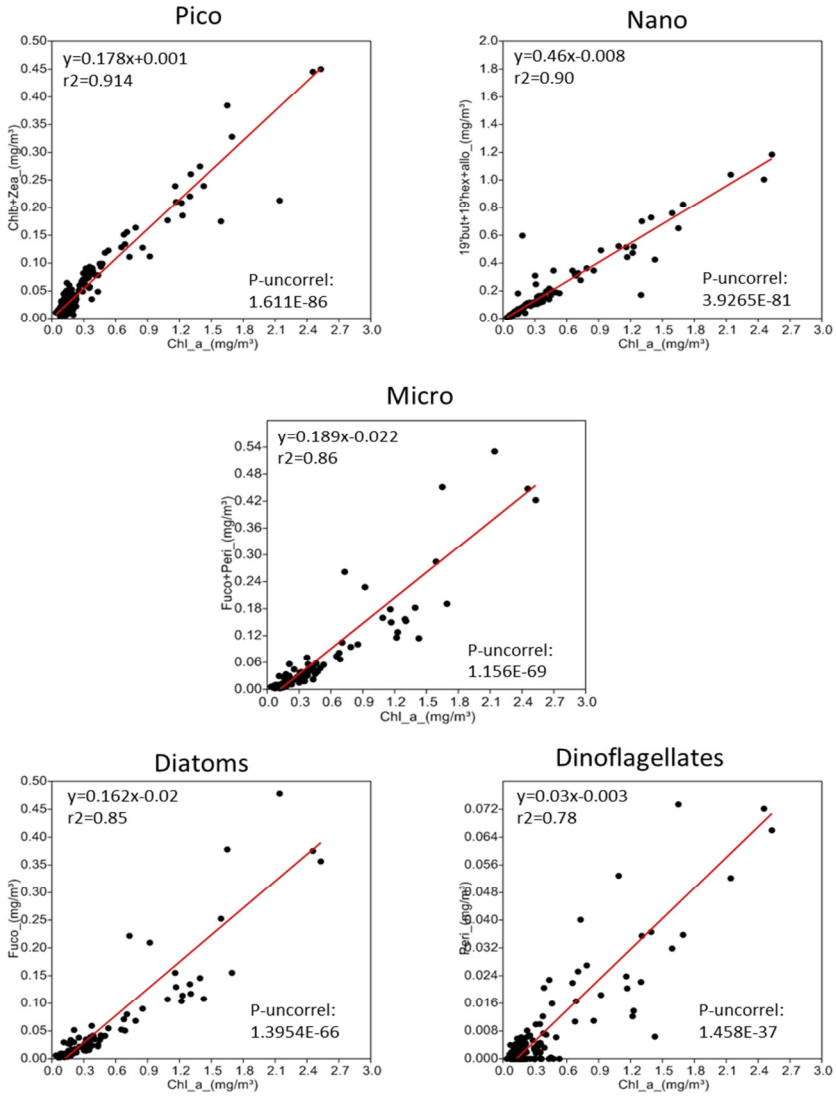

Figure 3.27 Regression analysis of the biomarker pigments versus the Total Chlorophyll *a* of samples collected during the WMED-BIOOPT2012 in the first 25 m of the water column.

The pico and nano classes correlate with the TChl a better than the micro one, and also show a smaller dispersion, indicating the presence of assemblage in which their proportion respect to the TChl a is rather constant. In the micro component, Diatoms (represented by Fucoxanthin) presents a higher linearity respect to Dinoflagellates (Peridinin).

The concentrations of the Total Chlorophyll *a* obtained by the HPLC were also been used to calibrate the fluorometer profiles. The regression curve follows (fig. 3.27):

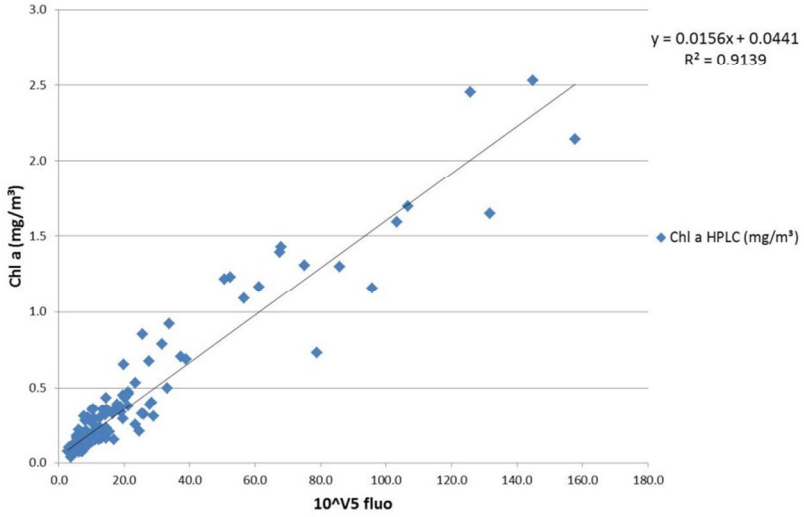

Figure 3.28 Sea Tech Fluorometer calibration from HPLC derived TChl *a*

where "V5 fluo" is the electric voltage of the fluorometer.

Samples were taken at 2 m, 10 m and 25 m. These depths were considered representative of the surface optical depth, layer involved in the Ocean Color acquisitions.

To obtain information on the distribution of the phytoplankton size and taxonomic (Dinoflagellates and Diatoms) classes in the water column deeper than 25 m, the Hirata et al., (2009) algorithm has been applied on the Total Chlorophyll *a* profiles.

Two transects, from coast to open sea, have been selected on the basis of their physical structures (transect 4 and 6, fig. 3.29 and 3.30 respectively). Both of them are characterized by an upwelling of colder and saltier waters, more marked in the transect 6. In correspondence of this doming there is also the Deep Chlorophyll Maximum, at ~ 40 m in the transect 4 (Station 54 and 55) and between 40 and 50 in the transect 6 (Station 67). The Hirata et al., (2009) algorithm has been used to estimate the contribution of each size class to the TChl *a*.

In the center of the dome micro results the size-component with the highest TChl a concentration, with a strong contribution from diatoms.

TRANSECT 4

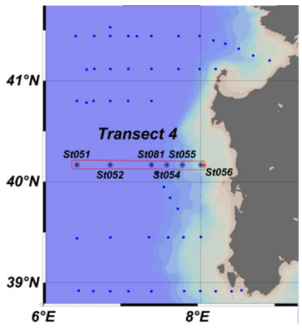

Figure 3.29 WMED-BIOOPT - Transect 4 – Vertical distribution of Physical (Temperature, Salinity and Density)and biological (Total Chlorophyll *a* and relative size and taxonomic classes composition) parameters

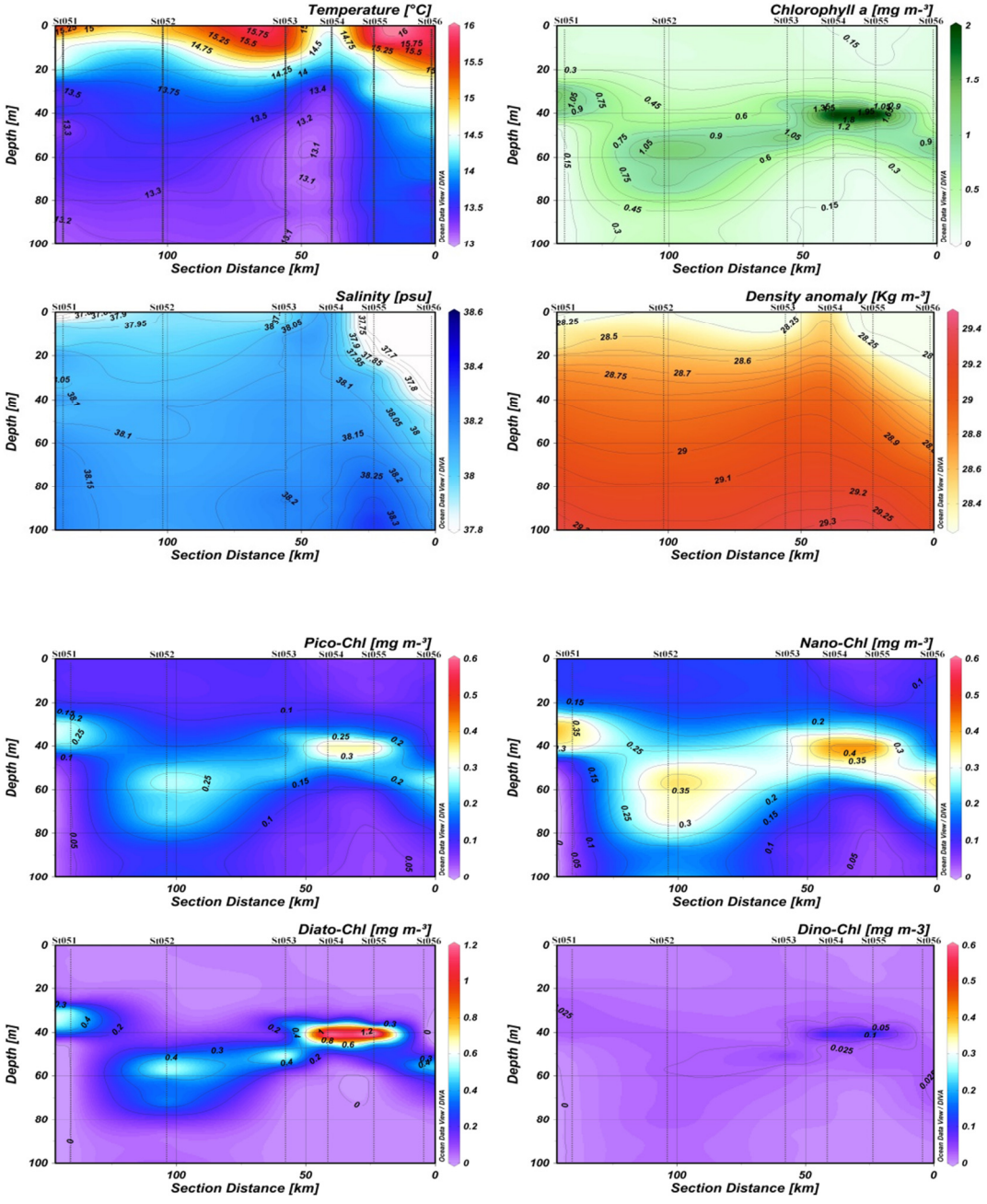

TRANSECT 6

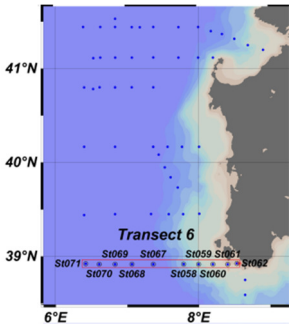

Figure 3.30 WMED-BIOOPT - Transect 6 – Vertical distribution of Physical (Temperature, Salinity and Density)and biological (Total Chlorophyll *a* and relative size and taxonomic classes composition) parameters

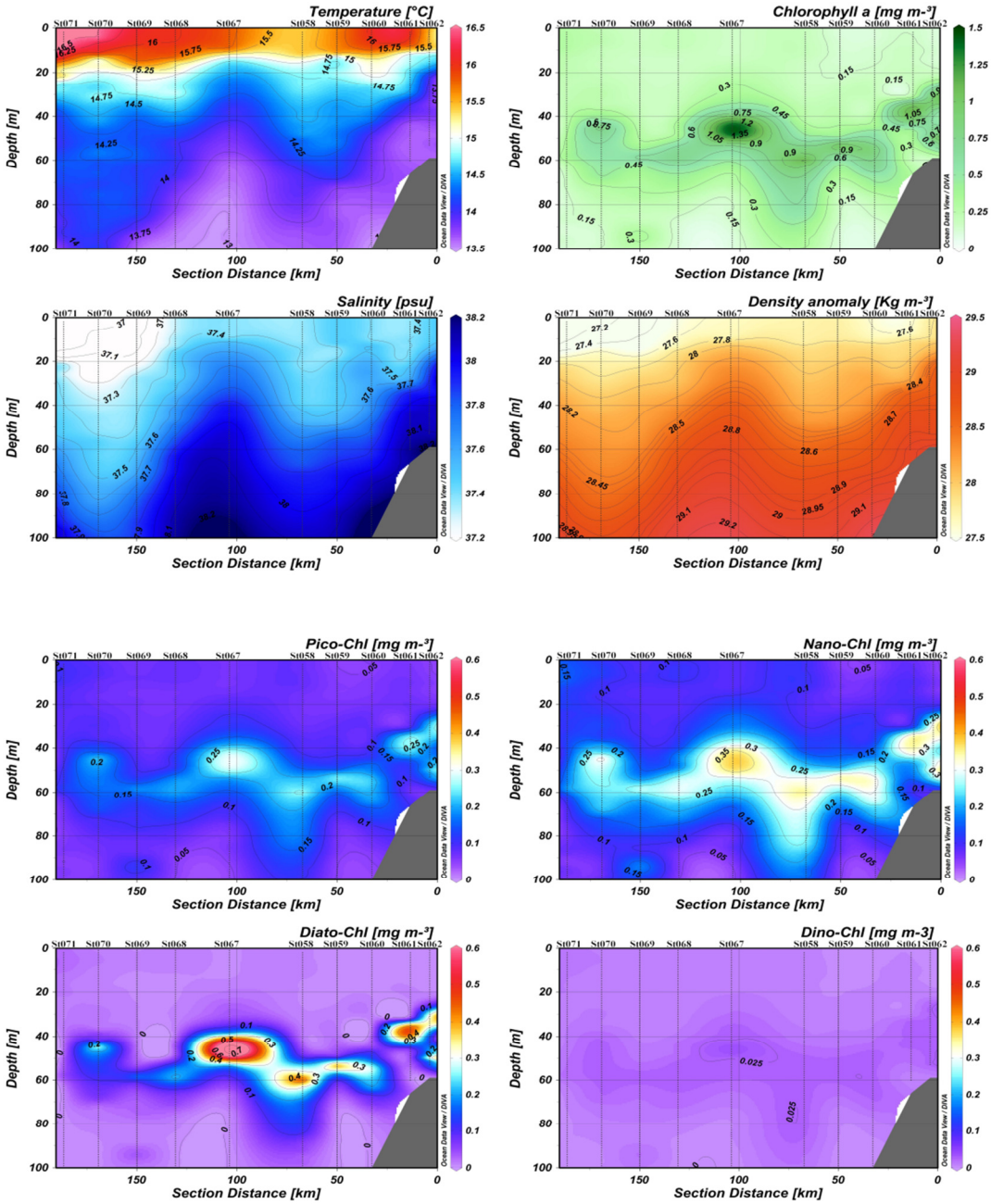

Micro is followed by nano and, at last, by pico. The contribution of the Dinoflagellates to the TChl *a* seems to be very low, not only in the DCM but also in the rest of the water column. Diatoms contribution dominates where TChl *a* concentration is higher, followed by nano and then by pico. In the areas with lower TChl *a* concentrations, as in this case the surface layer, the principal contribution can be ascribed to pico- and nano-size classes, while the micro contribution is nearly absent.

3.d.1 *Satellite* data

In figure 3.31 a Chlorophyll map representative of the cruise period is showed (27 March 2012). An important bloom area at Northwest of the Sardinia is observed. The station St067 of the transect 6 (fig. 3.32) is centered on a position probably associated to a small cyclonic structure (note the small yellow-red point in the circle of figure 3.31 at 39° N). Higher concentration of TChl *a* is evident in correspondence of the transect 4. The Hirata models has been applied to these data to obtain the TChl *a* concentrations related to the three size classes of pico-, nano- and micro-phytoplankton. This algorithm has also allowed to identify the specific contribution of Diatoms and Dinoflagellates to the TChl *a* of the micro component (fig. 3.33).

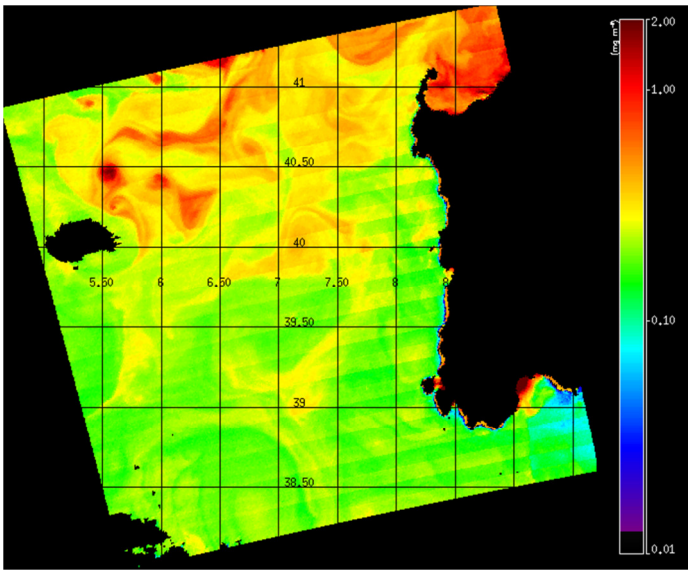

Figure 3.31 Chlorophyll map from MODIS data (27 March 2012)

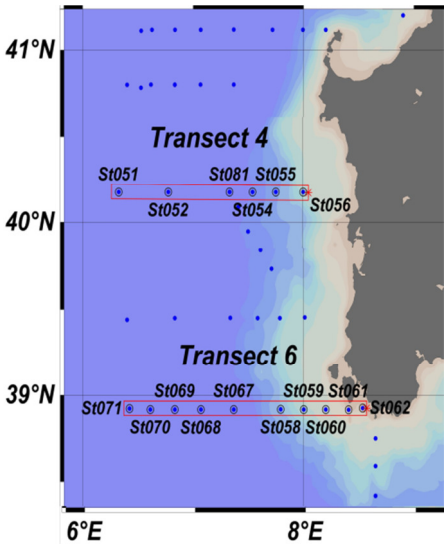

Figure 3.32 Geographyc position of the transects 4 and 6 of the WMED-BIOOPT2012 cruise and their stations

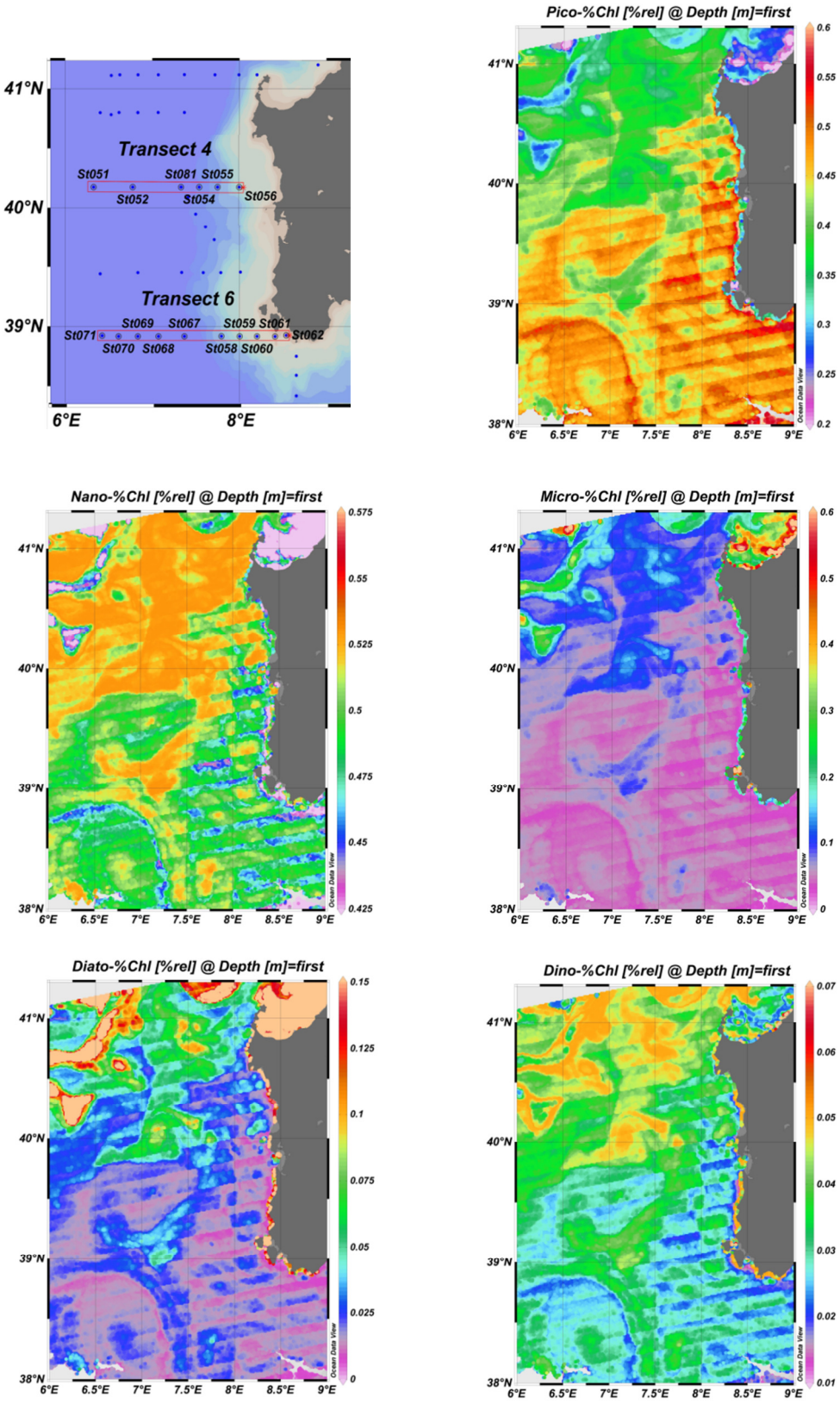

Figure 3.33 Spatial distribution of particle size (pico, nano and micro) and taxonomic (Diatoms and Dinoflagellates) classes from MODIS data (27 March 2012) from the Hirata et al., (2011) algorithm

The analysis of the MODIS images, in agreement with the previous *in situ* data (first 25 m of the water column), shows that, in correspondence of the stations involved in the DCM, the greater contribution to the Total Chlorophyll *a* is due to the nano-component (~ 0.5-0.525 mg m-³ in the transect 4 and 0.475-0.5 mg m-³ in the transect 6), immediately followed by pico-phytoplankton (~ 0.4 mg m-³ in the both transects) and then by micro (from 0 to 0.15 mg m-³ for the both transects). For the micro component, Diatoms seems to prevail in respect of Dinoflagellates. This trend is evident for the all stations of the two transects. In figure 3.34 the contributions of the all classes for each station of the two transects are reported.

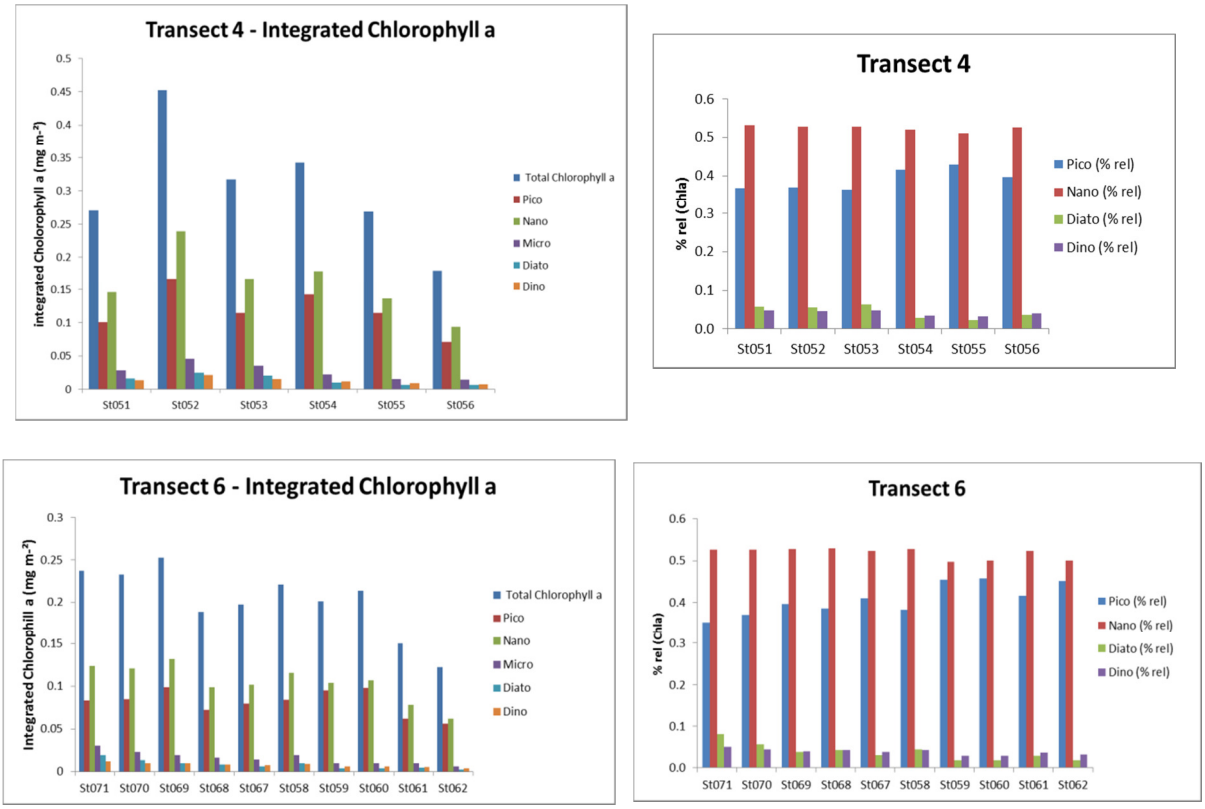

Figura 3.34 Contributes of the size (pico, nano and micro) and taxonomic (Diatoms and Dinoflagellates) classes to the Total Chlorophyll *a* in each station of the two transects.

4. DISCUSSION

The distribution of the phytoplankton size classes in terms of their relative contribution to the TChl *a* (Brewin et al., 2010/2011) and the number of sized-particles obtained from the algorithm of Kostadinov et al., (2009) reflects the general biological and physical characteristics of the Mediterranean sea.

The seasonal variability of the TChl *a* classes at basin scale shows a west-east gradient, linked to the very strong west-east gradient in subsurface nutrient concentration (Sioukou-Frangou et al., 2010) (fig. 4.1).

The climatological maps point out the typical cycle of temperate areas, with the highest concentrations in winter/early spring, when surface waters start to stabilize after the winter mixing and the phytoplankton blooms occur (Estrada, 1996), and minima concentrations in summer. The autumnal smaller bloom is not appreciable, instead TChl *a* concentration steadily from this season until the next spring bloom.

The coastal zones show a different pattern, affected by the river terrestrial input, sediment re-suspension and winds. Coastal clusters show higher productivity in November (cluster 6, Adriatic sea and Gulf of Gabès mainly, fig. 3.23), probably due to the increase of the mixed layer depth (D'ortenzio et al., 2003, fig. 4.2) and early autumn storm waves (Estrada et al., 1996). The winter cooling induces the break-up of the thermocline, with consequent deeper vertical mixing and nutrients enrichment in the surface waters in the whole Mediterranean Sea. In particular, in coastal waters, this phenomenon starts around November (Margalef and Castellví, 1967; Salat et al., 1978; Estrada et al., 1996). Land runoff is especially important in the north-western Adriatic sea, where it represents an important source of nutrients that, together with the limitation of the vertical mixing over shallow depths (Estrada et al., 1996) (fig. 4.2), tends to make this area one of the most productive, with the highest TChl *a* concentration for the whole year (see climatological maps and cluster 7, fig. 3.24).

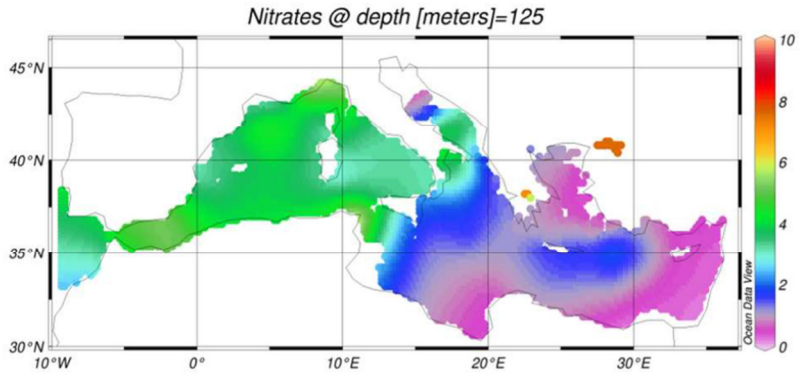

Figure 4.1 Average nitrate concentration (µmol l^{-1}) at 125m in winter (from Sioukou-Frangou et al., 2009)

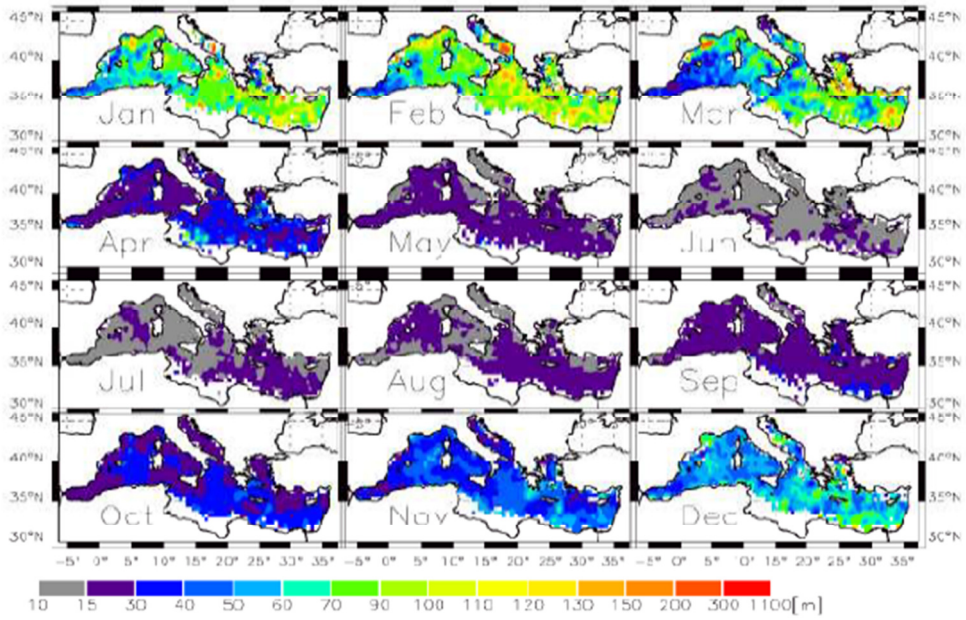

Figure 4.2 Mediterranean Mixed Layer Depth climatology (from D'Ortenzio et al., 2005)

Between the open sea areas with higher Chlorophyll concentrations, the Northwestern basin is characterized by the highest values (cluster 5, blooming area, fig. 3.22 and part of cluster 4, "intermittently blooming area", fig 3.21). In fact, the northern part of the western basin presents a cyclonic circulation, with an important doming, due to the "shelf/slope fronts" associated with the S-W northern current that flow on the continental side, and N-E currents on the Corsican, Sardinian and Balearic Islands side, which involves the Liguro-Provençal basin, the Gulf of Lion and the Balearic basin. This system plays an important role in the fertilization of this area (Estrada, 1996).

During winter cold and dry winds, the Mistral from out of the Rhone Valley and the Tramontana from the north side of the Pyrenees, occur in strong bursts of few days producing high sensible and latent heat fluxes contributing to a total ocean heat loss that can exceed 1000 Wm^{-2} (Leaman and Schott 1991). These forcing, after the precondition phase, can erode the weak stratification producing deep convection.

Fluctuations in the intensity of these phenomena have been related to inter-annual variations in primary production. The minimum of TChl *a* concentration in the center of the Gulf of Lion (fig. 3.6) in February is typical of areas of dense water formation (Santoleri et al., 2003). In this area, the mixing and down-welling of surface waters, causes a decrease of TChl *a* concentrations (Colella, 2006).

The Alboran Sea is another main zone that contributes to the productivity. Here, high Chlorophyll *a* concentrations are found all the year (see chapter 3, seasonal maps). This area is grouped into multiple clusters (3, 4, 5 and 6, see fig. 3.17) due to its complex hydrography (fig. 4.3). It is characterized by turbulent mixing in the Gibraltar Strait, that supplies nutrients to the euphotic layer by the Mediterranean water outflowing and by upwelling and frontal zone bounded to the anticyclonic gyres produced by the inflow of the Atlantic Water. Furthermore, the contribution of the Atlantic current, so enriched of nutrients, and strong dynamic activity along the Algerian coast able to generate meanders and eddies, can support phytoplankton growth (Estrada et al., 1996; Minas et al., 1984; Lohrenz et al., 1988; Taupier-Letage and Millot, 1988).

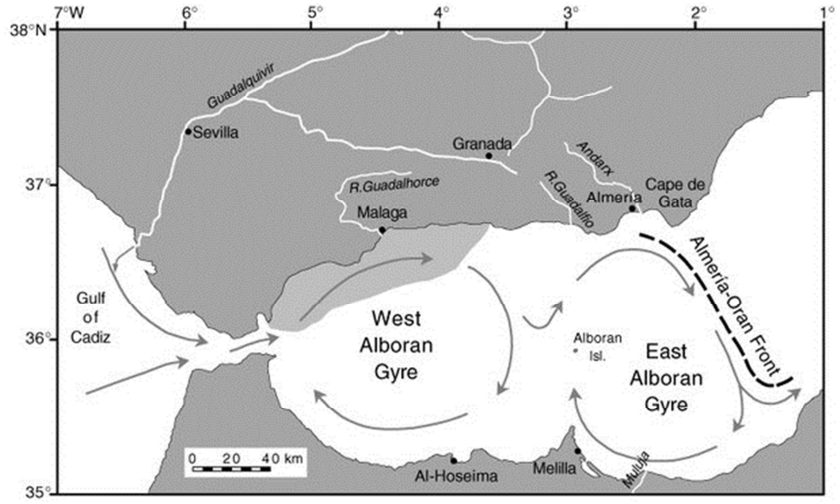

Figura 4.3 Alboran Sea hydrographic features [8]

Other important areas for the productivity are the cyclonic area in the North Tyrrhenian Sea, cyclonic Rhodes gyre in the North-Western Levantine Sea and the South Adriatic gyre with convective events during winter.

Lastly, intermittent coastal upwelling takes place in the Alboran Sea, Balearic Sea, Straits of Sicily, East Adriatic Sea and North-East Aegean Sea (Sioukou-Frangou et al., 2010), thus explaining the higher concentration of TChl *a* compared to their respective surrounding areas.

The distribution of the particles resulting from the Kostadinov model shows that small particles are always more abundant than the large ones. This is evidenced in all seasonal maps and in the seasonal and inter-annual cluster trends. A wide bibliography supported this observations (Chisholm et al., 1992; Sheldon and Parson, 1967; Sheldon et al., 1972). This qualitative inverse relationship between the size and local abundance of the organisms constitutes the conceptual base for the "ecological pyramid" of Elton, and its implications are involved in the analysis of food web dynamics (Chisholm et al., 1992; Platt and Denman, 1977,1978).

The Brewin et al., (2010/2011) approach supplies different information. It gives the fraction of each size classes to the Total Chlorophyll *a*. From the analysis of the seasonal and inter-annual variability of the three size classes it can been inferred that the relative micro-phytoplankton contribution increases with the increase of the Total Chlorophyll *a*. In the coastal areas, this is evidenced in particular in the North Adriatic Sea, in the Gulf of Gabès and in the South-Eastern area of the Levantine basin influenced by the outflow of the Nile river. High values of micro-TChl *a* are also found in the open sea in the North-Western basin in late winter/spring time, in correspondence to the areas involved in the phytoplanktonic bloom. Instead, the contribution of the small cells increases as the Total Chlorophyll a decreases. So the more oligotrophic eastern basin presents the higher pico-TChl *a* values for the whole year, and higher values are also present in the western basin in late-spring and summer. In general, nano-Chl *a* distribution seems to be quite constant during the whole year, with higher values in spring and late autumn/winter months, and lower in summer.

The predominance of the pico-phytoplankton in terms of particle number in the oligotrophic waters is well-known, also due to the effect of molecular diffusion on the feeding of the large cell in very low nutrient condition (Chisholm, 1992; Raven, 1998). The greater surface/volume ratio is another advantage in the floating of small cells. Oligotrophic regime is

also linked to the increase of the column water stratification in late spring-summer (see fig. 4.2). In this case, the nutrients are quickly depleted and at the same time the greater cells tend to sink faster than the smaller ones.

The number of pico-size particles is also predominant in the eutrophic waters, in which the pico-phytoplankton is advantaged by its r-strategy (Chisholm, 1992; Raven, 1998). But in situation of high concentrations of nutrients and mixing, as in late winter/early spring, Diatoms density, which have r-strategy too (Margalef et al., 1978; Estrada et al. 1996), also increase, concurring to the Total Chlorophyll *a* concentration. Diatoms are the principal components of the micro-phytoplankton, and thanks to the relations existent between size and pigmentary content, their relative contribute to the Total Chlorophyll *a* can be higher although with a lower number of particles.

The capability of the remote sensing techniques to detect biological information is limited to the first optical depth of the water column. This is also evident in the comparison of the vertical distribution of the *in-situ* collected data related to the WMED-BIOOPT2012 cruise and the corresponding satellite data. The match-up between these data shows that, in the studied stations, the community structure in terms of size and taxonomic classes (Diatoms and Dinoflagellates), as inferred from remote sensing, reflects well the *in-situ* pigmentary composition obtained from the first optical depth.

On the other hand, an ecological approach needs to take into account the whole euphotic layer. Having no means to exactly derive the actual vertical distribution of the chlorophyll concentration from surface measurements, a second choice is to apply a statistical approach that can provide the most probable chlorophyll vertical profile given the surface chlorophyll concentration.

The optical model of Morel and Berthon (1989) was applied in this study, with the aim to predict information on the vertical distribution of phytoplankton communities from chlorophyll profiles.

When the Brewin model is extended to the entire euphotic layer the contribution of the pico-component on the Total Chlorophyll *a* decrease, in favor of nano and micro ones due to the presence of the Deep Chlorophyll Maximum (DCM). This is also consistent with a scenario in which cells of greater dimensions tend to sink more than the small ones, in particular with the increase of the stratification.

5. CONCLUSIONS and PERPSECTIVES

In the present work three of the principal global models for the determination of the PSCs by satellite techniques has been studied, with the aim to investigate the Phytoplankton Size Classes distribution in the Mediterranean Sea. Two empirical model, Brewin et al., (2010/2011) and Hirata et al., (2010), has been tested by a consistent Mediterranean in-situ pigment subset obtained from SeaBASS dataset. On the basis of previous works (Gieskes et al., 2008; Vidussi et al. 2001; Uitz et al., 2006) new coefficients for the determination of the in-situ Mediterranean PSCs has been developed by a multiple regression analysis. Comparing the two models with these *in-situ* data, statistical analysis shows that Brewin algorithm perform better than the Hirata one's. So the Brewin model with the theoretical Kostadinov et al., (2009) algorithm, have been applied to a reanalysis of daily Chlorophyll *a* estimates, carried out by the MyOcean OC TAC, for the entire SeaWiFS mission (1998 - 2010).

The products obtained, displayed by climatological maps of the whole Mediterranean basin and seasonal trends centered on the D'Ortenzio Cluster areas, shows the predominance contribution of pico-phytoplankton on the TChl *a* all-around the year in the most oligotrophic areas and times. Instead the TChl *a* in coastal regions is always dominated by micro-phytoplankton. Intense bloom spring areas show an alternation. The pico is the principal component almost all year, except in the late winter-spring period when micro and nano contribute more to the higher TChl *a* concentrations. In terms of number of particles, the Kostadinov model shows a predominance of the pico-size particles in the whole basin. These considerations are in agreement with the main works on phytoplankton ecology (Chisholm et al., 1992; Raven et al., 1998) and with the Mediterranean phytoplankton distribution (i.e. Siokou-Frangou et al., 2010; Uitz et al., 2012 etc.). These two algorithms give different kind of information complementary to each other.

These results validate and support the importance of the satellite techniques also in the synoptic identification of the phytoplankton dimensional groups. Although the remote sensing observation is related only to the first optical depth of the water column, the information that

it's able to supply on the phytoplantonic dynamics and community structure are precious and represent a fundamental tool to investigate the marine ecosystem.

Future developments of this work want to take into account other theoretical algorithms (i.e. Alvain et al., 2005; 2009; Sathyendranath et al., 2004, etc) and a more ecological approach (Raitsos et al., 2008). The goal is to identify the more robust algorithm, able to outline the Mediterranean phytoplankton community in a more accurate way, with the aim of improving the understanding of its dynamics and contribute to a better estimate of the marine Primary Production.

Future intent is to extend this investigation to a longer time series, that also involves MODIS and MERIS data, in view of the ESA – Ocean Colour Climate Change, initiative that will realize a unique and consistent Ocean Colour time series.

Bibliography

Basset, A., Sangiorgio, F. and Sabetta, L., 2009. Nuovi approcci metodologici per la classificazione dello stato di qualità degli ecosistemi acquatici di transizione. Metodologie ISPRA

Basset, A., Sabetta, L., Sangiorgio, F., Pinna, M., mingoni, D., Fanizzi, F., Barbone, E., Galuppo, N., Fonda Umani, S., Reizopoulou, S., Nicolaidou, A., arvanitidis, C., Moncheva, S., Trajanova, A., Georgescu, L. and Beqiraj, S., 2008. Biodiversity conservation in Mediterranean and Black Sea lagoons: a trait-oriented approach to benthic invertebrate guilds. Aquatic conservation: marine and freshwater ecosystems. 18: S4-S15 (2008)

Berthon, J.-F., Zibordi, G., 2004. Bio-optical relationships for the northern Adriatic Sea. Int. J. Remote Sens., 25, 1527-1532

Brewin, R. J., Sathyendranath, S., Hirata, T., Lavender, S. J., Barciela, R. M., & Hardman-Mountford, N. J., 2010. A three-component model of phytoplankton size class for the Atlantic Ocean. Ecological Modelling, 221(11), pp. 1472-1483.

Brewin, R. J.W., Hardman-Mountford, N. J., Lavender, S. J., Raitsos, D. E., Hirata,T., Uitz, J., Devred, E., Bricaud, A., Ciotti, A., Gentili, B., 2011. An intercomparison of bio-optical techniques for detecting dominant phytoplankton size class from satellite remote sensing. Remote Sensing of Environment. 115(2), pp. 325-339.

Brewin, R. J. W., 2011. Detecting phytoplankton size class using satellite earth observation. Ph.D. Thesis

Brown, J. H., Gillooly, J. F., Allen, A. P., Savage, V. M. and West, G. B., 2004. Toward a metabolic theory of ecology. Ecology, 85(7), pp. 1771-1789

Casey, K.S., T.B. Brandon, P. Cornillon, and R. Evans, 2010. The Past, Present and Future of the AVHRR Pathfinder SST Program. Oceanography from Space: Revisited, eds. V. Barale, J.F.R. Gower, and L. Alberotanza, Springer. DOI: 10.1007/978-90-481-8681-5_16

Chisholm, S. W., 1992. Phytoplankton size. In: Primary Productivity and Biogeochemical Cycles in the Sea. Edited by P.G. Falkowski and A.D. Woodhead. Plenum Press, New York.

Claustre, H., & Marty, J. C., 1995. Specific phytoplankton biomasses and their relation to primary production in the tropical North Atlantic. Deep Sea Research Part I: Oceanographic Research Papers, 42(8), pp. 1475-1493.

Colella, S., 2007. La produzione primaria nel Mar Mediterraneo da satellite: sviluppo di un modello regionale e sua applicazione ai dati SeaWiFS, MODIS e MERIS. [PhD Thesis].

D'Alimonte, D., Mélin, F., Zibordi, G., Berthon, J.-F., 2003. Use of the novelty detection technique to identify the range of applicability of the empirical ocean color algorithms. IEEE Trans. Geosci. Remote Sens., 41, 2833-2843.

D'Ortenzio, F., Iudicone, D., de Boyer Montegut, C., Testor, P., Antoine, D., Marullo, S., Santoleri, R., Madec, G., 2005. Seasonal variability of the mixed layer depth in the Mediterranean Sea as derived from in situ profiles. Geophysical Research Letters, 32(12).

D'Ortenzio F. and Ribera d'Alcalà, M., 2009. On the trophic regimes of the Mediterranean Sea: a satellite analysis. Biogeosciences, 6, 1-10

Della Croce, N., Vietti, R. C., Danovaro, R., 1997. Ecologia e protezione dell'ambiente marino costiero. UTET libreria.

Devred, E., Sathyendranath, S. V. S. V. S., Stuart, V., Maass, H., Ulloa, O., Platt, T., 2006. A two-component model of phytoplankton absorption in the open ocean: Theory and applications. Journal of Geophysical Research: Oceans (1978–2012), 111(C3).

Estrada, M., 1996. Primary production in the northwestern Mediterranean. Scientia Marina, 60 (Supl.2): 55-64

Estrada, M. and Berdalet, E., 1996. Phytoplankton in a turbulent world. Scientia Marina, 61 (Supl. 1): 125-140

Falkowski, P. G., Scholes, R. J., Boyle,E., Canadell, J., Canfield, D., Elser, J., Gruber, N., Hibbard, K., Högberg, P., Linder, S., Mackenzie, F. T., Moore III, B., Pedersen, T., Rosenthal, Y., Seitzinger, S., Smetacek, V., and Steffen, W., 2000. The Global Carbon Cycle: A Test of Our Knowledge of Earth as a System. Science Vol. 290

Falkowski, P. G., 2001. Biogeochemical Cycles. Encyclopedia of Biodiversity. Academic Press

Falkowski, P. G., 2002. The Ocean's Invisible Forest. Scientific American

Falkowski, P. G. & Raven, J. A., 2007. Aquatic Photosynthesis. Princeton University Press,Second Edition

Gieskes, W. W. C., Kraay, G. W., Nontji, A., & Setiapermana, D., 1988. Monsoonal alternation of a mixed and a layered structure in the phytoplankton of the euphotic zone of the Banda Sea (Indonesia): A mathematical analysis of algal pigment fingerprints. Netherlands Journal of Sea Research, 22(2), pp. 123-137.

Goericke., R., & Repeta, D. J., 1993. Chlorophylls a and b and divinyl-chlorophylls a and b in the open subtropical North Atlantic Ocean. Mar. EcoL Prog. Ser, 101, pp. 307-313.

Gordon, H. R., Brown, O. B., Ewans,R. H., Brown, J. W., Smith, R. C., Baker, K. S., Clark, D. K., 1988. A semianalytical radiance model of ocean color, J. Geophys. Res., 93 (10) pp. 909–10, 924.

Hirata, T., Hardman-Mountford, N. J., Brewin, R. J. W., Aiken, J., Barlow, R., Suzuki, K., Isada, T., Howell, E., Hashioka, T., Noguchi-Aita, M., Yamanaka, Y., 2011. Synoptic relationships between surface Chlorophyll-a and diagnostic pigments specific to phytoplankton functional types. Biogeosciences, 8(2), pp. 311-327.

IOCCG (2000). Remote Sensing of Ocean Colour in Coastal, and Other Optically-Complex, Waters. Sathyendranath, S. (ed.), Reports of the International Ocean-Colour Coordinating Group, No. 3, IOCCG, Dartmouth, Canada.

JGOFS. June 1994. Chapter 14. Measurement of Chlorophyll a and Phaeopigments by Fluorometric Analysis. JGOFS Protocols. 5 pp

Junge, C. E. 1963, Air Chemistry and Radioactivity, Academic, New York.

Kirk, Jonn T. O., 1983. Light and photosynthesis in aquatic ecosystems. Cambridge University Press

Kostadinov, T.S., Siegel, D.A., Maritorena, S., 2009. Retrieval of the particle size distribution from satellite ocean color observations. Journal of Geophysical Research 114, C09015.

Lacombe, H., Gascard, J. C., Gonella, J., & Bethoux, J. P., 1981. Response of the Mediterranean to the water and energy fluxes across its surface, on seasonal and interannual scales. Oceanologica Acta, 4(2), pp. 247-255.

Lazzara L., Bianchi F., Falcucci M., Hull V., Modigh M., Ribera d'Alcalà M. (1990), Pigmenti clorofilliani. Nova Thalassia. 11: 207-223

Leaman K.D., and F. Schott, 1991: Hydrographic structure of the convection regime in the Gulf of Lions: Winter 1987. J. Phys. Oceanogr., 21, 573–596.

Lohrenz, S. E., Arnone, R. A., Wiesenburg, D. A., DePalma, I. P., 1988. Satellite detection of transient enhanced primary production in the western Mediterranean Sea (No. NORDA-JA-

333: 044: 88). NAVAL OCEAN RESEARCH AND DEVELOPMENT ACTIVITY STENNIS SPACE CENTER MS.

Lohrenz, S. E., Wiesenburg, D. A., de Palma, I. P., Johnson, K.S., Gustafson., D.E. – 1988. Interrelationships among primary production, chlorophyll, and environmental conditions in frontal regions of the Mediterranean Sea. Deep-Sea Res., 35, pp. 793-810.

Margalef, R., 1967. Some concepts relative to the organization of plankton. Oceanography and Marine Biology: an Annual Review, 5.

Margalef, R., 1997. Our Biosphere. Excellence in Ecology, 10. Edited by O. Kinne. Ecology Institute, Oldendorf (Germany).

Margalef, R., 1978. Life-forms of phytoplankton as survival alternatives in an unstable environment. Oceanol. Acta, 1: 493-509.

Margalef, R. and J. Castellví, 1967. Fitoplancton y producción primaria de la costa catalana, de julio de 1966 a julio de 1967. Inv. Pesq., 31: 491-502.

Mann, K. H. and Lazier, J. R., 2006. Dynamics of Marine Ecosystems: Biological-Physical Interactions in the Oceans, 3rd edn., Wiley-Blackwell, Inc..

McGillicuddy, D. J. Jr, Robinson, A. R., Siegel, D. A., Jannasch, H. W., Johnson, R., Dickey, T. D., McNeil, J., Michaels, A. F. and Knap, A. H., 1998. Influence of mesoscale eddies on new production in the Sargasso Sea. Nature 394: 263-266.

McGillicuddy, D. J. Jr, Johnson, R., Siegel, D. A., Michaels, A. F., Bates, N. R. and Knap, A. H., 1999. Mesoscale variations of biogeochemical properties in the Sargasso Sea. Journal of Geophysical Research, 104: 13381-13394.

Millot, C., Taupier-Letage, I., 2005. Circulation in the Mediterranean sea. In The Mediterranean Sea. Springer Berlin Heidelberg. pp. 29-66

Minas, H. J., Coste, B., Minas, M., 1984. Océanographie du détroit de Gibraltar et des parages annexes. Le Courr. du CNRS, 57: 10-18. Cent, Natl. de Rech. Sci. Paris

Mobley, Curtis D., 2004. Light and Water, Radiative Tranfer in Natural Waters. CD format

Morel, A., Berthon, J. F., 1989. Surface pigments, algal biomass profiles, and potential production of the euphotic layer: Relationships reinvestigated in view of remote-sensing applications. Limnol. Oceanogr, 34(8), pp. 1545-1562.

Mouillot, D., Spathris, S., Reizopoulou, S., Laugier, T., Sabetta, L., Basset, A., Do Chi, T., 2006. Alternatives to taxonomic-based approaches to assess changes in transitional water communities. Aquatic Conservation: Marine and Freshwater Ecosystems, 16: 469-482.

Organelli, E., Nuccio, N., Massi, L., 2007. Individuazione dei principali gruppi fitoplanctonici in base al loro contributo di assorbimento e retrodiffusione nella riflettanza. Ecologia Limnologia e Oceanografia: quale futuro per l'ambiente: 181-187. Ancona, 17 - 20 settembre 2007.

Platt, T., and Denman, K. L., 1977. Organization in the pelagic ecosystem, Helgolander wiss. Meeresunters, 30:575

Platt, T., and Denman, K. L., 1978. The structure of pelagic marine ecosystems, Rapp. P.-V. Reun. Cons. Perm. Int. Expor. Mer., 173:60

Raven, J. A., 1998. Small is beautiful. Functional Ecology, 12: 503-513.

Reynolds, R. A., Stramski, D., Mitchell B. G., 2001. A chlorophyll-dependent semianalytical reflectance model derivedfrom field measurements of absorption and backscattering coefficients within the Southern Ocean. J. Geophys. Res., 106 pp. 7125-7138.

Malanotte-Rizzoli, P., Artale, V., Borzelli-Eusebi, G. L., Brenner, S., Crise, A., Gacic, M., Kress, N., Marullo, S., Ribera d'Alcala, M., Sofianos, S., Tanhua, T., Theocharis, A., Alvarez, M., Ashkenazy, Y., Bergamasco, A., Cardin, V., Carniel, S., Civitarese, G., D'Ortenzio, F., Font, J., Garcia-Ladona, E., Garcia-Lafuente, J. M., Gogou, A., Gregoire, M., Hainbucher, D., Kontoyannis, H., Kovacevic, V., Krasakapoulou, E., Krokos, G., Incarbona, A., Mazzocchi, M. G., Orlic, M., Ozsoy, E., Pascual, A., Poulain, P.-M., Roether, W., Rubino, A., Schroeder, K., Siokou-Frangou, J., Souvermezoglou, E., Sprovieri, M., Tintore, J., and Triantafyllou, G., 2014. Physical forcing and physical/biochemical variability of the Mediterra-nean Sea : A review of unresolved issues and directions for future re-search. Special Issue: Physical, chemical and biological oceanography of the Mediterranean Sea. Handling Topic Editor: Dr. Mario Hoppema, mario.hoppema@awi.de. Status: Accepted Waiting for File Upload (OS).

Robinson, A. R., & Golnaraghi, M., 1995. The physical and dynamical oceanography of the Mediterranean sea.Ocean processes in climate dynamics: Global and Mediterranean examples, edited by P. Malanotte-Rizzoli and A. R. Robinson (pp. 255–306). Dordrecht, The Netherlands: Kluwer Academic Publishers.

Robinson, A. R., & Leslie, W. G., 2001. Mediterranean Sea circulation. Academic Press. pp. 1-19

Robinson, I. S., (2004). "Measuring the oceans from space: the principles and methods of satellite oceanography". Berlin, Germany, Springer/Praxis Publishing, 669pp.

Salat, J., Font, J., Cruzado, A., 1978. Datos oceanográficos frente a Barcellona. Datos Informativos. 5. pp. 1-73.

Santoleri, R., Banzon, V., Marullo, S., Napolitano, E., D'Ortenzio, F., Evans, R., 2003. Year-to-year variability of the phytoplankton bloom in the southern Adriatic Sea (1998–2000): Sea-viewing Wide Field-of-view Sensor observations and modeling study, J. Geophys. Res., 108, 8122.

Sathyendranath, S., Stuart, V., Cota, G., Maas, H. and Platt, T., 2001. Remote sensing of phytoplankton pigments: a comparison of empirical and theoretical approaches. International Journal of Remote Sensing 22: 249–273.

Sheldon, R. W. and Parson, T. R., 1967. A continuos size spectrum for particulate matter in the sea. J. Fish. Res. Bd. Can., 24:909

Sheldon, R. W., Prakash, A. and Sutcliffe, W. H., 1972. The size distribution of particles in the Ocean. Limnol. Oceanogr., 17:327.

Sieburth, J. M , Smetacek, V , Lenz, J , 1978. Pelagic ecosystem structure- Heterotrophic compartments of the plankton and their relationship to plankton size fractions Limnology and Oceanography 23, 1256-1263

Sieburth, J 1979. Sea microbes Oxford University Press New York.

Siokou-Frangou, I., Christaki, U., Mazzocchi, M. G., Montresor, M., Ribera d'Alcalá, M., Vaqué, D., Zingone, A., 2010. Plankton in the open Mediterranean Sea: a review. Biogeosciences, 7(5), pp. 1543-1586.

Taupier-Letage, I., & Millot, C., 1988. Surface circulation in the Algerian Basin during 1984. Oceanol. Acta, 9, pp. 119-131.

Taupier-Letage, I., Millot, C., 1988. Surface circulation in the Algerian Basin during 1984. Oceanol. Acta, 9, pp. 119-131.

Uitz, J., Claustre, H., Morel, A., Hooker, S. B., 2006. Vertical distribution of phytoplankton communities in open ocean: An assessment based on surface chlorophyll. Journal of Geophysical Research: Oceans (1978–2012), 111(C8).

Uitz, J., Stramski, D., Gentili, B., D'Ortenzio, F., Claustre, H., 2012. Estimates of phytoplankton class-specific and total primary production in the Mediterranean Sea from satellite ocean color observations. Global Biogeochemical Cycles, 26(2).

Vadrucci, M.R., Cabrini, M., Basset, A., 2007. Biovolume determination of phytoplankton guilds in transitional water ecosystems of Mediterranean Ecoregion. Transitional Waters Bulletin, 2: 83-102

Vidussi, F., Claustre, H., Manca, B. B., Luchetta, A., Marty, J. C., 2001. Phytoplankton pigment distribution in relation to upper thermocline circulation in the eastern Mediterranean Sea during winter. Journal of Geophysical Research: Oceans (1978–2012), 106(C9), 19939-19956.

Volpe, G., Santoleri, R., Vellucci, V., Ribera d'Alcala, M., Marullo, S., D'Ortenzio, F., 2007. The colour of the Mediterranean Sea: Global versus regional bio-optical algorithms evaluation and implication for satellite chlorophyll estimates, Remote Sens. Envi- ron., 107, 625–638

Werdell, P. J., & Bailey, S. W., 2005. An improved in-situ bio-optical data set for ocean color algorithm development and satellite data product validation. Remote Sensing of Environment, 98(1), pp. 122-140.

Wright, S. W., Jeffrey, S.W., Mantoura R.F.C., Llewellyn, C.A., Bjorn- land T., Repeta D., Welschmeyer, N., 1991. Improved HPLC method for the analysis of chlorophylls and carotenoids from marine phytoplankton. Mar. Ecol. Prog. Ser. 77, pp. 183-196 .

Websites:

1. http://modis.gsfc.nasa.gov/about/specifications.php
2. www.efremer.fr
3. http://catalogue.myocean.eu.org/static/resources/myocean/quid/MYO2-QUID-OC-MED-BS-V3.1-CNR-V4.0.pdf

4. http://seadas.gsfc.nasa.gov

5. http://catalogue.myocean.eu.org/)

6. http://pathfinder.nodc.noaa.gov

7. http://oceancolor.gsfc.nasa.gov/)

8. http://www.eoearth.org/view/article/149998/)